AD-A043 741 LOCKHEED MISSILES AND SPACE CO INC PALO ALTO CALIF PA--ETC F/G 11/6
CORRELATION OF MICROSTRUCTURE WITH FRACTURE TOUGHNESS PROPERTIE--ETC(U)
JAN 77 R E LEWIS, F A CROSSLEY N00019-75-C-0378
UNCLASSIFIED LMSC-D555813 NL

1 OF 2
AD A043 741

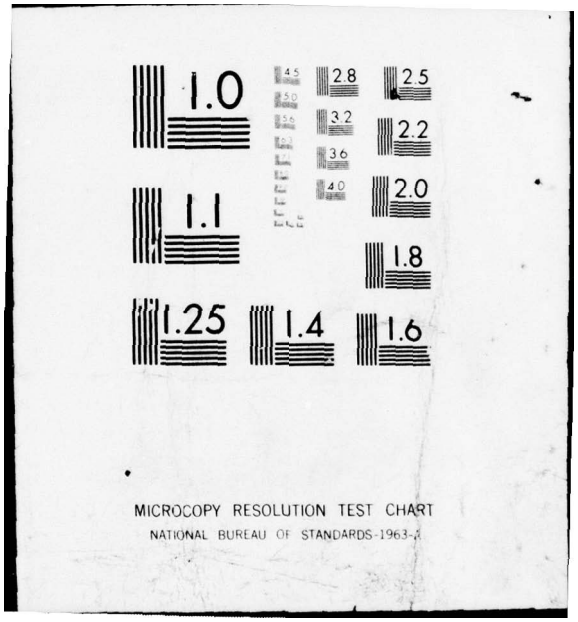
1.0
1.1
1.25
1.4
1.6
1.8
2.0
2.2
2.5
2.8
3.2
3.6
4.0
MICROCOPY RESOLUTION TEST CHART
NATIONAL BUREAU OF STANDARDS-1963-A

Report LMSC-D555813 N00019-75-C-0378

CORRELATION OF MICROSTRUCTURE WITH FRACTURE TOUGHNESS PROPERTIES IN METALS (PART III)

Richard E. Lewis
Frank A. Crossley

Lockheed Palo Alto Research Laboratory
Lockheed Missiles & Space Company, Inc.
A Subsidiary of Lockheed Aircraft Corporation
P.O. Box 504
Sunnyvale, California, 94088

10 January 1977

Final Report for Period 11 April 1975–10 January 1977

Approved for Public Release; Distribution Unlimited

Prepared for
Naval Air Systems Command
Code Air – 52031D
Washington, D.C., 20360

(9) Final rept. 11 Apr 75 - 10 Jan 77,

UNCLASSIFIED

SECURITY CLASSIFICATION OF THIS PAGE *(When Data Entered)*

REPORT DOCUMENTATION PAGE

READ INSTRUCTIONS BEFORE COMPLETING FORM

1. REPORT NUMBER

2. GOVT ACCESSION NO.

3. RECIPIENT'S CATALOG NUMBER

4. TITLE *(and Subtitle)*
(6) CORRELATION OF MICROSTRUCTURE WITH FRACTURE TOUGHNESS PROPERTIES IN METALS (PART III),

5. TYPE OF REPORT & PERIOD COVERED
Final Report for Period
11 Apr 1975 – 10 Jan 1977

6. PERFORMING ORG. REPORT NUMBER
(14) LMSC-D555813

7. AUTHOR(s)
(10) Richard E./Lewis
Frank A./Crossley

8. CONTRACT OR GRANT NUMBER(s)
(15) N00019-75-C-0378

9. PERFORMING ORGANIZATION NAME AND ADDRESS
Lockheed Missiles & Space Co., Inc.
3251 Hanover St., Palo Alto, Ca. 94304

10. PROGRAM ELEMENT, PROJECT, TASK AREA & WORK UNIT NUMBERS

11. CONTROLLING OFFICE NAME AND ADDRESS
(11) Naval Air Systems Command
Department of the Navy

12. REPORT DATE
10 Jan 1977

13. NUMBER OF PAGES
130 (12) 145p.

14. MONITORING AGENCY NAME & ADDRESS *(if different from Controlling Office)*

15. SECURITY CLASS. *(of this report)*
Unclassified

15a. DECLASSIFICATION/DOWNGRADING SCHEDULE

16. DISTRIBUTION STATEMENT *(of this Report)*

Approved for public release; distribution unlimited

17. DISTRIBUTION STATEMENT *(of the abstract entered in Block 20, if different from Report)*

18. SUPPLEMENTARY NOTES

19. KEY WORDS *(Continue on reverse side if necessary and identify by block number)*

Titanium alloy	Microstructures	ELI grade
Ti-6Al-4V	Fatigue crack growth rate	Standard grade
Fracture toughness	Mechanical properties	Effect of cooling rate
Stress corrosion cracking	Tensile properties	Short-range order
	Fractographs	

20. ABSTRACT *(Continue on reverse side if necessary and identify by block number)*

Ti-6Al-4V alloy, 1-in. plate was studied for the purpose of establishing a correlation between microstructures and fracture toughness, stress-corrosion cracking, and fatigue crack growth. Both standard and ELI grades, mill-annealed, vacuum-creep-furnace flattened and recrystallization-annealed were included. Reheat-treatments by duplex-annealing and beta- plus duplex-annealing were performed, including air and furnace cooling from the final annealing temperature. A total of 17 conditions were studied, complementing the 49 conditions previously studied on two contracts to Naval Air Systems Command. Tensile, fracture toughness, stress-corrosion cracking, and fatigue crack

DD FORM 1 JAN 73 1473 EDITION OF 1 NOV 65 IS OBSOLETE

UNCLASSIFIED 210118

SECURITY CLASSIFICATION OF THIS PAGE *(When Data Entered)*

growth properties were determined. Optical microscopy and scanning electron microfractography were employed. Six conditions studied previously were reexamined by transmission electron microscopy to investigate the effect of cooling rate on the interface phase between α and β phases and on development of short-range order in the α phase.

A coarse Widmanstätten $\alpha + \beta$ microstructure, resulting from beta- plus duplex-annealing, was found to exhibit the highest fracture toughness and stress-corrosion cracking resistance, and lowest fatigue crack growth rate from $<10^{-7}$ to 10^{-4} in./cycle. Mixtures of equiaxed α and Widmanstätten $\alpha + \beta$ were next best in combined fracture properties. The lowest toughness and about the lowest stress-corrosion cracking resistance were exhibited by equiaxed α, resulting from mill-annealing. High toughness but low stress-corrosion cracking resistance were exhibited by fine equiaxed α, resulting from recrystallization-annealing.

Cooling rate had a strong effect on stress-corrosion cracking resistance of microstructures containing Widmanstätten $\alpha + \beta$ and only a moderate effect on equiaxed microstructures. In both cases, slow furnace cooling reduces K_{Iscc} to as low as 28 ksi-in.$^{1/2}$, where as air cooling results in K_{Iscc} as high as 71 ksi-in.$^{1/2}$.

For the same heat-treatment, ELI grade exhibits higher toughness and stress-corrosion cracking resistance than standard grade. These differences are attributed to the lower aluminum and oxygen in the ELI grade.

Evidence of short-range order was found only in furnace-cooled product, both duplex-annealed and beta- plus duplex-annealed. In stress-corrosion cracking, short-range order appears to promote cleavage of α-phase and suppress secondary cracking along α - β interfaces. Slow cooling rates promote the growth of the interface phase, but the effect of the interface phase on stress-corrosion cracking is unclear.

PREFACE

This report is an account of the work performed at the Lockheed Palo Alto Research Laboratory on the Correlation of Microstructure with Fracture Toughness Properties in Metals for the U.S. Naval Air Systems Command, Contract N00019-75-C-0378 from 11 April 1975 to 10 January 1977. The work was performed in the Metallurgy and Composites Laboratory, managed by Dr. T. E. Tietz. The principal investigator was R. E. Lewis, assisted by F. A. Crossley, A. T. Davinroy, R. W. Harrington, H. A. Kawayoshi, and A. H. Heynan. Included also is some of the work performed by Dr. C. Hartley, Professor of Materials Science, University of Florida, Gainesville, Florida, when at the Lockheed Palo Alto Research Laboratory on a National Science Foundation Fellowship, summer of 1975. The project monitor was W. T. Highberger, Code Air – 52031D, Naval Air Systems Command, Washington, D.C.

ABSTRACT

Ti-6Al-4V alloy, 1-in. plate was studied for the purpose of establishing a correlation between microstructures and fracture toughness, stress-corrosion cracking, and fatigue crack growth. Both standard and ELI grades, mill-annealed, vacuum-creep-furnace flattened and recrystallization-annealed were included. Reheat-treatments by duplex-annealing and beta- plus duplex-annealing were performed, including air and furnace cooling from the final annealing temperature. A total of 17 conditions were studied, complementing the 49 conditions previously studied on two contracts to Naval Air Systems Command. Tensile, fracture toughness, stress-corrosion cracking, and fatigue crack growth properties were determined. Optical microscopy and scanning electron microfractography were employed. Six conditions studied previously were reexamined by transmission electron microscopy to investigate the effect of cooling rate on the interface phase between α and β phases and on development of short-range order in the α phase.

A coarse Widmanstätten $\alpha + \beta$ microstructure, resulting from beta- plus duplex-annealing, was found to exhibit the highest fracture toughness and stress-corrosion cracking resistance, and lowest fatigue crack growth rate from $<10^{-7}$ to 10^{-4} in./cycle. Mixtures of equiaxed α and Widmanstätten $\alpha + \beta$ were next best in combined fracture properties. The lowest toughness and about the lowest stress-corrosion cracking resistance were exhibited by equiaxed α, resulting from mill-annealing. High toughness but low stress-corrosion cracking resistance were exhibited by fine equiaxed α, resulting from recrystallization-annealing.

Cooling rate had a strong effect on microstructures containing Widmanstätten $\alpha + \beta$ and only a moderate effect on equiaxed microstructures. In both cases, slow furnace cooling reduces K_{Iscc} to as low as 28 ksi-in.$^{1/2}$, where air cooling results in K_{Iscc} as high as 71 ksi-in.$^{1/2}$.

For the same heat-treatment, ELI grade exhibits higher toughness and stress-corrosion cracking resistance than standard grade. These differences are attributed to the lower aluminum and oxygen in the ELI grade.

Evidence of short-range order was found only in furnace cooled product, both duplex-annealed and beta- plus duplex-annealed. In stress-corrosion cracking, short-range order appears to promote cleavage of α-phase and suppress secondary cracking along α - β interfaces. Slow cooling rates promote the growth of the interface phase, but the effect of interface phase on stress-corrosion cracking is unclear.

CONTENTS

Section		Page
	PREFACE	iii
	ABSTRACTS	v
	TABLES	ix
	ILLUSTRATIONS	x
1.0	INTRODUCTION	1
	1.1 The Need for Correlating Microstructure With Fracture Toughness Properties	1
	1.2 Microstructure Versus Properties in α-β Titanium Alloys	2
	1.3 Results of First Year's Study	5
	1.4 Results of Second Year's Study	7
	1.5 Activities for Current Study	10
2.0	MATERIALS AND METHODS	12
	2.1 Materials, Processing, and Heat Treatment	12
	2.2 Mechanical Properties Tests	13
	2.2.1 Tensile Properties	13
	2.2.2 Fatigue Crack Growth and Fracture Toughness	14
	2.2.3 Stress-Corrosion Crack Growth Threshold	16
	2.3 Metallography and Fractography	17
	2.3.1 Metallography	17
3.0	RESULTS AND DISCUSSION	19
	3.1 Relationship of Fracture Toughness and Stress-Corrosion Cracking Resistance to Tensile Properties	19
	3.2 Relationship of Microstructures to Mechanical Properties	21
	3.2.1 Mill-Annealed Plate	22
	3.2.2 Vacuum Creep Furnace-Flattened (VCFF) Plate	26
	3.2.3 Recrystallization-Annealed Plate	29

Section			Page
	3.3	Fatigue Crack Growth	30
		3.3.1 General Comments	30
		3.3.2 Mill-Annealed Plate	30
		3.3.3 Vacuum Creep Furnace-Flattened Plate	31
		3.3.4 Recrystallization-Annealed Plate	31
		3.3.5 Comparison of As-Received Conditions	31
		3.3.6 Effect of Microstructural Condition on Fatigue Life of Structures	31
	3.4	Effect of Cooling Rate on the Interface Phase and Short-Range Order	33
		3.4.1 Results of Duplex-Annealing	33
		3.4.2 Results of Beta Treatment Followed by Duplex-Annealing	34
		3.4.3 Discussion of Results	35
4.0		SUMMARY AND CONCLUSIONS	38
		REFERENCES	41
		DISTRIBUTION LIST	127

TABLES

Table		Page
I	Ti-6Al-4V 1-In. Plate Mill Products	46
II	Summary of Titanium 6Al-4V, 1-In. Plate Conditions Studied	47
III	Comparison of Heat-Treatment Cooling Rates	48
IV	Summary of Mechanical Properties Grouped By Mill Heat-Treatment Product and Ranked By Fracture Toughness	49
V	Interplanar Spacings for Phases Observed in Ti-6Al-4V	50

ILLUSTRATIONS

Figure		Page
1	Processing Schedule for Ti-6Al-4V 1-in. Plate	51
2	Cooling Curves for Ti-6Al-4V 1-in. Plate. Laboratory treatments cooled from 1775°F and 1450°F; mill treatments cooled from 1810°F and 1450°F. Thermocouple located 1/2 in. below surface at center of plates	52
3	Tensile Specimen	53
4	Compact Tension Specimen Used for K_{Ic}, da/dN Versus ΔK, and K_{Iscc} Tests	54
5	Fracture Toughness Versus Yield Strength Comparison for the Seventeen Conditions of Ti-6Al-4V 1-in. Plate	55
6	Stress-Corrosion Cracking Index (K_{Iscc}) Versus Yield Strength Comparisons for Thirteen Conditions of Ti-6Al-4V 1-in. Plate	56
7	Ti-6Al-4V Condition 50. Mill-annealed, standard grade, 1-in. plate, *as-received*. K_{Ic} = 45 ksi-in.$^{1/2}$, K_{Iscc} = 45 ksi-in.$^{1/2}$, F_{ty} = 147 ksi	57
8	SEM Fractographs of Ti-6Al-4V Condition 50	58
9	Ti-6Al-4V Condition 51. Mill-annealed, standard grade, 1-in. plate, 1775°F-1/2h-AC. K_{Ic} = 65 ksi-in.$^{1/2}$, K_{Iscc} = 44 ksi-in.$^{1/2}$, F_{ty} = 137 ksi	59
10	SEM Fractographs of Ti-6Al-4V Condition 51	60
11	Ti-6Al-4V Condition 53. Mill-annealed, standard grade, 1-in. plate, 1775°F-1/2h-AC, 1450°F-1h-FC. K_{Ic} = 55 ksi-in.$^{1/2}$, K_{Iscc} = 45 ksi-in.$^{1/2}$, F_{ty} = 140 ksi	61
12	SEM Fractographs of Ti-6Al-4V Condition 53	62
13	Ti-6Al-4V Condition 54. Mill-annealed, ELI grade, 1-in. plate, as-received. K_{Ic} = 60 ksi-in.$^{1/2}$, F_{ty} = 144 ksi	63
14	SEM Fractographs of Ti-6Al-4V Condition 54	64
15	Ti-6Al-4V Condition 55. Mill-annealed, ELI grade, 1-in. plate, 1775°F-1/h-AC, 1450°F-1h-AC. K_{Ic} = 74 ksi-in.$^{1/2}$, F_{ty} = 136 ksi	65
16	SEM Fractographs of Ti-6Al-4V Condition 55	66
17	Ti-6Al-4V Condition 57. Mill-annealed, ELI grade, 1-in. plate, 1775°F-1/2h-AC, 1450°F-1h-FC. K_{Ic} = 72 ksi-in.$^{1/2}$, F_{ty} = 139 ksi	67

Figure		Page
18	SEM Fractographs of Ti-6Al-4V Condition 57	68
19	Ti-6Al-4V Condition 60. Mill-annealed, ELI grade, 1-in. plate, 1825°F-1/2h-AC, 1775°F-1/2h-AC, 1450°F-1h-AC. K_Q = 95 ksi-in.$^{1/2}$, K_{Iscc} = 72 ksi-in.$^{1/2}$, F_{ty} = 123 ksi	69
20	SEM Fractographs of Ti-6Al-4V Condition 60	70
21	Ti-6Al-4V Condition 63. Vacuum creep-flattened, standard grade, 1-in. plate, as-received. K_{Ic} = 70 ksi-in.$^{1/2}$, K_{Iscc} = 40 ksi-in.$^{1/2}$, F_{ty} = 136 ksi	71
22	SEM Fractographs of Ti-6Al-4V Condition 63	72
23	Ti-6Al-4V Condition 64. Vacuum creep-flattened, standard grade, 1-in. plate, 1775°F-1/2h-AC, 1450°F-1h-AC. K_{Ic} = 64 ksi-in.$^{1/2}$, K_{Iscc} = 28 ksi-in.$^{1/2}$, F_{ty} = 133 ksi	73
24	SEM Fractographs of Ti-6Al-4V Condition 64	74
25	Ti-6Al-4V Condition 66. Vacuum creep-flattened, standard grade, 1-in. plate, 1775°F-1/2h-AC, 1450°F-1h-FC. K_{Ic} = 74 ksi-in.$^{1/2}$, K_{Iscc} = 29 ksi-in.$^{1/2}$, F_{ty} = 134 ksi	75
26	SEM Fractographs of Ti-6Al-4V Condition 66	76
27	Ti-6Al-4V Condition 67. Vacuum creep-flattened, standard grade, 1-in. plate, 1825°F-1/2h-AC, 1775°F-1/2h-AC, 1450°F-1h-AC. K_{Ic} = 80 ksi-in.$^{1/2}$ K_{Iscc} = 54 ksi-in.$^{1/2}$, F_{ty} = 127 ksi	77
28	SEM Fractographs of Ti-6Al-4V Condition 67	78
29	Ti-6Al-4V Condition 69. Vacuum creep-flattened, standard grade, 1-in. plate, 1825°F-1/2h-AC, 1775°F-1/2h-AC, 1450°F-1h-FC. K_{Ic} = 82 ksi-in.$^{1/2}$, K_{Iscc} = 32 ksi-in.$^{1/2}$, F_{ty} = 132 ksi	79
30	SEM Fractographs of Ti-6Al-4V Condition 69	80
31	Ti-6Al-4V Condition 70. Vacuum creep-flattened, ELI grade, 1-in. plate, as-received. K_{Ic} = 71 ksi-in.$^{1/2}$, K_{Iscc} = 50 ksi-in.$^{1/2}$, F_{ty} = 138 ksi	81
32	SEM Fractographs of Ti-6Al-4V Condition 70	82
33	Ti-6Al-4V Condition 71. Vacuum creep-flattened, ELI grade, 1-in. plate, 1775°F-1/2h-AC, 1450°F-1h-AC. K_{Ic} = 84 ksi-in.$^{1/2}$, K_{Iscc} = 38 ksi-in.$^{1/2}$, F_{ty} = 134 ksi	83
34	SEM Fractographs of Ti-6Al-4V Condition 71	84

Figure		Page
35	Ti-6Al-4V Condition 73. Vacuum creep-flattened, ELI grade, 1-in. plate, 1775°F-1/2h-AC, 1450°F-1h-FC. K_{Ic} = 76 ksi-in.$^{1/2}$, K_{Iscc} = 28 ksi-in.$^{1/2}$, F_{ty} = 138 ksi	85
36	SEM Fractographs of Ti-6Al-4V Condition 73	86
37	Ti-6Al-4V Condition 76. Recrystallization-annealed, standard grade, 1-in. plate, as-received. K_Q = 85 ksi-in.$^{1/2}$, F_{ty} = 127 ksi	87
38	SEM Fractographs of Ti-6Al-4V Condition 76	88
39	Ti-6Al-4V Condition 75. Recrystallization-annealed, ELI grade, 1-in. plate, as-received. K_{Ic} = 82 ksi-in.$^{1/2}$, K_{Iscc} = 36 ksi-in.$^{1/2}$, F_{ty} = 132 ksi	89
40	SEM Fractographs of Ti-6Al-4V Condition 75	90
41	Fatigue Crack Growth Behavior in Ti-6Al-4V Condition 50. Mill-annealed, standard grade, 1-in. plate, as-received. K_{Ic} = 45 ksi-in.$^{1/2}$, K_{Iscc} = 45 ksi-in.$^{1/2}$, F_{ty} = 147 ksi	91
42	Fatigue Crack Growth Behavior in Ti-6Al-4V Condition 51. Mill-annealed, standard grade, 1-in. plate, 1775°F-1/2h-AC, 1450°F-1h-AC. K_{Ic} = 65 ksi-in.$^{1/2}$, K_{Iscc} = 44 ksi-in.$^{1/2}$, F_{ty} = 137 ksi	92
43	Fatigue Crack Growth Behavior in Ti-6Al-4V Condition 53. Mill-annealed, standard grade, 1-in. plate, 1775°F-1/2h-AC, 1450°F-1h-FC. K_{Ic} = 55 ksi-in.$^{1/2}$, K_{Iscc} = 45 ksi-in.$^{1/2}$, F_{ty} = 140 ksi	93
44	Fatigue Crack Growth Behavior in Ti-TAl-4V Condition 54. Mill-annealed, ELI grade, 1-in. plate, as-received. K_{Ic} = 60 ksi-in.$^{1/2}$, F_{ty} = 144 ksi	94
45	Fatigue Crack Growth Behavior in Ti-6Al-4V Condition 55. Mill-annealed, ELI grade, 1-in. plate, 1775°F-1/2h-AC, 1450°F-1h-AC. K_{Ic} = 74 ksi-in.$^{1/2}$, F_{ty} = 136 ksi	95
46	Fatigue Crack Growth Behavior in Ti-6Al-4V Condition 57. Mill-annealed, ELI grade, 1-in. plate, 1775°F-1/2h-AC, 1450°F-h-FC. K_{Ic} = 72 ksi-in.$^{1/2}$, F_{ty} = 139 ksi	96
47	Fatigue Crack Growth Behavior in Ti-6Al-4V Condition 60. Mill-annealed, ELI grade, 1-in. plate, 1825°F-1/2h-AC, 1450°F-1h-AC, K_Q = 95 ksi-in.$^{1/2}$, K_{Iscc} = 72 ksi-in.$^{1/2}$,	97
48	Fatigue Crack Growth Behavior in Ti-6Al-4V Condition 63. Vacuum creep-flattened, standard grade, 1-in. plate, as-received. K_{Ic} = 70 ksi-in.$^{1/2}$, K_{Iscc} = 40 ksi-in.$^{1/2}$, F_{ty} = 136 ksi	98

Figure		Page
49	Fatigue Crack Growth Behavior Ti-6Al-4V Condition 64. Vacuum creep-flattened, standard grade, 1-in. plate, 1775°F-1/2h-AC, 1450°F-1h-AC. K_{Ic} = 64 ksi-in.$^{1/2}$, K_{Iscc} = 28 ksi-in.$^{1/2}$, F_{ty} = 133 ksi	99
50	Fatigue Crack Growth Behavior in Ti-6Al-4V Condition 66. Vacuum creep-flattened, standard grade, 1-in. plate, 1775°F-1/2h-Ac, 1450°F-1h-FC. K_{Ic} = 74 ksi-in.$^{1/2}$, K_{Iscc} = 29 ksi-in.$^{1/2}$, F_{ty} = 134 ksi	100
51	Fatigue Crack Growth Behavior in Ti-6Al-4V Condition 67. Vacuum creep-flattened, standard grade, 1-in. plate, 1825°F-1/2h-AC, 1775°F-1h-AC. K_{Ic} = 80 ksi-in.$^{1/2}$, K_{Iscc} = 54 ksi-in.$^{1/2}$, F_{ty} = 127 ksi	101
52	Fatigue Crack Growth Behavior in Ti-6Al-4V Condition 69. Vacuum creep-flattened, standard grade, 1-in. plate, 1825°F-1/2h-AC, 1775°F-1/2h-AC, 1450°F-1h-FC. K_{Ic} = 82 ksi-in.$^{1/2}$, K_{Iscc} = 32 ksi-in.$^{1/2}$, F_{ty} = 132 ksi	102
53	Fatigue Crack Growth Behavior in Ti-6Al-4V Condition 70. Vacuum creep-flattened, ELI grade, 1-in. plate, as-received. K_{Ic} = 71 ksi-in.$^{1/2}$, K_{Iscc} = 50 ksi-in.$^{1/2}$, F_{ty} = 138 ksi	103
54	Fatigue Crack Growth Behavior in Ti-6Al-4V Condition 71. Vacuum creep-flattened, ELI grade, 1-in. plate, 1775°F-1/2h-AC, 1450°F-1h-AC. K_{Ic} = 84 ksi-in.$^{1/2}$, K_{Iscc} = 38 ksi-in.$^{1/2}$, F_{ty} = 134 ksi	104
55	Fatigue Crack Growth Behavior in Ti-6Al-4V Condition 73. Vacuum creep flattened, ELI grade, 1-in. plate, 1775°F-1/2h-AC, 1450°F-1h-FC. K_{Ic} = 76 ksi-in.$^{1/2}$, K_{Iscc} = 28 ksi-in.$^{1/2}$, F_{ty} = 138 ksi	105
56	Fatigue Crack Growth Behavior in Ti-6Al-4V Condition 76. Recrystallization-annealed, standard grade, 1-in. plate, as-received. K_Q = 85 ksi-in.$^{1/2}$, F_{ty} = 127 ksi	106
57	Fatigue Crack Growth Behavior in Ti-6Al-4V Condition 75. Recrystallization-annealed, ELI grade, 1-in. plate, as-received. K_{Ic} = 82 ksi-in.$^{1/2}$, K_{Iscc} = 36 ksi-in.$^{1/2}$, F_t = 132 ksi	107
58	Fatigue Crack Growth Comparison of Mill-Annealed Ti-6Al-4V 1-in. Plate, Standard Grades: As-Received (Condition 50); Duplex-Annealed, Air-Cooled (Condition 51); and Duplex-Annealed, Furnace-Cooled (Condition 53)	108
59	Fatigue Crack Growth Comparison of Mill-Annealed Ti-6Al-4V 1-in. Plate, ELI Grades: As-Received (Condition 54); Duplex-Annealed, Air-Cooled (Condition 55); Duplex-Annealed, Furnace-Cooled (Condition 57); and Beta + Duplex-Annealed, Air-Cooled (Condition 60)	109

Figure		Page
60	Fatigue Crack Growth Comparison of Vacuum Creep-Flattened Ti-6Al-4V, 1-in. Plate, Standard Grades: As-Received (Condition 63); Duplex-Annealed, Air-Cooled (Condition 64); Duplex-Austenitized, Furnace-Cooled (Condition 66); Beta + Duplex-Annealed, Air-Cooled (Condition 67); and Beta + Duplex-Annealed, Furnace-Cooled (Condition 69)	110
61	Fatigue Crack Growth Comparison of Vacuum Creep-Flattened Ti-6Al-4V, 1-in. Plate, ELI Grade: As-Received (Condition 70); Duplex-Austenitized, Air-Cooled (Condition 71); and Duplex-Austenitized, Furnace-Cooled (Condition 73)	111
62	Fatigue Crack Growth Comparison of Recrystallization-Annealed Ti-6Al-4V, 1-in. Plate, Standard Grade (Condition 76) and ELI Grade (Condition 75)	112
63	Fatigue Crack Growth Comparisons of As-Received Ti-6Al-4V, 1-in. Plate: Mill-Annealed – Stanard (Condition 50), – ELI (Condition 54); Vacuum Creep-Flattened – Standard (Condition 63), – ELI (Condition 70); Recrystallization-Annealed – Standard (Condition 76), – ELI (Condition 75)	113
64	Effect of Heat Treatment on Crack Depth During Life of Structure Subjected to Constant Amplitude Fatigue. Beta plus duplex-annealing is 1825°F-1/2h-AC, 1755°F-1/2h-AC, 1450°F-1h-AC (this study). Duplex annealing cycle is 1775°F-1/2h-AC, 1450°F-1h – cooled as noted; mill-annealing cycle is 1450°F-1h-AC (after Ref. 7)	114
65	Ti-6Al-4V, 1-in. Plate, Effect of Heat-Treatment on Structural Life Predicted by Computer Modelling. Beta plus duplex-annealing cycle is 1825°F-1/2h-AC, 1775°F-1/2h-AC, 1450°F-1h-AC (this study). Duplex-annealing cycle is 1775°F-1/2h-AC, 1450°F-1h-water-quenched (WQ), air-cooled (AC), or furnace-cooled (FC); mill-annealing cycle is 1450°F-1h-AC (after Ref. 7)	115
66	Ti-6Al-4V Conditon 31, 2(R), and 32 From the First and Second Year s Studies. 1-in. Plate, 1775°F-1/2h-AC, 1450°F-1h – cooled as noted. 3000× (after Ref. 2)	116
67	Ti-6Al-4V Conditions 31, 2(R), and 32; Duplex-Annealed and Water-Quenched, Air-Cooled, or Furnace-Cooled, Respectively	117
68	Ti-6Al-4V Condition 31: Duplex-Annealed and Water-Quenched	118
69	Ti-6Al-4V Condition 2(R): Duplex-Annealed and Air-Cooled	119
70	Ti-6Al-4V Condition 32: Duplex-Annealed and Furnace-Cooled	120
71	Diffraction Pattern From Duplex-Annealed and Furnace-Cooled Specimen Showing Diffuse Spots at (h/2, k/2, ℓ)	121

Figure		Page
72	Ti-6Al-4V Conditions 33, 7, and 34 From the First and Second Year's Studies. 1-in. Plate, 1850°F-1/2h-AC, 1775°F-1/2h-AC, 1450°F-1h – cooled as noted. 3000× (after Refs. 1 and 2)	122
73	Ti-6Al-4V Conditions 33, 7, and 34; Beta-Treated, Duplex-Annealed, and Water-Quenched, Air-Cooled, or Furnace-Cooled, Respectively	123
74	Diffraction Pattern From Beta-Treated and Duplex-Annealed Furnace-Cooled Specimens Showing Diffuse Spots at (h/2, k/2, ℓ)	124
75	Fracture Surfaces of Ti-6Al-4V Stress-Corrosion Cracked Specimens; Duplex-Annealed and Water-Quenched or Furnace-Cooled	125
76	Fracture Surfaces of Ti-6Al-4V Stress-Corrosion Cracked Specimens; Beta-Treated, Duplex-Annealed, and Water-Quenched or Furnace-Cooled	126

1.0 INTRODUCTION

1.1 THE NEED FOR CORRELATING MICROSTRUCTURE WITH FRACTURE TOUGHNESS PROPERTIES

High-performance military aircraft and space structures use a number of strong, tough metallic materials. Particularly for tension-critical components, certain alpha-beta titanium alloys exhibit an excellent combination of high strength, low density, and high toughness. Of the various alpha-beta alloys, Ti-6Al-4V is by far the most commonly used. This alloy exhibits an attractive yield strength-to-density range from 0.6 to 0.8×10^6 in. and at the same time can be highly resistant to elastically unstable fracture, salt water, or salt air stress corrosion cracking, and fatigue initiation and crack growth. The latter properties are particularly important for naval aircraft.

Reliable performance of such structures requires a successful combination of (1) accurate design and stress analysis for the intended service requirements, (2) quality control to screen out unacceptable flaws and defects in the fabricated parts, and (3) control of mechanical properties including fracture toughness, fatigue, and stress corrosion cracking resistance in the structural materials. The third item is the focus of interest in the present study.

Because compositional and processing variations of alpha-beta titanium alloys widely affect both microstructure and mechanical properties, a need exists to develop useful correlations between them. A number of studies have been conducted with the aim of developing such correlations. Unfortunately, most have not systematically explored the relationship of microstructure to plane strain fracture toughness (K_{Ic}).

A systematic study of these factors was initiated for the Naval Air Systems Command in 1972 by Lockheed Missiles & Space Company, Inc. Results of the first and second year's activities have been previously reported [1,2]* and are summarized in Sections

*Numbers in parenthesis refer to references appearing at the end of this report.

1.3 and 1.4. The third, and concluding, year's activities are the subject of the present report.

1.2 MICROSTRUCTURE VERSUS PROPERTIES IN α-β TITANIUM ALLOYS

Alpha-beta titanium alloys, as illustrated by Ti-6Al-4V, exhibit a variety of microstructures. Through relatively simple differences in processing and heat treatment, an α-β alloy may exhibit equiaxed $\alpha + \beta$ or acicular $\alpha + \beta$ microstructures or mixtures of these two. Additionally, acicular $\alpha + \beta$ microstructures may be those formed by nucleation and (diffusion-controlled) growth on moderate or slow cooling from β or by martensitic (i.e., shear) transformation (α'). Aging of α' causes precipitation hardening of β, resulting in a significant strength increase.

These microstructures exhibit a wide range of strength and fracture toughness properties. In Ti-6Al-4V, tensile yield strength range is from 110 to 165 ksi, while fracture toughness, K_{Ic}, ranges from ~ 40 to over 100 ksi-in.$^{1/2}$. Generally, with higher strength, the range of tougness declines, but the minimum tougness observed is essentially independent of yield strength[1,2]. For any combination of strength and toughness, many small variations in composition (O,H) and processing history (cooling rate from annealing in the β or $\alpha + \beta$ field) may affect subcritical crack growth behavior; fatigue crack growth rate below 10^{-5} in./cycle and K_{Iscc}.

Recommendations of Ti-6Al-4V microstructure exhibiting the optiumum combination of toughness, subcritical crack growth, and strength are clearly not in agreement. Stubbington recommends a matrix of Widmanstätten (nucleation and growth transformation) $\alpha + \beta$ with a small percentage of equiaxed α.[3] Paton el al. recommend a fine equiaxed α resulting from recrystallization annealing (RA)[4]. This heat treatment was devised to minimize the large variation in toughness of equiaxed α exhibited by the mill annealed (MA) product. RA plate usually exhibits a moderately high yield strength (130 – 140 ksi) along with a high fracture toughness (> 75 ksi-in.$^{1/2}$). The fatigue crack growth rate of RA plate for ΔK = 20 ksi-in.$^{1/2}$ and R = 0.1 has been

observed to be superior to MA plate, but inferior to β-annealed plate[4]. β-annealing (BA) involves heating to above the β-transus followed by air cooling. RA plate does not exhibit a high threshold for stress corrosion cracking, K_{Iscc}, in aqueous chloride solutions[5]. This is attributed to the absence of acicular α as in Widmanstätten $\alpha + \beta$, which, when present, may act to promote secondary or branching crack growth, thereby absorbing more energy in crack propagation[4].

Greenfield and Margolin[6], Crossley and Lewis[1,2], and Paton et al.[4] identify coarse Widmanstätten $\alpha + \beta$ as having attractive properties. This structure results from BA treatment or BA followed by duplex annealing (DA). The microstructure consistently exhibits a high fracture toughness (> 80 ksi-in.$^{1/2}$) and high fatigue crack growth resistance[2,4]. As-transformed Widmanstätten $\alpha + \beta$ exhibits a somewhat lower yield strength than equiaxed α and a much lower yield strength than aged α'. It may also exhibit a lower tensile ductility than equiaxed α in terms of reduction of area.

The coarse acicular (Widmanstätten) $\alpha + \beta$ microstructure can exhibit a superior K_{Iscc}, as mentioned previously. However, it should be kept in mind that certain processing treatments can result in a serious degradation of K_{Iscc} in this as well as other microstructures. This degradation results from slow or very slow cooling from annealing in the $\alpha + \beta$ field. The effect was reported by Lewis and Crossley[2] and is a topic of increasing interest[7]. It is further investigated in the present study.

Some users of Ti-6Al-4V prefer to specify aged acicular α', developed by solution-treating and aging (STA) or overaging (STOA). STA and STOA are advantageous for applications that require the highest yield strength, only a low or moderate fracture toughness, a high fatigue endurance limit, and usually involve plane stress rather than plane strain conditions. Such applications are not in the majority compared with MA, RA, BA, or DA processed products because of the restrictions in meeting fracture toughness requirements of many aerospace structures and the heavy sections involved. In some cases, however, STA is a preferred condition of Ti-6Al-4V for critically stressed pressure vessels because of a high K_{Iscc} in the presence of certain liquid propellants.[8]

One must also consider inherent defects and processing defects as well as microstructure. Inherent defects include alpha-stabilized inclusions and alpha segregation and are discussed in the first year's study[1]. Processing defects include oxygen and hydrogen contamination, development of as-transformed Widmanstätten structure, and precipitation of Ti_3Al or an ordering of Ti-Al. Oxygen and hydrogen are commonly known to affect fracture properties in titanium, while oxygen also affects strength. Oxygen contamination most frequently results from insufficient removal of contaminated surfaces from hot-worked parts or parts heat-treated in air, or castings made in an oxide-coated mold. Hydrogen contamination may result from improper pickling, or from heat-treating in a reducing atmosphere.

Crystallographic texture influences both strength and fracture properties in α-β titanium alloys. Cross-rolling of Ti-6Al-4V sheet to produce strong basal texture normal to the plane of the sheet was used to fabricate spherical pressure vessels exhibiting a biaxial yield strength of 217 ksi[9]. Fatigue crack propagation and fracture toughness in textured Ti-6Al-2Sn-4Zr-6Mo (Ti-6246) alloy are quite sensitive to orientation of crack plane and growth direction[10]. At low values of ΔK, the fastest crack growth occurs in a plane containing the highest density of basal planes and growth direction parallel to rolling direction. It is postulated that this may be due to environmental effects promoting cleavage on near-basal planes[4]. Fatigue fracture surfaces in both Ti-6Al-4V and Ti-6246 exhibiting high growth rate at low ΔK do contain large areas of cleavage, often in the form of long "tongues" encompassing many α cells[1, 2, 12]. Meyn and Sandoz have shown that cleavage in α Ti occurs approximately 15 degrees from the basal plane[13]. It is probable that crystallographic texture is especially important at low stress intensities, where the plastic zone size in front of the crack tip is significantly smaller than the α cell size, and in the presence of moist air or salt water, environmental cracking along preferred cleavage planes may be a strong factor in crack growth. This would pertain to fatigue at low ΔK and for sustained loading stress corrosion crack growth threshold, K_{Iscc}.

1.3 RESULTS OF FIRST YEAR'S STUDY

Activities and Results

The Lockheed Palo Alto Research Laboratory initiated a study in 1972 to investigate and correlate macrostructures with fracture toughness and other properties in titanium alloys. This study was performed from 1 June 1972 to 30 September 1973 for the Naval Air Systems Command, Washington, D.C., under Contract N00019-72-C-0545. It was designed to be part of a continuing program extending over a period approximately three years. The complete results of this first year's activity were reported as LMSC-D356114.[1] A summary of this activity is as follows.

Ti-6Al-4V alloy was studied in three mill product forms for the purpose of establishing a correlation between microstructure and fracture toughness. The mill products were: 1-in. plate characteristic of material being supplied for the F-14 and F-15 fighter programs, 2.4-in. plate characteristic of material being supplied for the B-1 bomber program and 4 × 4-in. forged billets. Mill product, processing, and heat treatment variables produced 28 microstructural conditions. Mechanical properties determined were: tension test, plane strain fracture toughness and crack growth rate. Metallographic means employed were: light microscopy, scanning electron microfractography, and a limited amount of transmission electron microscopy.

Observed fracture toughness values varied from 47 to 111 ksi-in.$^{1/2}$. Conditions having K_{Ic} values less than 60 ksi-in.$^{1/2}$ were characterized by an absence of acicular α resulting from the nucleation and (diffusion dependent) growth transformation of β. The most significant finding was that commercial-size plates of 1-in. or more thickness air cooled from high in the α-β phase field do not have the same microstructures as similarly heat treated smaller volumes that are commensurate with test specimen blanks. The as-received 1-in. and 2.4-in. plates of Ti-6Al-4V were found to have an equiaxed, predominantly α structure having the lowest fracture toughness values measured in this study; i.e., about 48 ksi-in.$^{1/2}$ Heat treatments similar to those reported for the as-received conditions of the plates were applied to test specimen blanks. These treatments produced microstructures consisting of equiaxed primary α plus acicular

α resulting from nucleation and growth transformation of the β phase that existed at the annealing temperature. These conditions had fracture-toughness values ranging from 62 to 111 ksi-in.$^{1/2}$ in contrast to the 48 ksi-in.$^{1/2}$ for the as-received conditions.

It appears that commercial size heavy plates cool so slowly, because of their mass, that the β phase is consumed by the primary α growing into it, rather than by its nucleation and growth transformation. The former preserves the equiaxed condition existing at the solution treatment temperature, while the latter produces the familiar acicular product. This finding suggests a word of caution concerning structures resulting from working and annealing in the α-β phase field: large structures of Ti-6Al-4V cannot be expected to have either the microstructure or the fracture toughness associated with test specimens unless cooling rate from annealing treatment is approximately the same.

The fatigue crack propagation rate was found to vary widely among the different microstructures. For example, at a stress intensity range of 30 ksi-in.$^{1/2}$ and R = 0.1, the crack propagation rate was 3×10^{-6} in. per cycle for as-quenched martensite, 3×10^{-5} to 10^{-4} in. per cycle for coarse equiaxed α, and 3×10^{-5} to 8×10^{-4} in. per cycle for Widmanstätten, fine equiaxed α or worked Widmanstätten structures.

A correlation was found between microstructures and microfractographic features. Primary α was associated with cleavage (lower fracture toughness and high fatigue crack growth rates at low ΔK). Wholly, or nearly so, acicular structures having platelets greater than 1 μm in thickness, and full martensitic (unaged) structures were associated with the higher fracture toughness values and lower fatigue crack growth rates. Their fracture surfaces were characterized by the presence of large (> 20 μm) voids.

The major conclusion of this study is that for solution treatment below the β transus unless the microstructure contains a significant amount of acicular α formed by nucleation and growth transformation of α (rather than martensitically), plane strain fracture toughness will be less than 60 ksi-in.$^{1/2}$. It would appear that microstructurally equiaxed heavy plates currently produced by the mills are not cooled rapidly enough from annealing treatment to produce the type of microstructure associated with fracture toughness of more than 50 ksi-in.$^{1/2}$.

1.4 RESULTS OF SECOND YEAR'S STUDY

The study to investigate and correlate microstructures with fracture toughness and other properties in titanium was continued from 21 November 1973 to 21 January 1975 under Contract N00019-74-C-0161. The complete results of this activity were reported in LMSC-D454884[2]. A summary of this activity is as follows.

Ti-6Al-4V in three product forms and Ti-6Al-6V-2Sn-0.7Fe-0.7Cu (Ti-662) in one product form was studied. The Ti-6Al-4V mill products were: 1-in. plate characteristic of material supplied for the F-14 and F-15 fighter programs, 2.4-in. plate characteristic of material supplied for the B-1 Bomber program, and 4- × 4-in. forged billets. Mill product, processing, and heat-treatment variables produced 21 microstructural conditions. In Ti-6Al-4V, effects of cooling rate (water quenching, air cooling, furnace cooling) from annealing in the $\alpha-\beta$ phase field were studied. Some conditions involving beta annealing followed by duplex annealing in the $\alpha-\beta$ field were included. The effects of hydrogen from 34 to 150 ppm on duplex annealed, 1-in. plate were studied. Equiaxed α and α-segregated, worked Widmanstätten forged billets were studied in the duplex annealed and solution-treated and aged conditions. Cooling rates were varied from the final annealing temperature. In Ti-662, the as-received (mill annealed) plate was recrystallization annealed various ways and also solution-treated and aged. Mechanical properties determined were: tensile, plane strain critical stress intensity factor (K_{Ic}), fatigue crack growth (da/dN versus ΔK), and salt water stress corrosion cracking, threshold stress intensity (K_{Iscc}). Microstructures were examined by light optical microscopy, scanning electron microfractography, and some transmission electron microscopy.

In Ti-6Al-4V, 1-in. plate, fracture toughness values varied from 34 to 85 ksi-in.$^{1/2}$. In general, microstructure exhibiting the lowest toughness was predominantly equiaxed α, a mixture of equiaxed α plus Widmanstätten $\alpha+\beta$ was of intermediate toughness, and essentially all Widmanstätten $\alpha+\beta$ was the most tough. Cooling rate from the final annealing temperature (1450°F) was found to affect strength, toughness, fatigue crack growth, and K_{Iscc}. Slow furnace cooling produced the lowest

K_{Iscc} and highest fatigue crack growth rates at low ΔK, but K_{Ic} and yield strength were about the same as for air cooling. Water quenching produced the lowest K_{Ic} and yield strength but fatigue crack growth rates at low ΔK were significantly lower and K_{Iscc} was higher than for either air cooling or furnace cooling. These effects are consistent with a model involving Ti_3Al precipitation, but TEM examination failed to reveal any indication of such precipitation.

In Ti-6Al-4V, 2.4-in. plate, reannealing at 1450°F-1h followed by air cooling developed very large equiaxed α cells. This structure exhibited the lowest yield strength (108 ksi) and highest toughness (K_Q = 118 ksi-in.$^{1/2}$) of any conditions investigated in both the first and second year's studies. Crack growth rates below 10^{-5} in./cycle were relatively unaffected by stress intensity range, ΔK, from 10 to 25 ksi-in.$^{1/2}$. Fractographic examination of the fatigue surface revealed cleavage and striation formation across some of the equiaxed α cells. These cells were separated by rough surfaces containing faint fatigue striations. The starting microstructure (as-received condition) appeared to be either severely worked Widmanstätten, very slowly cooled from above the β-transus, or some form of coarse, recrystallization annealed structure.

In Ti-6Al-4V forged billet, duplex annealing of the initially equiaxed α structure produced a mixture of equiaxed α and patches of coarse Widmanstätten $\alpha + \beta$. When air cooled from 1450°F, this condition exhibited the best combination of toughness, stress-corrosion cracking resistance, and yield strength of all the conditions in the present study (K_{Ic} = 77 ksi-in.$^{1/2}$, K_{Iscc} = 58 ksi-in.$^{1/2}$, and F_{ty} = 122 ksi). The same thermal treatment of the α-segregated, worked Widmanstätten billet resulted in similar toughness and yield strength; K_{Iscc} was not measured (first year's study). Furnace cooling from 1450°F resulted in a negligible change in microstructural appearance, and only minor changes in toughness (-9 percent) and yield strength (+ 8 percent). However, the furnace cooled condition was severely degraded in stress corrosion cracking threshold, K_{Iscc} = 24 ksi-in.$^{1/2}$, a 61-percent loss compared to the duplex annealed and air cooled forged billet, initially equiaxed α.

The equiaxed α forged billet exhibited poor properties when solution-treated and aged. Toughness was 43 and 56 ksi-in.$^{1/2}$ (two separate test results), yield strength was 112 ksi, and K_{Iscc} was 40 ksi-in.$^{1/2}$. The unusually low strength is attributed to lean β existing at the high solution-treating temperature, 1775°F, resulting in an unusually complete $\beta \rightarrow \alpha$ transformation on quenching. Since α' ages much more slowly than retained β, the condition was underaged.

Toughness, fatigue crack growth rate, stress-corrosion cracking resistance, and strength in 1-in. Ti-6Al-4V duplex annealed (air cooled) plate were found to be insensitive to hydrogen contents from 34 to 150 ppm. The microstructure for these conditions was equiaxed α + Widmanstätten $\alpha + \beta$.

Toughness of the as-received, equiaxed Ti-662 1-in. annealed plate was poor – 47 ksi-in.$^{1/2}$, whereas yield strength was good – 147 ksi. Reannealing this plate in a variety of ways to produce equiaxed α + Widmanstätten structures resulted in significantly increasing toughness with either no or a minor (5-percent) loss in yield strength. However, the best result (K_{Ic} = 71 ksi-in.$^{1/2}$ and F_{ty} = 140 ksi) can also be realized in Ti-6Al-4V plate processed to produce a similar microstructure. STA treatment of the Ti-662 plate resulted in a toughness and strength combination that offers no advantage over solution-treated and aged Ti-6Al-4V 1-in. plate. The increased vanadium content of Ti-662 compared with Ti-6Al-4V produces a more supersaturated α'. K_{Iscc} was not measured in Ti-662.

Fatigue crack-growth behavior was found to vary widely with condition and alloy. In general, furnace cooling from within the α-β phase field increased fatigue crack growth rates below $\Delta K = 20$. Below $\Delta K = 20$, Ti-662 exhibited significantly higher rates than Ti-6Al-4V air cooled from the final annealing temperature, and about the same (high rates) as Ti-6Al-4V, furnace cooled in the final anneal.

The major conclusion of the second year's study is that furnace cooling from 1450°F in annealing Ti-6Al-4V plate or forged billet significantly degrades subcritical crack

growth resistance (fatigue crack growth rate is high below $\Delta K = 20$ and K_{Iscc} is low). Water quenching, air cooling, and furnace cooling from 1450°F annealing temperature did not result in any significant differences in light optical microstructural appearance, even at 3000 ×. Thus, optical examination of microstructures annealed at 1450° F gives no clue to the cooling rate.

1.5 ACTIVITIES FOR CURRENT STUDY

Major questions regarding cooling rate effects on annealing Ti-6Al-4V were formulated in the first and second year's studies. Slow cooling rates are believed to have detrimental effects on the resistance to stress-corrosion behavior in other titanium alloys.[14-17] Although the deleterious effect of furnace cooling from 1450°F is consistent with a model involving precipitation of Ti_3Al, no direct evidence of such precipitation was found. In Ti-6Al-4V, only diffuse superlattice reflections have been observed, more characteristic of short-range order in primary α grains than large-scale precipitation of coherent Ti_3Al partioles.[18]

Because Ti-6Al-4V continues to be the most widely used titanium alloy for aerospace structural applications, and annealing treatments are most commonly used, the current study focuses on cooling rate effects in Ti-6Al-4V. Two different grades of plate (standard and ELI) and three different mill-processing conditions (mill anneal, vacuum creep-flatten, and recrystallization anneal) were used as starting materials. Of particular interest is the vacuum creep-flattened (VCF) plate, in which, by nature of the massiveness of the apparatus, very slow cooling rates from annealing temperature occur. Because cooling rate comparison between laboratory and mill-rocessing plates is desired, documentation is included of cooling rates incurred in the various mill-processing treatments. These cooling curves can then be compared directly with laboratory treatment cooling curves obtained in the second year's study.[2]

Laboratory processing treatments include duplex annealing with and without a prior beta anneal. Air cooling and furnace cooling from the final (1450°F) annealing

temperature are used, in order to encompass actual cooling rates expected in annealing of complex, large structural components.

Mechanical properties to be measured and microstructural examination methods include the same ones used in the previous two studies. A further examination was performed of possible differences in substructure as affected by cooling rate. Transmission electron microscope examination of selected conditions experiencing different cooling rates from 1450°F was undertaken to examine effects of cooling rate on the interface phase and look further for evidence of precipitation of Ti_3Al or ordering in α cells, particularly in furnace cooled conditions exhibiting low resistance to stress-corrosion cracking.

A comparison of predicted fatigue life of different microstructural conditions is included using actual fatigue crack growth rate curves and an LMSC-developed computerized integration technique. Fatigue life comparisons obtained this way illustrate meaningful differences in fracture properties between different microstructural conditions. The maximum stress and stress amplitude used for fatigue life predictions are reasonable values pertaining to high-performance military aircraft.

2.0 MATERIALS AND METHODS

2.1 MATERIALS, PROCESSING, AND HEAT TREATMENT

The form, source, and chemistry of the Ti-6Al-4V plate are summarized in Table I. The processing schedule to produce the different mill heat-treated plates is given in Fig. 1. This processing schedule is identical for both standard and ELI grade com-compositions. Heat-treatment schedules for the various conditions are presented in Table II.

Cooling curves from the RMI production facility for mill air cooling and mill vacuum creep-flattening are included in Fig. 2 along with similar curves for laboratory annealing involving air cooling and furnace cooling. The mill air cooling curves are from thermocouples affixed to the center of 1- × 20- × 24-in. plates processed through the RMI electric roller-hearth furnace used for heat-treating large plates. The VCF cooling curve is from thermocouples embedded between 1- × 20- × 24-in. plates in the RMI furnace used for vacuum creep-flattening large plates. In both cases, heat-treating of the relatively small plates was designated to be comparable to that employing normal production processing of large plates for aircraft structures. Methods used for obtaining the laboratory cooling rate data were previously reported.[2] A comparison of cooling rates at 1000°F for both laboratory and mill heat-treatments is presented in Table III.

Conditions 50, 51, and 53 provide characterization of the as-received standard grade, mill-annealed plate and the effect of subsequent duplex annealing, including air cooling and furnace cooling from the final annealing temperature, 1450°F.

Conditions 54, 55, and 57 provide characterization of the as-received ELI grade, mill-annealed plate and the effect of the same subsequent duplex annealing as above. Condition 60 permits evaluation of reannealing just above the β-transus to develop an all-Widmanstatten $\alpha + \beta$ structure, then followed by the same duplex annealing

treatments. A β-transus of 1820 ± 2°F was determined by heating a series of specimens to various temperatures between 1800 and 1830° F in air for 1/2 hour, water quenching, and examining metallographically.

Conditions 63, 64, and 65 provide characterization of the as-received standard grade, vacuum creep-flattened (VCF) plate, and the effect of subsequent duplex annealing. Conditions 67 and 69 were selected to evaluate standard grade, VCF plate, beta-annealed, then duplex annealed with air cooling and furnace cooling from 1450°F.

Conditions 70, 71, and 73 provide characterization of the as-received ELI grade, VCF plate, and the effect of duplex annealing with air cooling and furnace cooling from 1450°F.

Conditions 75 and 76 provide characterization of as-received, recrystallization annealed ELI and standard grade plates.

The mill heat-treatment schedules for MA, VCF, and RA are included in the Processing Schedule, Fig. 1.

Check analyses of composition of each of the six plates were performed and included in Table I. Check analyses agreed closely in all cases with the mill analyses with the exception of hydrogen. As both analyses are reportedly standardized frequently for hydrogen against NBS-supplied specimens, there is no rational explanation for the observed differences in hydrogen. It is quite unusual for mill products to have hydrogen contents less than 35 to 40 ppm and so a basis exists for probably disregarding the check analyses for hydrogen.

2.2 MECHANICAL PROPERTIES TESTS

2.2.1 Tensile Properties

The tensile properties – ultimate strength, 0.2 percent offset yield strength, percent elongation at fracture, and percent reduction in area – were determined in accordance

with the requirements of the applicable ASTM standards. The tensile test specimen configuration is shown in Fig. 3. Specimen orientation was long transverse in both the standard grade and ELI grade plates. One test was conducted for each of the 17 microstructural conditions. Loads were applied with a Tinius Olsen multirange 120,000-lb capacity hydraulic testing machine. The accuracy of this machine meets or exceeds the accepted ASTM standard of 1 percent of indicated load. The specimens were loaded at a strain rate of 0.005 in./in./min to yield, then increased to approximately 0.020 in./in./min to fracture. Strains were measured with an ASTM class B-1, LVDT extensometer. Individual load-elongation curves were autographically recorded for each specimen tested. These records were used to obtain the load at 0.2-percent offset strain and ultimate load for calculation of yield and ultimate strengths, respectively.

The percent elongation was computed from gage marks preplaced on the specimen. The percent reduction in area was computed from measurements of the cross-sectional diameter at the necked-down region compared with the original diameter at the same locus.

2.2.2 Fatigue Crack Growth and Fracture Toughness

For each heat-treatment condition, two specimens of the same configuration were employed for evaluating fatigue crack growth rate behavior (da/dN vs. ΔK). One of these specimens was also used to obtain a value of the fracture toughness index, K_{Ic} or K_Q. A third specimen of this same configuration but with the addition of a threaded hole was used for obtaining K_{Iscc}, the threshold stress-corrosion cracking index. The specimen configuration selected was the compact tension (CT) type shown in Fig. 4. This specimen type has the advantage of requiring the smallest volume of material to obtain plane-strain conditions and also is covered by an appropriate ASTM specification.[19] Orientation of each specimen was TL, i.e., the crack plane normal to the long transverse direction in the plate or transverse in the billet, and crack growth direction parallel to the longitudinal or rolling direction.

In each specimen, the starter notch was sharpened to fatigue crack acuity by low stress tension-tension sinusoidal loading. The maximum load in precracking was closely controlled, so that the plastic zone produced at the crack tip did not interfere with subsequent da/dN determinations. The precrack length was nominally 0.75 in. ($a/W = 0.3$).

The pair of da/dN specimens for each heat-treatment condition was tested in the following way. The first specimen was loaded sinusoidally in tension-tension at a frequency of 10 to 20 Hz, and a minimum-to-maximum load ratio of 0.1 (i.e., $R = 0.1$). The cyclic load was adjusted to provide crack growth rate data in the range of 10^{-5} to $> 10^{-4}$ in. per cycle. The load range was maintained at a constant value as the crack extended to obtain incremental ranges of crack-growth data. The crack length was periodically monitored by a traveling telescope capable of resolving 0.0001-in. change. The cycle count was obtained from a digital ramp function generator, calibrated for the sinusoidal load frequency applied to the specimen by a closed-loop, electrohydraulic fatigue unit. A graph of crack length (ordinate) versus cycles (abscissa) was constructed. Data were obtained in this manner to the maximum extent of useful subcritical crack length of the specimen, approximately 1.78 in.

The second specimen was used to obtain fatigue crack growth rate data in the same manner as the first specimen, but with two differences. One difference was that the cyclic load was periodically adjusted downwards to provide crack growth rate data in the range of 10^{-5} to $\sim 10^{-7}$ in. per cycle. Initial growth data after each load change was disregarded until a crack length change at least 20 × the calculated plastic zone size occurred. This way, crack growth retardation effects were eliminated from the data analyzed. The other difference was that the fatigue crack length was extended to between 1.15 to 1.40 in. ($0.45 \leq a/W \leq 0.55$). Thus, the second specimen provided complementary data to the first specimen, and the final fatigue crack length was in the appropriate range for subsequent testing to obtain a fracture toughness value, K_{Ic} or K_Q.

After fatigue testing, the second specimen was removed from the axial fatigue unit, and a crack opening displacement (COD) gage was affixed. This specimen was then loaded to failure to obtain a valid plane-strain fracture toughness index, according to ASTM Standard E399-74. During this test, load (ordinate) versus COD (abscissa) was autographically recorded. The conditional stress intensity factor (K_Q) was then calculated from the equation:

$$K_Q = C\, P_Q / Ba^{1/2}$$

where C is a function of the dimensionless ratio of the crack length to specimen length, P_Q is the conditional value of the critical load as defined in the ASTM specification, B is the specimen thickness and is the average crack length from the load line. The function, C, is expressed in polynomial form[20] as:

$$C = 30.96\,(a/W) - 195.8\,(a/W)^2 + 730.6\,(a/W)^3 - 1186.3\,(a/W)^4 + 754.6\,(a/W^5$$

where W is the specimen length measured from the load line.

When the K_Q value was obtained, it was then determined whether K_Q equals a valid K_{Ic}. Two major tests and a number of minor tests are applied to make this determination. The major tests are $1.00 \leq P_{max}/P_Q \leq 1.10$ and B, a, W-a, and $H \geq 2.5(K_Q/F_{ty})^2$, where P_{max} is the maximum load obtained in the test, and H is the height of the specimen from the crack plane. The minor tests involve rate of loading, crack shape, and a number of other factors detailed in the ASTM specification.

2.2.3 Stress-Corrosion Crack Growth Threshold

The specimen for measuring the threshold stress-corrosion cracking index, K_{Iscc}, was precracked by fatigue loading sinusoidally at R = 0.1 and to extend the precrack to a length approximately 0.77 in. from the load line. The specimen was then loaded in a tensile test machine with a special inverted load frame holding the specimen. An

ultrasonic crack follower was attached to the specimen during loading so that increments of crack growth as small as 0.005 in. would be detected. A 3-1/2-percent aqueous salt solution (NaCl) was injected in the specimen notch and fatigue precrack. The specimen was loaded slowly until a crack growth rate of between 0.01 to 0.1 in. per hour was achieved. At this load, the inverted load frame was secured to wedge open the specimen and the test machine load removed from the specimen. The load frame contains a strain-gaged element that is calibrated to read pounds applied to the specimen. The specimen with load frame attached was then positioned in a small container of salt water so that the crack tip and uncracked portion of the specimen were constantly immersed. A reading of load and surface crack length was made each day for the first week or longer, then each three to five days thereafter. After 8,000 to 10,000 min of total exposure time, the specimen was removed from the bath and a terminal value of load (P_Q) and surface crack length, a_f, were used to calculate (an estimated value of) K_Q using the above equation. This value of K_Q is used as an estimate of K_{Iscc}. Verification of K_{Iscc} is required by fatigue cracking the exposed specimen at a maximum stress intensity of 0.3 to 0.5 of the estimated K_{Iscc}. This marks the furthest extent of environmental crack grwoth. When the specimen was broken open, a final determination of effective crack length at arrest of environmental growth in the salt water solution could be calculated from measurements of crack shape on the fracture surface. The final load on the specimen, while in the salt solution, and the effective crack length are then used to calculate a final, verified value of K_{Iscc}.

In the event that the final crack length exceeded an a/W value of 0.7, the results were disregarded and no value of K_{Iscc} is reported.

2.3 METALLOGRAPHY AND FRACTOGRAPHY

2.3.1 Metallography

Metallographic samples were prepared for light microscopy by electrolytic polishing. The electrolytic polishing conditions for a 0.3-in.^{2} surface area employed 30 V and 1.5 A at 23°C for 2 min in an electrolyte comprised of 175-ml methyl alcohol and

2.5-ml H_2SO_4. The samples were etched by immersion for 30 sec in a room-temperature solution of 5-cc fluoboric acid (HBF_4), 5-cc nitric acid (HNO_3), and 90-ml distilled water.

Thin-foil electron transmission studies were done with a Siemens Elmiskop 1A-125kV electron microscope at 100 or 125 kV using a universal specimen stage with a double-tilt specimen cartridge. Slices 0.040- to 0.060-in. thick were cut normal both to the rolling plane and the rolling direction using a carbide cutoff wheel. These were then ground to 0.015 in. on a DISCOPLAN surface grinder. The slices were chemically thinned in a solution of 65-percent HN_3 > 18-percent HF, and 17-percent H_2O at 50°F to approximately 0.005-in. thickness. Disks 2.3 mm in diameter were than punched from the slices with an E. F. Fullam Model 1178 specimen grid punch, and the disks were electrolytically thinned in a Fishione twin-jet polisher until a small hole was formed in the center.

The solution used to electropolish the foils was 30-ml perchloric acid (60-vol percent), 300-ml methyl alcohol, and 175-ml n-butyl alcohol, recommended by Blackburn and Williams.[21] It was found to reliably produce satisfactory foils when a bath temperature of < -13°F and an applied voltage of 15V were maintained.

3.0 RESULTS AND DISCUSSION

3.1 RELATIONSHIP OF FRACTURE TOUGHNESS AND STRESS-CORROSION CRACKING RESISTANCE TO TENSILE PROPERTIES

Fracture toughness, stress-corrosion cracking index, and tensile properties are presented in Table 4. The conditions studied vary widely in both fracture toughness, K_{Ic}, and stress-corrosion cracking index, K_{Iscc}, with tensile yield strength, F_{ty}. Figures 5 and 6 are summaries comparing these properties for Ti-6Al-4V conditions investigated in the current year.

For structural applications where fatigue loading and sustained stress in a salt water environment are both unimportant, then the designer wants the highest combination of toughness and yield strength. Where fatigue loading and sea water environment is present, such as for naval aircraft and other aircraft operating near or over the oceans, then the highest combination of fatigue life, K_{Iscc}, K_{Ic}, and strength is preferred.

As shown in Fig. 5, seven conditions exhibit a toughness in excess of 75 ksi-in.$^{1/2}$, and at the same time have yield strengths ranging from 125 to 138 ksi. For toughness-critical structures, all of these conditions would be desired by the aircraft designer. The top seven conditions include both standard and ELI grade material, representing mill-annealed (MA), vacuum creep furnace-flattened (VCFF), and recrystallization-annealed mill-processing. Only two of these seven are as-received plate: Conditions 75 and 76, both recrystallization-annealed, which have a characteristic equiaxed $\alpha + B$ microstructure resulting from the RA treatment. Of the seven highest toughness conditions, only two of these also exhibit a high K_{Iscc}, as shown in Fig. 6. These are Conditions 60 and 67, both of which have been processed to develop a coarse Widmanstätten structure, essentially free of any equiaxed α.

Condition 50, mill-annealed, standard grade plate, exhibits the lowest toughness (45 ksi-in.$^{1\ 2}$) of the 17 conditions characterized, but it has a high-yield yield strength, 147 ksi. With regard to salt water stress-corrosion cracking, Condition 50 is

reasonably resistant, $K_{Iscc} \cong 45$ ksi-in.$^{1/2}$, and nine conditions have an inferior stress-corrosion cracking resistance. Of these inferior conditions, many have acicular $\alpha + \beta$ rather than all equiaxed α structures.

From a standpoint of combined high toughness, high stress-corrosion cracking resistance and acceptable strength, Condition 60 is without peer. This combination of properties is not equalled by any of the 14 Ti-6Al-4V conditions characterized in the previous study.[2] The best combination of mechanical properties in the second year's study was exhibited by Condition 37 (K_{Ic} = 77 ksi-in.$^{1/2}$, K_{Iscc} = 58 ksi-in.$^{1/2}$, and F_{ty} = 122 ksi). This is a duplex-annealed and air-cooled forged billet, initially having an equiaxed α structure, but after the DA treatment, it is predominantly Widmanstätten $\alpha + \beta$ with some moderately small equiaxed α cells remaining.

Of all the conditions studied in the current year, there is a general relation between strength and toughness. Below a yield strength of 135 ksi, toughness varies from 68 to over 90 ksi-in.$^{1/2}$. At yield strengths above 135 ksi, the maximum toughness declines rapidly with increased strength. With the exception of aged and unaged martenistic structures (α') evaluated in the first year's study,[1] this trend appears to be representative for the upper bound of annealed Ti-6Al-4V conditions, regardless of grade, mill process, or reheat-treatment condition. Many conditions, however, fall short or far short of this upper bound of strength and toughness. It is important to identify those factors which reduce toughness and strength from the optimum "trend" line.

As illustrated in Fig. 5, ELI grade conditions come closer to defining the "upper bound" of combined strength and toughness. This has been recognized generally for some time. A limitation of practical consequence from routinely specifying ELI grade products for combined strength and toughness is, of course, the premium price compared to the standard grade composition.

Based on K_{Iscc} and F_{ty} comparisons, Fig. 6, the optimum combination of these properties is not particularly dependent upon grade, but upon processing history. The lowest combination is exhibited by VCFF product, furnace-cooled MA product, and RA product. All of these three products involve a slow cooling rate history, either in mill processing, or in reheat-treatments.

The highest stress-corrosion cracking resistance observed in studies to date is exhibited by an ELI grade, Condition 60. Unfortunately, K_{Iscc} for the standard grade condition processed in an identical way was not obtained; consequently, a direct comparison of effect of grade on optimum stress-corrosion cracking resistance is not possible.

As observed in the previous studies, percent elongation is relatively insensitive to grade and process history. Reduction in area is also insensitive to grade and process history, except for Condition 60 which exhibits a 19-percent reduction in area, between 40 and 55 percent lower than all the other conditions. This low reduction in area has been observed before[1,2] and may be considered a shortcoming by some designers. It should be noted that there is no particular correlation between reduction in area and fracture toughness, K_{Ic}. Low reduction in area may affect toughness as measured in the Charpy impact test or mildly notched bar tensile test, but these properties were not measured.

In summary, for the conditions studied there is no general correlation between K_{Ic} or K_{Iscc} with tensile properties. There is, however, a relationship between optimum K_{Ic} and K_{Iscc} with tensile yield strength, with both properties declining with increased strength. ELI grade is more likely to exhibit the optimum toughness for yield strengths below ~ 143 ksi. Process history, rather than grade, has the dominant effect on K_{Iscc}, with air-cooling in the final heat-treatment promoting optimum combination of stress-corrosion cracking resistance and strength.

3.2 RELATIONSHIP OF MICROSTRUCTURES TO MECHANICAL PROPERTIES

Microstructures and fracture surface (fractographic) features of the various conditions investigated are shown in Figs. 7 through 40. The mechanical properties of interest for relating to structure are fracture toughness, K_{Ic}, and yield strength, F_{ty}. Because of its practical interest for naval aircraft, the threshold stress intensity factor for salt water cracking, K_{Iscc}, is also compared. Fatigue crack growth rate is also important, and is compared in a subsequent section.

The optimum material for naval aircraft applications is one which exhibits the highest combination of strength, toughness, stress-corrosion cracking resistance and fatigue life.

3.2.1 Mill-Annealed Plate

Microstructures and fractographic features of conditions starting with mill-annealed plate are shown in Figs. 7 through 20. Standard grade conditions are discussed first, followed by ELI grade conditions.

3.2.1.1 Condition 50 – Standard grade, mill-annealed plate, as received

The microstructure is equiaxed $\alpha + \beta$, typical of MA plate finished relatively low in the $\alpha + \beta$ phase field. As reported by the supplier, final plate temperature upon rolling was ~ 1500°F. The toughness of this microstructure is the lowest measured in the current study, K_{Ic} = 45 ksi-in.$^{1/2}$. This is attributed to the propensity for equiaxed α cells to fail by the low-fracture energy mode, cleavage, rather than a high-energy mode, transgranular ductile rupture. Inspection of the microfractographic modes in fast fracture, Fig. 8(c), shows planar cracking separated by transgranular ductile rupture. The planar cracking is not clearly transgranular cleavage, but may be a mixture of cleavage and grain boundary separation. The transgranular ductile rupture surfaces are "gnarled" and are characterized by rather flat, poorly defined dimples. Such dimples indicate a low-energy absorption fracture process, compared to deep, spheroidal cavities formed in fracture of high toughness materials.

Stress-corrosion cracking resistance of this condition is not particularly high, but it is essentially the same value as K_{Ic}. The fracture mode is a combination of large areas of cleavage, Fig. 8(e), separated by poorly defined, rather flat dimpled areas, Fig. 8(e) and (f). Secondary cracking in the cleavage areas is not present, thus indicating a minimum influence of crack branching, and its attendant increase in crack propagation resistance.[4]

3.2.1.2 Condition 51 – Standard grade, mill-annealed plate, duplex-annealed, and air-cooled

Condition 51 results from duplex-annealing and air-cooling Condition 50. The microstructure contains patches of Widmanstatten $\alpha + \beta$, transformed from β cells by the 1775°F treatment. Although yield strength has dropped 7 percent to 137 ksi, toughness has increased 51 percent to 68 ksi-in.$^{1/2}$, when compared with Condition 50 properties. K_{Iscc}, however, is unaltered. The fracture surfaces resulting from elastically unstable (fast) fracture and from stress-corrosion cracking are similar in appearance to Condition 50, except patches of fine, equiaxed dimples [right side of Fig. 10(c)]. These patches may be indicative of the higher toughness of the acicular (Widmanstätten) $\alpha + \beta$ microstructure.[1–3]

3.2.1.3 Condition 53 – Standard grade, mill-annealed plate, duplex-annealed, and furnace-cooled

Condition 53 results from the same mill product (Condition 50), and reheat-treated the same way as Condition 51, but is furnace-cooled from 1450°F. Fracture toughness (K_{Ic} = 53 ksi-in.$^{1/2}$) is 18 percent lower than Condition 51. K_{Iscc} remains unaffected by heat-treatment. A distinct etching effect is evident in many of the equiaxed α cells, Fig. 11. The cause of this is as yet unknown but is postulated to be related to increased sensitivity of the equiaxed α to possible hydrogen pick-up in the electropolishing or etching procedure.[22] As will be shown later, slow furnace-cooling, as performed in this condition, results in the development of short-range order in α-cells. This ordering is believed to be a significant contribution to lowering environmentally assisted crack growth. Apparently, K_{Iscc} is unaffected by slow furnace-cooling in this case as the starting material (mill-annealed plate) is almost entirely equiaxed α. Equiaxed α is known to be less resistant to environmentally assisted cracking than acicular α structure (Widmanstatten $\alpha + \beta$ or martensitic α').[4]

3.2.1.4 Condition 54 – ELI grade, mill-annealed plate, as-received

Condition 54, ELI grade, mill-annealed plate, exhibits almost the same yield strength (144 ksi), but a significantly higher fracture toughness (K_{Ic} = 60 ksi-in.$^{1/2}$) than the standard grade, mill-annealed plate, Condition 50. Although the microstructural appearance is the same (compare Figs. 13 and 7), the fractographic features in elastically unstable fracture show smaller-diameter and more clearly defined deeper dimples in the higher toughness ELI grade material, compare Figs. 14(c) and 8(c). The difference in toughness is attributed to the lower oxygen content of the ELI grade: 0.128 w/o versus 0.175 w/o for the standard grade. Oxygen content is known to affect the toughness in mill-annealed Ti-6Al-4V. Some authors postulate that increased oxygen in standard grade compared to ELI grade reduces toughness by promoting planar slip.[4] Ordering of oxygen has been postulated to occur in equiaxed α Ti-6Al-4V after certain thermal treatments.[23] If this is the case, the higher oxygen content of the standard grade would be more susceptible to ordering, and associated effects on fracture toughness. Ordering in mill-annealed Ti-6Al-4V could possibly occur upon slow cooling from an annealing temperature of 1450°F. Lim et al. have shown that for a Ti-8 weight percent

Al alloy aged high in the α-β phase field, an increase in oxygen content from 600 ppm to 1200 ppm decreases the fracture strain from 20- to 1-percent elongation and slightly increases the yield strength.[24] This effect was attributed to an observed increase in Ti_3Al precipitation with increased oxygen. Thus, for mill-annealed plate, ELI grade is preferred over the standard grade, because it exhibits higher toughness without being significantly lower in strength or ductility.

3.2.1.5 Condition 55 – ELI grade, mill-annealed plate, duplex-annealed, and air-cooled

Condition 55 involves duplex-annealing and air-cooling the ELI, mill-annealed plate. Compared to the latter (Condition 54), a significant increase (23 percent) in toughness results and with only a minor decrease (6 percent) in strength. As for Condition 51, the duplex-anneal causes a significant amount of Widmanstätten $\alpha + \beta$ to form, with a minority fraction remaining equiaxed α cells. The fracture surface exhibits an extensive amount of small, well-formed, ductile rupture dimples, consistent with the observed high toughness.

K_{Iscc} was not measured for this condition (nor for Conditions 54 and 57), as too long a crack grew in the specimen before arrest occurred, obviating data analysis. Comparison of stress-corrosion crack fracture surfaces, however, suggests that the duplex-annealed and air-cooled treatment raised K_{Iscc}. Compare Figs. 16(e) and 14(e). Transgranular cleavage predominates in both cases, but the cleavage crack planes are more irregularly oriented to one another in the former, suggesting somewhat higher resistance to crack growth.

3.2.1.6 Condition 57 – ELI grade, mill-annealed plate, duplex-annealed, and furnace-cooled

This treatment is represented by Condition 57. Compared with duplex-annealing and air-cooling, Condition 55, furnace-cooling has a negligible effect on yield strength (F_{ty} = 139 ksi, a 2-percent increase) and fracture toughness (K_{Ic} = 72 ksi-in.$^{1/2}$, a 3-percent decrease). Unfortunately, K_{Iscc} was not measured for this condition.

The ELI grade conditions contain more Widmanstätten $\alpha + \beta$ than the standard grade conditions heated to 1775°F, as lower oxygen content of the former lowers the $\alpha \rightarrow \beta$ transformation. The higher volume fraction of Widmanstätten $\alpha + \beta$ usually results in a higher toughness.[3] Ordering in α may also contribute to the difference in toughness. Whether ordering of oxygen[23] or ordering of aluminum is postulated,[24] the lower oxygen content of the ELI grade would affect either reaction. The lower oxygen content in the ELI grade means increased solubility of aluminum in α-titanium,[25, 26] thereby reducing the propensity for ordering of Al to occur in slow cooling.

Fractographic features in both Conditions 55 and 57 reveal an interesting relationship to microstructure. In the elastically unstable, fast-fracture mode, both conditions exhibit almost entirely transgranular ductile rupture, see Figs. 16(c) and (d) and 18(c) and (d). The ductile rupture is of two types – nucleation and growth of relatively small spheroidal or ellipsoidal cavities and nucleation and growth of relatively large "stretch" zones. One such stretch zone is visible in Fig. 18(d), just to the right of center. It is postulated that such zones nucleate and grow preferentially in the Widmanstätten $\alpha + \beta$ patches. The occasional transgranular cleavage regions visible in Fig. 18(c) are postulated to occur solely or preferentially in equiaxed α cells, oriented so that the basal plane normal is ± 15 degrees from the tensile axis, consistent with previous observations.[13] The predominance of transgranular ductile rupture mechanisms in the elastically unstable fracture surfaces is consistent with the relatively high toughness measured.

3.2.1.7 Condition 60 – ELI grade, mill-annealed plate, beta-annealed, duplex-annealed, and air-cooled

The equiaxed α structure of mill-annealed Condition 54 is transformed entirely to a coarse Widmanstätten $\alpha + \beta$ structure by the beta-anneal, duplex-anneal and air-cooling treatment of Condition 60. The prior β grain size was not measured but is > 200 μm. This condition exhibits an exceptionally high fracture toughness (K_Q = 91, and 99 ksi-in.$^{1/2}$, two separate results) and stress-corrosion cracking resistance (K_{Iscc} = 72 ksi-in.$^{1/2}$), while strength is lower than other conditions (F_{ty} = 123 ksi). Compared to the as-received, ELI grade, mill-annealed product,

Condition 54, these properties represent a 52- to 65-percent increase in fracture toughness, by far the highest K_{Iscc} of any condition in the current study (Fig. 6), and a 15-percent loss in yield strength. As will be shown, the fatigue crack growth behavior of this condition is a significant improvement over all the other mill-annealed, ELI conditions.

The coarse Widmanstätten structure fractures microscopically by nucleation and transgranular growth of both small cavities and large stretch zones in elastically unstable fracture; see Figs. 20(c) and (d). There is a complete absence of low-fracture energy modes – grain boundary separation or transgranular cleavage. In the case of stress-corrosion cracking, the microfractographic mode is unique, see Figs. 20(e) and (f). Large stretch zones have formed, with their axes parallel and in the microscopic crack propagation direction, towards 11 o'clock in Fig. 20. Note that the stretch zone axes in stress-corrosion cracking are parallel to the stretch zone axes in the elastically unstable fracture surface. Stress-corrosion crack growth is probably controlled by the rate of cross-slip in a large plastic zone.

Except for the lower reduction in area – 19 versus 32 to 42 percent – than in the other conditions, the coarse Widmanstätten $\alpha + \beta$ structure exhibits outstanding properties for application to high toughness, environmental cracking resistant aircraft structures.

3.2.2 Vacuum Creep Furnace Flattened (VCFF) Plate

Microstructures and fractographic features of conditions starting with VCFF plate are shown in Figs. 21 through 36. Both standard and ELI grades are discussed together, because of their close similarity in microstructural appearance.

3.2.2.1 Condition 63 – As-received, VCFF plate

Conditions 63 and 70 are the standard grade and ELI grade, as-received plates, respectively. The microstructure in both cases is equiaxed α; see Figs. 21 and 31. The higher oxygen grade, Condition 63 shows a distinctive etching effect, Fig. 21. The VCFF product has experienced a cooling rate at the mill that is similar to slow furnace-cooling in

the laboratory, see Fig. 2 and Table 3. This etching effect is most likely caused by hydrogen absorbed preferentially into the α-titanium[22,27,28]. As will be discussed later, the etching effect is believed to be an indirect evidence of development of short-range order in the α-phase, and in the present case, the slow cooling rate is the cause of such ordering. The enhanced etching effect in the standard grade, Condition 63, when compared to the very slight etching effect in the ELI grade, Condition 70, is attributed to the higher oxygen content in the former. Higher oxygen reduces solubility of Al in Ti,[25] resulting in an increased propensity for ordering to occur on furnace cooling in Condition 63 than in Condition 70. If short range order is more fully developed in Condition 63, then the stress-corrosion cracking index, K_{Iscc}, would be lower also. This is observed: in Condition 63, K_{Iscc} = 40 ksi-in.$^{1/2}$ and in Condition 70, K_{Iscc} = 50 ksi-in.$^{1/2}$. From a design standpoint, if heavy sections of Ti-6Al-4V are to be annealed, then the most rapid quench possible should be used, commensurate with control of distortion due to thermal strains. Also, ELI grade would be less susceptible to development of short-range order than would standard grade, thus assuring a higher resistance to subcritical crack growth, such as salt water sustained load cracking or fatigue crack growth in air or salt water.

3.2.2.2 Conditions 64, 66, 71, and 73 – VCFF plate, reheat-treated by duplex-annealing and air- or furnace-cooling

These treatments are represented by Conditions 64 and 66 for standard grade, and 71 and 73 for ELI grade. Conditions 64 and 71 are air-cooled, 66 and 73 are furnace-cooled, all from 1450°F. In all four cases, duplex-annealing increases the fracture toughness over the as-received conditions. However, duplex-annealing lowers the stress-corrosion cracking index, K_{Iscc}, in all cases. This is believed due to some degree of Al segregation resulting in short-range order in the original VCFF products, and upon reheat-treating, the short-range order reoccurs in the α-phase. Aluminum segregation once obtained is very difficult to eliminate.[28] Thus, the reheat-treating causes some transformation from equiaxed α to Widmanstätten $\alpha + \beta$ to occur, but cleavage at low stress intensities with salt water present still occurs readily through retained equiaxed α cells; see (e) and (f) of Figs. 24, 26, 34, and 36. Etching effects attributed to hydride formation are especially visible in equiaxed α cells in the air-cooled products, Condition 64

(Fig. 23) and Condition 71 (Fig. 33), and are less visible in the furnace-cooled products, for reasons that are not obvious. See Figs. 25 and 35.

Again, the superiority of ELI over standard grade is illustrated, as is the deleterious effect of furnace cooling on the stress-corrosion cracking index, K_{Iscc}. When furnace cooled from 1450°F in the duplex anneal cycle, both standard and ELI grades are degraded to K_{Iscc} of 29 and 28 ksi-in.$^{1/2}$, respectively.

3.2.2.3 Conditions 67 and 69 – VCFF plate, reheat-treated by beta-annealing, duplex-annealing, and air- or furnace-cooling

Only standard grade plate was heat-treated by this cycle. Condition 67 is air cooled, and Condition 69 is furnace cooled from 1450°F. Heating to 1825°F for 1/2 hour has caused almost a complete transformation from the originally all equiaxed α, Fig. 21, to relatively ccarse Widmanstätten $\alpha + \beta$, Figs. 27 and 29. The prior β grain size is still rather small in both cases, as during the β anneal, some equiaxed α was retained, which inhibits coarsening of the β-grain size.

Compared with duplex-annealing, the β-anneal, duplex anneal combination results in a higher fracture toughness, almost the same yield strength, and a higher stress-corrosion cracking index, K_{Iscc}. This is believed due to the superior ability of the acicular α structure to resist environmentally assisted crack growth, and also to plastically deform more readily than equiaxed α. The increase in toughness of the coarse acicular α structure appears to be related to its lower propensity to fracture transgranularly by cleavage, as in equiaxed α cells. This lower propensity for cleavage of acicular α than in equiaxed α may be due to a difference in elastic constraint within each α cell or possibly a difference in bond strength between atoms due to a different composition in the two forms of α phase and a different degree of short-range order developed during annealing and upon cooling. Also, the transformation from equiaxed α to Widmanstätten $\alpha + \beta$ would have some effect of "randomizing" crystallographic texture that may be present in the equiaxed α, VCFF plate.

Because texture was not characterized for the materials studied, the possible role of texture on fracture behavior in the current study can only be conjectured. Because

all the materials used in this study were straight rolled from 4 1/2-in.-thick press-forged slab to 1-in. plate, some degree of transverse basal texture is to be expected. This texture may have an effect on fracture properties in the present study, somewhat parallel to that observed by Harrigan et al.[10] Fracture toughness specimens oriented in the TL direction[19] would have the tensile axis parallel to the direction containing the largest population of basal poles in transversely textured plate. Thus, cleavage of equiaxed α is promoted in this specimen orientation, as cleavage in α-cells occurs preferentially $\sim$ 15 degrees from the basal plane.[13]

3.2.3 Conditions 75 and 76 – Recrystallization-Annealed Plate

Recrystallization annealed plate was characterized as-received from the mill in both standard grade, Condition 76, and ELI grade, Condition 75. Both exhibit the rather uniform equiaxed $\alpha + \beta$ structure typical of recrystallization-annealed plate; see Figs. 37 and 39. As observed in other certain other conditions, the ELI grade exhibits a distinct etching effect, especially in the core of the equiaxed α cells, Fig. 37. This effect is almost completely absent in the standard grade, Fig. 39. Both grades exhibit almost the same mechanical properties, with the standard grade having the higher toughness (K_Q = 85 ksi-in.$^{1/2}$ versus 82 and 83 ksi-in.$^{1/2}$, two separate test results) and lower yield strength (127 ksi versus 132 ksi). These differences may be considered within experimental error, and thus are not significant. No explanation is offered for the difference in etching effect.

Although K_{Iscc} was not successfully measured for Condition 76, standard grade, the ELI grade exhibits only 36 ksi-in.$^{1/2}$. Compared with the other three as-received conditions for which K_{Iscc} was measured, this value is the lowest. A comparison of stress-corrosion fractographic features does not reveal any particular differences in fracture mode for these various equiaxed α products; cleavage is a rather dominant fracture mode in all of them. Compare (e) and (f) of Figs. 9, 22, and 32 with Fig. 40.

One might conclude from these few results that for recrystallization annealed plate, strength and toughness of the standard grade are as good as the ELI grade.

3.3 FATIGUE CRACK GROWTH

3.3.1 General Comments

The characteristic fatigue crack growth rate data for the seventeen conditions studied are plotted in Figs. 41 through 57. Each figure of crack growth rate, da/dN, versus cyclic stress intensity range, Δk, indicates the value of K_{Ic} (1-R), the assumed asymptote for the crack growth curve at a rate of 1 in./cycle.

The fatigue crack growth curves generally follow a sigmoidal shape, with the upper asymptote being K_{Ic} (1-R) and the lower asymptote the value of ΔK at crack growth rates below 10^{-8} in./cycle. Because no data at that low growth rate were obtained, the lower asymptote, or fatigue crack growth threshold, is not plotted on the figures.

Fractographic features of the fatigue crack surface of each condition studied are shown in (a) and (b) of Figs. 8, 10, 12 ... 40. The macroscopic crack growth direction is towards 11 o'clock in each case. The location photographed is at mid-thickness and at a location having a macroscopic crack growth rate of between 10^{-7} and 10^{-6} in./cycle.

3.3.2 Mill-Annealed Plate

The fatigue crack growth rate curves for mill annealed, standard grade and ELI grade conditions are compared in Figs. 58 and 59, respectively. Below 10^{-5} in./cycle, all of the mill-annealed conditions exhibit almost the same fatigue crack growth behavior, except Condition 60, ELI grade, β-annealed, duplex annealed and air cooled. It was shown previously that this condition exhibits a high toughness and stress-corrosion cracking index. I also exhibits significantly lower fatigue crack growth rate than any of the other conditions in the present study. Only one condition in the Second Year's study[2] was significantly better than Condition 60. That was Condition 18, 4- × 4-in. forged billet, α-segregated, worked Widmanstätten, duplex annealed as follows: 1750°F-2h-AC, 1450°F-1h-AC. In the First Year's study,[1] as-quenched martensitic α' exhibited a lower fatigue crack-propagation rate than any others in the entire study.

3.3.3 Vacuum Creep Furnace-Flattened Plate

The fatigue crack growth rate curves for VCFF standard grade and ELI grade conditions are compared in Figs. 60 and 61, respectively. All eight conditions compare closely with one another, and with all conditions in the current study except Condition 60.

3.3.4 Recrystallization-Annealed Plate

The crack growth rate curves for RA standard grade and ELI grade conditions are compared in Fig. 62. Over the entire crack growth range, the growth rates are almost identical. A somewhat lower apparent threshold, ΔK_o, is indicated for the ELI grade. This is consistent with a model involving hydrogen-assisted fatigue crack growth rate approaching threshold; the ELI grade has the lower oxygen content (1680 ppm versus 1290 ppm) and slightly higher hydrogen content, 91 ppm versus 31 ppm. If the recrystallization annealing cycle developed any short-range order, it would more readily occur in the higher oxygen condition, as oxygen reduces the solid solubility of aluminum in α-Ti. Al segregation is also a factor.

3.3.5 Comparison of As-Received Conditions

Fatigue crack growth behavior of the six as-received conditions are compared in Fig. 63. All six conditions are rather close in fatigue behavior, with the three ELI grades – MA, VCF, and RA – exhibiting the highest fatigue crack growth rates below a stress intensity range of ΔK = 10 ksi-in.$^{1/2}$, and the three standard grades the lowest rates. The microstructure in all six conditions is equiaxed α. The relationship of crack growth rate at low ΔK does not correlate with stress-corrosion cracking index, where ELI grades having comparable process histories exhibit a high K_{Iscc}.

3.3.6 Effect of Microstructural Condition on Fatigue Life of Structures

Figure 47 shows the fatigue crack growth behavior of Condition 60 (ELI grade, mill-annealed plate, beta annealed, duplex annealed and air cooled), the lowest growth rate of all conditions in the current study over the entire ΔK range. Using the computer

crack growth model previously developed,[1,7] a fatigue crack growth comparison of this coarse Widmanstätten structure was made with mill-annealed and duplex-annealed conditions previously reported.[7] These are Condition 1 for as-received mill-annealed plate and Conditions 31, 2(R), and 32[2] for mill-annealed plate, duplex-reannealed and water-quenched, air-cooled, and furnace-cooled, respectively. Figures 64 and 65 present the comparison obtained by iterative crack growth procedures and the da/dN versus ΔK data pertinent to each microstructural condition. An initial flaw size of 0.02-in. was assumed and is a reasonable size that would escape detection by NDI in production fabrication of a complex titanium airframe structure.

The coarse Widmanstätten microstructure of Condition 60 is shown to be significantly superior to the equiaxed α of Condition 1 or the equiaxed α + Widmanstätten $\alpha + \beta$ of Conditions 31, 2(R) or 32. Both cycles to failure and critical flaw size are larger for Condition 60. A flaw growing by fatigue during service in this microstructure is more likely to be detected before failure occurs than in the equiaxed α or equiaxed $\alpha + \beta$ Widmanstätten $\alpha + \beta$ microstructures.

Yoder et al. found a coarse Widmanstätten structure resulting from beta annealing Ti-6Al-4V plate to have superior fatigue crack growth behavior over mill-annealed plate.[30] Their beta annealing schedule was 1900°F-1/2h-Cool at 752°F/h to RT, 1400°F-2h-AC. The mill-annealed plate schedule was 1450°F-1h-MAC. Eylon and Pierce[31] found beta annealed (1900°F-1h-AC, 1350°F-4h-AC) plate to exhibit superior high cycle notched fatigue strength at 10^7 cycles over equiaxed α (both mill-annealed and recrystallization-annealed plates), and two variations in equiaxed α + Widmanstätten $\alpha + \beta$ plates. They suggest that the fatigue performance of acicular alpha microstructures is controlled by the size of the nucleating crack. At low stress, the nucleated crack is limited in size to the width of a single alpha needle, while at high stresses, the nucleated crack may be as large as an entire colony of similarly aligned alpha needles. Thus, the Widmanstätten microstructure in Condition 60 is expected to have excellent notched fatigue strength as well as high fracture toughness, and K_{Iscc}, and fatigue crack growth life in aircraft structures.

3.4 EFFECT OF COOLING RATE ON THE INTERFACE PHASE AND SHORT RANGE ORDER

Duplex-annealed and beta-annealed plus duplex-annealed conditions from the previous studies[1,2] were reexamined by transmission electron microscopy in detail. Of particular interest was the effect of cooling from the final annealing temperature, 1450°F. The heat treatments used were identical to those used in the current study except that the beta annealing temperature was 1850°F, rather than 1825°F.

3.4.1 Results of Duplex-Annealing

Optical micrographs of the material tested by Lewis et al.[7] are shown in Fig. 66. In all cases the microstructure consists of a mixture of equiaxed primary α and acicular secondary α plus β. Two features of these micrographs are of interest in the context of subsequent TEM studies. First, the average width of β ribs decreases slightly as the cooling rate decreases. This was not measured quantitatively, but it is consistent with growth of acicular α, which would be expected to occur as cooling rate from higher temperatures is decreased. Second, there is a distinctly different etching response of the α, which becomes more pronounced as the cooling rate decreases. This response appears first as a delineation of α-β interfaces by a region extending about 0.3 μm into the β. Both air-cooled and furnace-cooled samples exhibit this effect. The furnace-cooled samples also show mottling within some acicular α grains.

Transmission electron micrographs of the same three conditions are shown in Fig. 67. Because of the high magnification, it is not possible to show both primary α and acicular $\alpha + \beta$ in the same field-of-view. All three views shown are of acicular α and β ribs (light in Figs. 66a and 66b, dark in Fig. 66c). In all three conditions, there exists a structure in the α - β interfaces which exhibits diffraction contrast different from that of the α and β ribs. The width of this structure in Fig. 66b is approximately the same as that of the outlining observed in Figs. 65b and 65c. There also appears to be less of this feature in the water-quenched sample than in the air-cooled and furnace-cooled material.

Micrographs of the interfaces at a higher magnification are shown in Figs. 68, 67, and 70. These reveal a structure similar in appearance to the "interface phase" previously observed in this alloy.[4,32,33] Although the widths of the β ribs are different in the three micrographs, it should be noted that these are not uniform throughout a given material, as shown in Fig. 66. However, the width of the interface phase relative to the β rib increases with increasing cooling rate. This point is illustrated by a comparison of the dark-field micrographs, Figs. 68, 69, and 70, which were taken with reflections from the interface phase.

Selected area-diffraction patterns of the regions shown in Figs. 68, 69, and 70 exhibit reflections from α, β and a face-centered cubic phase with lattice parameter of 4.4 ± 0.1 Å. This latter finding is in agreement with the analysis of Rhodes and Williams.[33] More than one orientation of the face-centered cubic phase was often present. For example, the diffraction pattern of the region shown in Fig. 68 showed two [112] zones, rotated approximately 90 deg about the [112] axis. It was not always possible to determine the orientation relationships among the three phases because of superimposed reflections. The interplanar spacings for the α, β and face-centered cubic phases are given in Table V.

Evidence of short-range order was occasionally found in primary α grains of the furnace-cooled material. A typical diffraction pattern of a $[11\bar{2}0]_\alpha$ zone illustrating this point is shown in Fig. 71. Extra reflections occur at (h/2, k/2, ℓ) locations, which is consistent with a DO_{19} (Ti_3Al) superlattice. No discrete particles could ever be imaged from these reflections, since they were too diffuse to be observed on the viewing screen of the microscope. The extra reflections only became apparent on careful observation of the photographic plate. No evidence of short-range order was observed in water-quenched or air-cooled material, nor was it present in all primary α grains of the furnace-cooled samples. This finding is consistent with earlier findings of Williams and Blackburn on this alloy.[18]

3.4.2 Results of Beta Treatment Followed by Duplex Annealing

This heat-treatment results in the Widmanstätten structure, consisting of platelets of secondary α separated by β ribs. Optical micrographs of the material tested

by Lewis et al. are shown in Fig. 72. Outlining of the α-β interfaces is still apparent in the higher magnification micrographs, but no evidence of the etching attack within α grains is observed.

The structure of these specimens is shown in low-magnification transmission electron micrographs in Fig. 73. It is evident that slow-cooling promotes delineation of the interface phase as in the case of duplex-annealed material without the prior beta treatment.

Selected area diffraction analysis indicated that short-range order was present in some α grains of the beta-treated and duplex-annealed, furnace-cooled material. This is illustrated in Fig. 74. No dislocation pairs typical of long-range ordered material were ever observed in grains which exhibited superlattice reflections.

3.4.3 Discussion of Results

Slower cooling rates promote delineation of the interface phase in both duplex-annealed and beta-treated and duplex-annealed material. In all cases the interface phase was composed of a high density of thin plates extending from the interface into the alpha phase. No examples of a monolithic layer between the phases were observed. No structure within alpha grains was observed which would explain the etching effect in air-cooled and furnace-cooled material. However, the furnace-cooled material did show evidence of short-range order in some alpha grains.

The interface phase is face-centered cubic with a lattice parameter of 4.4 ± 0.1 Å, in agreement with the findings of Rhodes and Williams.[33] Although it was not possible to make a complete determination of the orientation relationships between α, β, and interface phases, diffraction patterns were similar in some cases to those identified by Rhodes and Williams as arising from alpha and beta having the Burgers orientation plus reflections from a "non-Burgers alpha," while in other cases they were identical to the example given by Blackburn of hydride platelets in the alpha phase of Ti-8Al-1Mo-1V (Ti-811) alloy.[27] Habit planes of the interface phase are also those of hydride in the alpha phase of Ti-811.[34]

The true situation regarding the effect of hydrogen in the stress-corrosion behavior of titanium alloys remains unclear. It has long been recognized that hydrogen content sufficient to cause intergranular precipitation of hydride or precipitation within alpha grains is detrimental to mechanical properties.[35,36] These studies indicate that hydrogen contents in excess of 150 ppm are required to cause observable effects. However, there is evidence that much lower hydrogen contents can affect the susceptibility to stress-corrosion and sustained load cracking resistance.[37,38,39] It is also significant that these hydrogen-associated fractures are accompanied by cracking along alpha-beta interfaces, or by cracks initiated at alpha-beta interfaces.[36,37,38]

Alpha-beta interfaces are known to be preferred sites for hydride nucleation.[27,34,36,40] Hydrogen has also been shown to collect at these interfaces and within the beta grains even when no hydrides are observed.[41] It has also been observed that hydrides can nucleate heterogeneously on slip bands at hydrogen contents much lower than those required for precipitation in the alpha grains.[34,35] Interphase interfaces would be expected to provide similar high-energy sites for heterogeneous nucleation.

Recent evidence suggests that the interface phase does not decompose on heating in vacuum at 200° to 400°C.[33] The amount of hydrogen in typical alloys also does not seem sufficient to account for the amount of interface phase observed.[33] However, the structure and habit plane of the phase is that of hydride. The interface phase is very likely associated with the hydrogen content of the material, whether it forms as a defect hydride or stabilizes a f.c.c. solid-solution phase.

A fractographic examination was performed of the stress-corrosion cracked specimens of both heat-treatment conditions, water-quenched and furnace-cooled. Fracture surfaces of the duplex annealed specimens are shown in Fig. 75. Regardless of cooling rate, the fracture mode is amost entirely cleavage, with a few small patches failing by ductile rupture. Cleavage of almost all of the equiaxed α is probable, and some of the Widmanstätten patches also fracture by cleavage. Separation along $\alpha-\alpha$, $\alpha-$ Widmanstätten $\alpha+\beta$, and $\alpha-\beta$ phase boundaries appears to occur, but only in local instances.

Cooling rate from 1450° F was found to significantly affect fracture mode. In a water-quenched specimen, significant secondary cracking occurs along Widmanstätten α-β rib boundaries [see Fig. 76(a)]. These boundaries are also the locus of the interface phase. Also, some portions of β between the α platelets appear to have failed by microvoid nucleation and growth, a high-energy fracture mode. In comparison furnace-cooling suppresses the propensity for both secondary cracking along Widmanstätten α-β boundaries and ductile rupture within β [see Fig. 76(b)]. These observations contribute to the number of factors possibly involved in cooling rate effects on K_{Iscc}. Secondary cracking along α-β platelet boundaries provides a more tortuous path for crack growth, requiring a higher driving force (macroscopic stress intensity). Secondary cracking along the α-β boundaries may be promoted in the water-quenched product because cooling rate does affect morphology and may affect properties of the interface phase. Additionally, rapid quenching may develop a significantly higher residual stress between the α platelets and β ribs due to differences in tensile properties and coefficients of thermal expansion between the α and β phases. As cooling rate affects development of short-range order in the α phase, secondary cracking between α platelets and β ribs may be suppressed in the furnace-cooled product. Short-range order in the furnace-cooled product may significantly lower the transgranular cleavage crack growth resistance in salt water.

Short-range order in α suppresses tensile ductility and increases elastic modulus. Alpha-beta-annealed specimens exhibit a tensile modulus of elasticity of 16.6, 17.1–17.9, and 19.8 million psi, respectively for water-quenched, air-cooled, and furnace-cooled conditions. For the same conditions, reduction in area is 37, 28, and 24 percent, respectively.[2] For the same applied tensile strain, increased elastic modulus of α would increase tensile stress in β normal to the α-β boundaries, due to the Poisson strain component in α. The interface phase in the furnace-cooled specimen, therefore, may have either a higher tensile strength or stress-corrosion cracking resistance, as secondary cracking between α platelets is suppressed.

Development of short-range order in α due to slow cooling may be the dominant factor affecting stress-corrosion cracking resistance of either microstructural condition, and the role of the interface phase may be secondary.

4.0 SUMMARY AND CONCLUSIONS

A study of $\alpha + \beta$ titanium was continued for the purpose of establishing a correlation between miscrostructure and fracture toughness. In the current year, T-6Al-4V was studied. The Ti-6Al-4V mill products were both standard and ELI grade 1-in. plate in the mill-annealed, vacuum-creep-furnace flattened, and recrystallization-annealed conditions characteristic of material supplied for high performance military aircraft.

Reheat-treatments by duplex- and beta- plus duplex-annealing with air or furnace cooling from the final annealing temperature were included to make a total of 17 microstructural conditions. The types of microstructure included equiaxed α (from mill-annealing and from recrystallization-annealing), mixtures of equiaxed α and Widmanstätten $\alpha + \beta$ (from duplex-annealing), and coarse Widmanstätten (from beta-plus duplex-annealing). Tensile properties, plane strain fracture toughness, stress-corrosion cracking threshold in salt water, and fatigue crack growth behavior in air were determined. Microstructures were characterized by optical metallography and scanning electron microfractography. Six microstructural conditions of Ti-6Al-4V studied previously were characterized by transmission electron microscopy and scanning electron microfractography. These conditions involved duplex-annealing and beta-plus duplex-annealing, water-quenched, air-cooled, and furnace-cooled from the final annealing temperature.

Composition and heat-treatment were found to have a relatively minor effect on tensile properties, with yield strength ranging from a low of 123 to a high of 147 ksi-in.$^{1/2}$. Heat-treatment was found to have a major effect and composition a minor effect on fracture toughness (K_{Ic} or K_Q) and stress-corrosion cracking threshold (K_{Iscc}). Equiaxed α microstructure exhibited both low and high toughness (from 45 ksi-in.$^{1/2}$ for standard grade, mill-annealed, to 85 ksi-in.$^{1/2}$ for standard grade, recrystallization-annealed). Equiaxed α plus Widmanstätten $\alpha + \beta$ microstructure was consistently higher in toughness than equiaxed α (53 to 89 ksi-in.$^{1/2}$ for duplex-annealing of various mill products). A coarse Widmanstätten $\alpha + \beta$ resulting from

beta- plus duplex-annealing produced the highest range of toughness (79 to 99 ksi-in.$^{1/2}$). In all cases, the high toughness is associated with Widmanstätten $\alpha + \beta$ microstructure formed by nucleation and growth transformation from β and low toughness associated with relatively large equiaxed α cells.

Stress-corrosion cracking threshold in microstructures containing Widmanstätten $\alpha + \beta$ were found to be strongly dependent upon cooling rate from final annealing temperature, with K_{Iscc} for slow furnace cooling as low as 27 ksi-in.$^{1/2}$ and for air cooling as high as 71 ksi-in.$^{1/2}$. In microstructures consisting entirely of equiaxed $\alpha + \beta$, cooling rate had a minor influence: K_{Iscc} ranged from 40 to 50 ksi-in.$^{1/2}$. The high thresholds are attributed to the beneficial role of acicular α platelets and secondary crack branching along α - β boundaries in the Widmanstätten $\alpha + \beta$, provided short range order is not present due to slow cooling, and low thresholds to the propensity for equiaxed α cells to environmentally crack by cleavage, regardless of degree of short range order that may have been developed. Short range order in Widmanstätten $\alpha + \beta$ reduces K_{Iscc} by both suppressing crack branching along α - β interfaces and promoting crack growth by cleavage across acicular α platelets.

Composition was found to affect stress-corrosion cracking. For the same microstructure type and cooling rate, ELI grade exhibited a higher K_{Iscc} than standard grade. This difference is attributed to the difference in oxygen concentration affecting solubility of aluminum in the α-phase, which in turn strongly affects propensity for short range order and fracture mode.

Of the seventeen conditions studied, fatigue crack growth rate was similar between 10^{-5} and 10^{-4} in./cycle. Below 10^{-5} in./cycle, conditions involving slow furnace cooling exhibited the highest growth rates. The all Widmanstätten, air cooled ELI grade exhibited the lowest crack growth rate over the entire range from $<10^{-7}$ to 10^{-4} in./cycle, and has the longest computed fatigue life in a simulated aircraft structural application.

As revealed by TEM, slower cooling rates promote the growth of the interface phase between α and β ribs. Slow cooling from 1450°F promotes short range order in

the α-phase in both duplex-annealed and beta- plus duplex-annealed plate. The role of the interface phase in toughness and environmental cracking resistance is unclear. Development of short-range order is believed to have a major effect on environmental cracking resistance by affecting plastic deformation in the α-phase.

REFERENCES

1. F. A. Crossley and R. E. Lewis, "Correlation of Microstructure with Fracture Toughness Properties in Metals," Report No. LMSC-D356114, Lockheed Palo Alto Research Laboratory, Palo Alto, California, to Naval Air Systems Command. Contract N00019-72-C-0545, 30 September 1973

2. R. E. Lewis and F. A Crossley, "Correlation of Microstructure with Fracture Toughness Properties in Metals (Part II)," Report No. LMSC-D454884, Lockheed Palo Alto Research Laboratory, Palo Alto, California, to Naval Air Systems Command, Contract N00019-74-C-0161, 21 January 1975

3. C. A. Stubbington, "Metallurgical Aspects of Fatigue and Fracture in Titanium Alloys," Specialists Meeting on Alloy Design for Fatigue and Fracture Resistance, Brussels, Belgium, 13–19 April 1975, AGARD Conference Proceedings No. 185, p. 3–1

4. N. E. Paton, J. C. Williams, J. C. Chestnut, and A. W. Thompson, "The Effects of Microstructure on the Fatigue and Fracture of Commercial Titanium Alloys," op. cit., p. 4–1

5. I. W. Hall and C. Hammond, "The Relationship Between Crack Propagation Characteristics and Fracture Toughness in $\alpha + \beta$ Titanium Alloys," Titanium Science and Technology (Vol. 2), Plenum Press, New York, 1973, p. 1365

6. M. A. Greenfield and H. Margolin, "The Interrelationship of Fracture Toughness and Microstructure in a Ti-5.25% Al-5.5% V-0.9% Fe-0.5% Cu Alloy," Met. Trans., V. 2, 1971, p. 841

7. R. E. Lewis, J. G. Bjeletich, T. M. Morton, and F. A. Crossley, "Effect of Cooling Rate on Fracture Behavior of Mill-Annealed Ti-6Al-4V," ASTM STP 601, 1976, p. 371

8. J. C. Lewis and J. T. Kenny, "Sustained Load Crack Growth Design for Ti-6Al-4V Titanium Alloy Tanks Containing Hydrazine," AIAA Paper No. 76-769, presented at AIAA/SAE Propulsion Conference, Palo Alto, Ca., July 1976

9. J. M. Fitzpatrick, F. A. Crossley, and R. E. Lewis, "Texture Strengthening of Ti-6Al-4V," Metals Eng'g Quarterly, February 1972, p. 27

10. M. J. Harrigan, A. W. Sommer, P. G. Reimers, and G. A. Alers, "The Effect of Rolling Texture on the Fracture Mechanics Properties of Ti-6Al-2Sn-4Zr-6Mo Alloy," Titanium Science and Technology (Vol. 2), Plenum Press, New York, 1973, pp. 1297–1320

11. D. N. Fager and W. F. Spurr, "Some Characteristics of Aqueous Stress Corrosion in Titanium Alloys," TRANS ASM, 61, 1968, p. 238

12. J. C. Williams, N. E. Paton, P. J. Stocker, and H. L. Marcus, Space Shuttle Materials (Vol. 3), S.A.M.P.E., Azusa, California, 1971, p. 643

13. D. A. Meyn and G. Sandoz, "Fractography and Crystallography of Subcritical Crack *Propagation in High Strength Titanium Alloys*," TRANS–AIME, 245, 1969, p. 1253

14. S. R. Seagle, R. R. Seeley, and G. S. Hall, "The Influence of Composition and Heat Treatment on the Aqueous-Stress Corrosion of Titanium," Applications Related Phenomena in Titanium Alloys, ASTM STP 432, 1968, p. 170

15. I. R. Lane and J. L. Cavallaro, "Metallurgical and Mechanical Aspects of the Sea-Water Stress Corrosion of Titanium," Applications Related Phenomena in Titanium Alloys, ASTM STP 432, 1968, p. 147

16. M. J. Blackburn and J. C. Williams, "Metallurgical Aspects of Stress-Corrosion Cracking in Titanium Alloys," Fundamental Aspects of Stress Corrosion Cracking, ed. R. Stahle et al., NACE, Houston, 1969, p. 620

17. J. D. Boyd and R. G. Hoagland, "The Relation Between Surface Slip Topography and Stress-Corrosion Cracking in Ti-8 Wt. % Al," Proc. Intn'l Symposium on Stress-Corrosion Mechanisms, Atlanta, Ga., (NACE) 1971

18. J. C. Williams and M. J. Blackburn, "A Comparison of Phase Transformations in Three Commercial Titanium Alloys," ASM Transactions Quarterly, V. 60, No. 3, 1967, p. 373

19. "Standard Method of Test for Plane Strain Fracture Toughness of Metallic Materials," Amer. Soc. for Testing and Materials, Designation: E 399-74, July 1974

20. J. M. Barsom, "Fatigue-Crack Propagation in High Yield-Strength Steels," Engineering Fracture Mechanics, Vol. 2, No. 4, June 1971, p. 301

21. M. J. Blackburn and J. C. Williams, "Preparation of Thin Foils of Titanium Alloys," TMS-AIME, V. 239, 1967, p. 287

22. H. Margolin and H. Portisch, "Hydrogen-Induced Expansions in Titanium-Aluminum Alloys," Trans. AIME, Vol. 242, Sep 1968, p. 1901

23. G. Welsch, G. Lütjering, K. Gazioglu, and W. Bunk, "Deformation Characteristics of Age-Hardened Ti-6Al-4V, "Deutsche Forschungs- und Versuchsanstalt für Luft- und Raumfahrt, Institut fur Werkstofforschung, Cologne, Germany, 1975

24. J. Y. Lim, C. J. McMahon, Jr., D. R. Pope, and J. C. Williams, "The Effect of Oxygen on the Structure and Mechanical Behavior of Aged Ti-8 Wt Pct Al," Vol. 7A, January 1976, p. 139

25. F. A. Crossley, "Effects of the Ternary Additions: O, S, Zr, Cb, Mo, and V on the $\alpha/\alpha + Ti_3Al$ Boundary of Ti-Al Base Alloys," Trans. AIME, Vol. 245, Sep 1969, p. 1963

26. F. A. Crossley, "Kinetics of Ti_3 Al Grain Boundary Precipitation in Ti-Al Binary and Ti-Al-X Ternary Alloys and Correlation with Mechanical Properties," Met. Trans., Vol. 1, 1970, p. 1921

27. M. J. Blackburn, "Relationship of Microstructure to Some Mechanical Properties of Ti-8Al-1V-1Mo," ASM Transactions Quarterly, V. 59, No. 4, 1966, p. 694

28. F. A. Crossley, "Titanium-Rich End of the Titanium-Aluminum Equilibrium Diagram," Trans. AIME, V. 235, No. 8, 1966, p. 1174

29. M. J. Blackburn, "The Ordering Transformation in Titanium: Aluminum Alloys Containing Up to 25 at. pct. Aluminum," Trans. AIME, V. 239, August 1967, p. 1200

30. G. R. Yoder, L. A. Cooley, and T. W. Crooker, "A Transition to Enhanced Fatigue Crack Propagation Resistance in a β-Annealed Ti-6Al-4V Alloy of Commercial Purity," paper presented at the Second International Conference on Mechanical Behavior of Materials, Boston Massachusetts, 16–20 August 1976

31. E. Eylon and C. M. Pierce, "Effect of Microstructure on Notch Fatigue Properties of Ti-6Al-4V," Met Trans., V. 7A, January 1976, p. 111

32. Chesnutt, J. C., Frandsen, J. D., Tompson, A. W. and Williams, J. C., "Influence of Metallurgical Factors on the Fatigue Crack Growth Rate in Alpha-Beta Titanium Alloys," Quarterly Report (Oct. 1, 1974 to December 31, 1974) on Contract F33615-74-C-5067, Rockwell International Science Center, Thousand Oaks, California, p. 2

33. Rhodes, C. G. and Williams, J. C., "Observations of an Interface Phase in the α/β Boundaries in Titanium Alloys," Met. Trans., V. 6A, 1975, p. 1670

34. Boyd, J. D., "Precipitation of Hydrides in Titanium Alloys," ASM Transactions Quarterly, V. 62, No. 4, 1969, p. 977

35. Berger, L. W., Williams, D. N. and Jaffee, R. J., "Hydrogen in Titanium-Aluminum Alloys," TMS-AIME, V. 212, 1958, p. 509

36. Jaffee, R. J., "The Physical Metallurgy of Titanium Alloys," Progress in Metal Physics, V. 7, Pergamon Press, 1958, p. 65

37. Martinod, H. and Vassel, A., "Stress Cracking of a Titanium Alloy in Salt Water and Various Organic Media," Proc. of La Chambre Syndicale des Producteurs d'Aciens Fins et Speciaux et l' Union Syndicale des Industries Aeronautiques: Ameliriation des Performances des Acirs a Temperature Ambiante et a' Haute Temperature, Paris, June 1973, discussion p. 57

38. Meyn, D. A., "Effect of Hydrogen in Fracture and Inert Environment Sustained Load Cracking Resistance of α-β Titanium Alloys," Met. Trans., V. 5, 1974, p. 2405

39. Howe, D. G. and Goode, R. J., "Effects of Heat-Treating Environmental Conditions on the Stress-Corrosion Cracking Resistance of Several Titanium Alloys," Applications Related Phenomena in Titanium Alloys, ASTM STP 432, 1968, p. 189

40. Pittinato, G. F. and Hanna, W. D., "Hydrogen in β-Transformed Ti-6Al-4V," Met. Trans., V. 3, 1972, p. 2905

41. Tiner, N. A., Mackay, T. L., Asanmaa, S. K. and Ingersoll, R. G., "Use of Electron Microautoradiography for Evaluating Microsegregation of Hydrogen in Titanium Alloys," ASM Transactions Quarterly, V. 61, No. 2, 1968, p. 195

Table I

Ti-6Al-4V 1-IN. PLATE MILL PRODUCTS

Grade	RMI Heat No.	Lot No.	Mill Process	Analysis*	Chemistry (Weight Percent)						
					Al	V	Fe	C	H	O	N
Standard	892482	02	MA	RMI	6.7	4.0	0.18	0.02	0.0057	0.175	0.011
				Check	6.45	4.08	0.167	0.02	0.0022	0.18	0.013
		03	VCF	RMI	6.7	4.0	0.18	0.02	0.0051	0.174	0.011
				Check	6.40	4.18	0.17	0.016	0.0016	0.16	0.008
		04	RA	RMI	6.7	4.0	0.18	0.02	0.0031	0.168	0.011
				Check	6.48	4.35	0.159	0.016	0.002	0.17	0.01
ELI	802334	05	MA	RMI	6.1	4.0	0.19	0.02	0.0048	0.128	0.018
				Check	6.03	4.13	0.168	0.013	0.002	0.13	0.017
		06	VCF	RMI	6.1	4.0	0.19	0.02	0.0099	0.14	0.018
				Check	6.13	4.33	0.173	0.011	0.0018	0.11	0.021
		07	RA	RMI	6.1	4.0	0.19	0.02	0.0091	0.129	0.018
				Check	6.20	4.08	0.162	0.011	0.0018	0.14	0.017

*RMI Analyses are average of top and bottom of plate ingot except H and O which are from 1-in. plate.
Check analyses are by Oregon Metallurgical Corp. from 1-in. plate.

Table II

SUMMARY OF TITANIUM 6Al-4V, 1-IN. PLATE CONDITIONS STUDIED

Condition Number	Grade	Mill Heat-Treatment[a]	Microstructural Type[b]	Abbreviated Description of Heat-Treatment[c]	Reheat-Treatment
50	Standard	MA	E	MA	None (as-received)
51	Standard	MA	E + W	DA(AC)	1775°F-1/2h-AC, 1450°F-1h-AC
53	Standard	MA	E + W	DA(FC)	1775°F-1/2h-AC, 1450°F-1h-FC
54	ELI	MA	E	MA	None (as-received)
55	ELI	MA	E + W	DA(AC)	1775°F-1/2h-AC, 1450°F-1h-AC
57	ELI	MA	E + W	DA(FC)	1775°F-1/2h-AC, 1450°F-1h-FC
60	ELI	MA	Coarse W	BA + DA(AC)	1825°F-1/2h-AC, 1775°F-1/2h-AC, 1450°F-1h-AC
63	Standard	VCF	E	MA	None (as-received)
64	Standard	VCF	E + W	DA(AC)	1775°F-1/2h-AC, 1450°F-1h-AC
66	Standard	VCF	E + W	DA(FC)	1775°F-1/2h-AC, 1450°F-1h-FC
67	Standard	VCF	Coarse W	BA + DA(AC)	1825°F-1/2h-AC, 1775°F-1/2h-AC, 1450°F-1h-AC
69	Standard	VCF	Coarse W	BA + DA(FC)	1825°F-1/2h-AC, 1775°F-1/2h-AC, 1450°F-1h-FC
70	ELI	VCF	E	VCF	None (as-received)
71	ELI	VCF	E + W	DA(AC)	1775°F-1/2h-AC, 1450°F-1h-AC
73	ELI	VCF	E + W	DA(FC)	1775°F-1/2h-AC, 1450°F-1h-FC
75	ELI	RA	E	RA	None (as-received)
76	Standard	RA	E	RA	None (as-received)

(a) MA = mill anneal
VCF = vacuum creep-flatten
RA = recrystallization anneal

(b) E = equiaxed (primary) $\alpha + \beta$
E + β = equiaxed α + (nucleation and growth formation) Widmanstätten
W = Widmanstätten

(c) DA = duplex anneal
BA = beta anneal
(AC) = air-cooled from 1450°F
(FC) = furnace-cooled from 1450°F

Table III

COMPARISON OF HEAT-TREATMENT COOLING RATES

Symbol	Facility	Medium	Furnace Temperature (°F)	Cooling Rate at 1000°F (°F/min)
AC	Laboratory Furnace	Air	1450	69
MAC	RMI Electric Roller Hearth	Air	1450	27
			1810	75
FC	Laboratory Furnace	Air	1450	0.77
VCF	RMI Vacuum Creep-Flattening Furnace	Heavy Platens	1450	0.83

AC = laboratory anneal, air-cool
MAC = mill anneal, air-cool
FC = laboratory anneal, furnace-cool
VCF = mill vacuum creep-flatten

Table IV

SUMMARY OF MECHANICAL PROPERTIES[a] GROUPED BY MILL HEAT-TREATMENT PRODUCT AND RANKED BY FRACTURE TOUGHNESS

Condition Number	Grade	Microstructure Type[b]	Reheat-Treatment[c]	K_{Ic} (or K_Q) (ksi-in.$^{1/2}$)	K_{Iscc} (ksi-in.$^{1/2}$)	F_{ty} (ksi)	F_{tu} (ksi)	Elongation (%)	RA (%)	E (10^6 psi)
MILL ANNEALED										
60	ELI	Coarse W	BA + DA(AC)	(91),(99)	72	123	137	12	19	19
55	ELI	E + W	DA(AC)	74	–	136	145	13	37	18.2
57	ELI	E + W	DA(FC)	72	–	139	147	13	35	20.1
51	Std	E + W	DA(AC)	68,62	44	137	145	15	35	19.2
54	ELI	E	None (as-received)	60	–	144	153	13	33	19.5
53	Std	E + W	DA(FC)	53,57	45	140	147	16	34	18.9
50	Std	E	None (as-received)	45	~45	147	153	17	42	18.2
VACUUM CREEP-FLATTENED										
71	ELI	E + W	DA(AC)	(89),83	38	134	144	14	32	19.5
69	Std	Coarse W	BA + DAC(FC)	85,79	32	132	145	13	35	18.5
67	Std	Coarse W	BA + DA(AC)	81,79	54	127	140	16	32	17
73	ELI	E + W	DA(FC)	77,75	28	138	148	17	36	19.3
66	Std	E + W	DA(FC)	74,75	29	134	142	15	33	18.8
70	ELI	E	None (as-received)	71	50	138	149	13	34	19.9
63	Std	E	None (as-received)	64,77	40	136	145	16	31	17.9
64	Std	E + W	DA(AC)	69,59	28	133	142	16	35	17.8
RECRYSTALLIZATION ANNEALED										
76	Std		None (as-received)	85	–	127	142	–	33	17.6
75	ELI		None (as-received)	82,83	36	132	143	15	34	18.4

(a) Description of Headings:

- K_{Ic} – fracture toughness index, where $2.5\,(K_Q/F_{ty})^2 < 1.00$ in.
- K_Q – trial value of fracture toughness index
- K_{Iscc} – stress-corrosion cracking threshold
- F_{ty} – 0.2% offset tensile yield
- F_{tu} – ultimate tensile strength
- Elongation – elongation in 1 in.
- RA – reduction in area
- E – Young's Modulus

(b) E = equiaxed (primary) $\alpha + \beta$

E + W = equiaxed $\alpha +$ (nucleation and growth formation) Widmanstätten $\alpha + \beta$

W = Widmanstätten $\alpha + \beta$

(c) See abbreviated descriptions of heat-treatments in Table II.

Table V

INTERPLANAR SPACINGS FOR PHASES OBSERVED IN Ti-6Al-4V[(a)]

α(HCP) a = 2.924 Å c = 4.673 Å		β(b.c.c) a = 3.238 Å		γ(f.c.c) a = 4.40 Å	
{hk·l}	d(Å)	{hkl}	d(Å)	{h k l}	d(Å)
10.0	2.533			111	2.54
00.2	2.336	110	2.290		
10.1	2.227			200	2.20
10.2	1.718	200	1.619	220	1.56
11.0	1.463				
11.1	1.396				
10.3	1.327	211	1.322	311	1.33
20.0	1.267				
11.2	1.240			222	1.27
20.1	1.223				
00.4	1.168	220	1.145		
20.2	1.114			400	1.10
11.3	1.066				
10.4	1.061	310	1.024	331	1.01
20.3	0.983			420	.984
21.0	0.958	222	0.935		
21.1	0.938				
11.4	0.913				
21.2	0.886	321	0.865		
10.5	0.877				
20.4	0.859				
30.0	0.844	400	0.810		
21.3	0.816				

[(a)] Lattice parameters for the α and β phases were determined from an x-ray diffractometer scan of the as-received material.

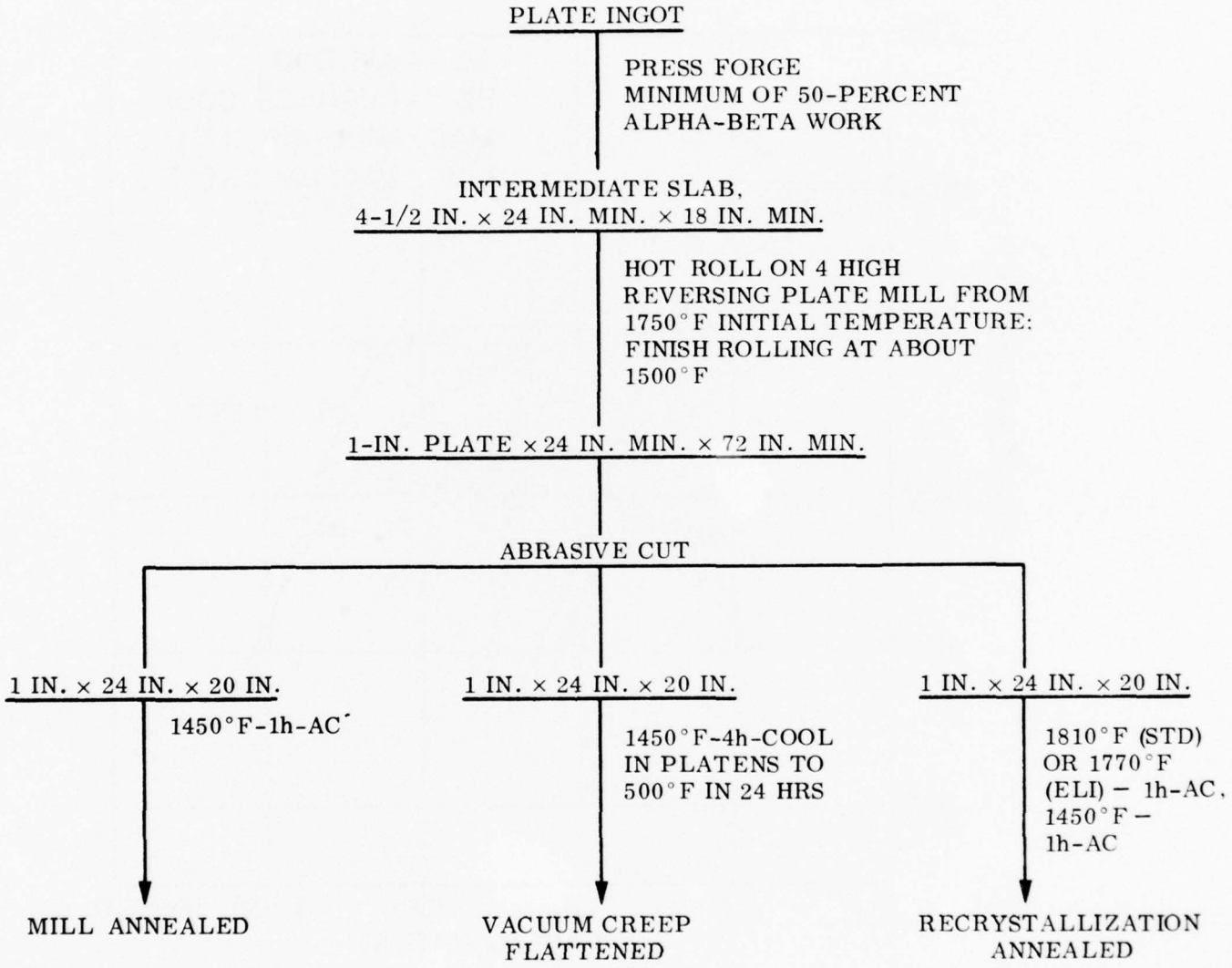

Fig. 1 Processing Schedule for Ti-6Al-4V 1-in. Plate

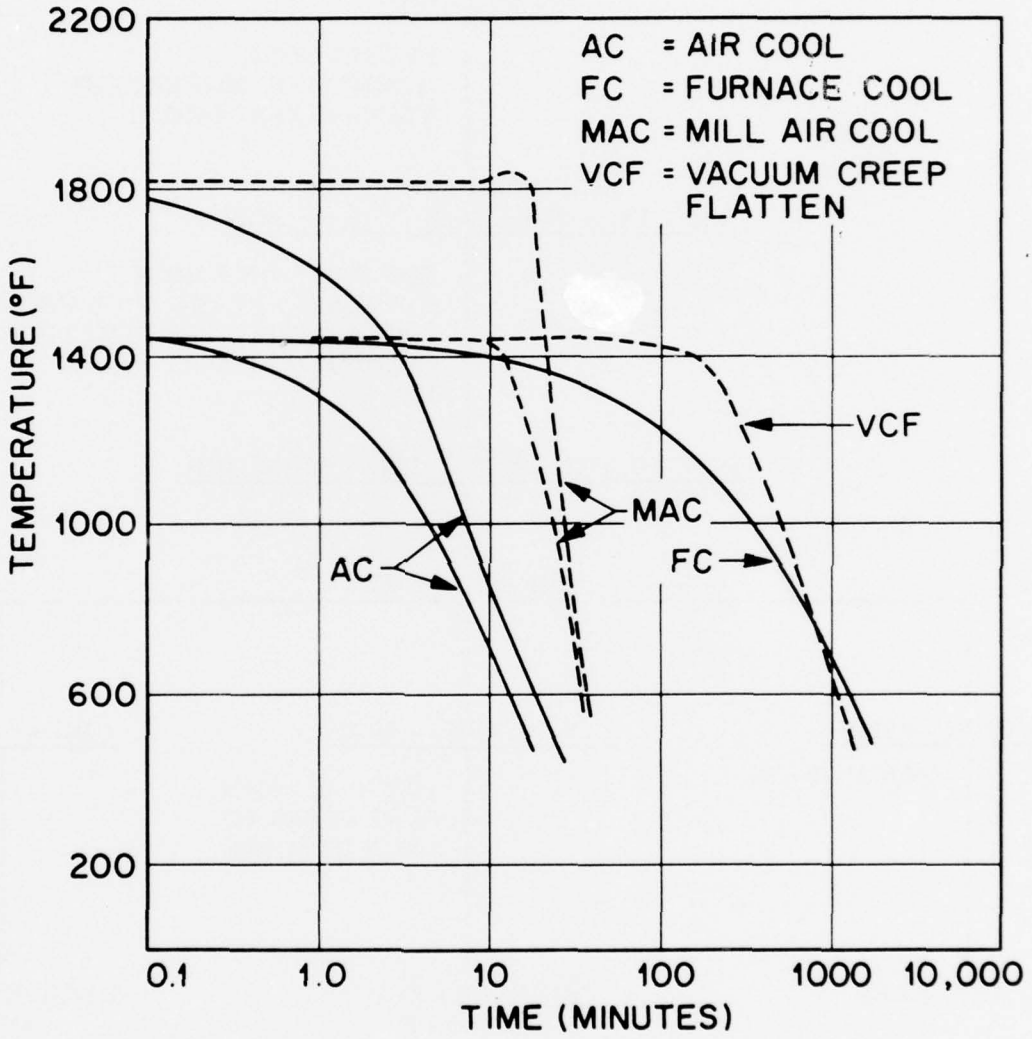

Fig. 2 Cooling Curves for Ti-6 Al-4V 1-in. Plate. Laboratory treatments cooled from 1775°F and 1450°F; Mill treatments cooled from 1810°F and 1450°F. Thermocouple located 1/2 in. below surface at center of plates

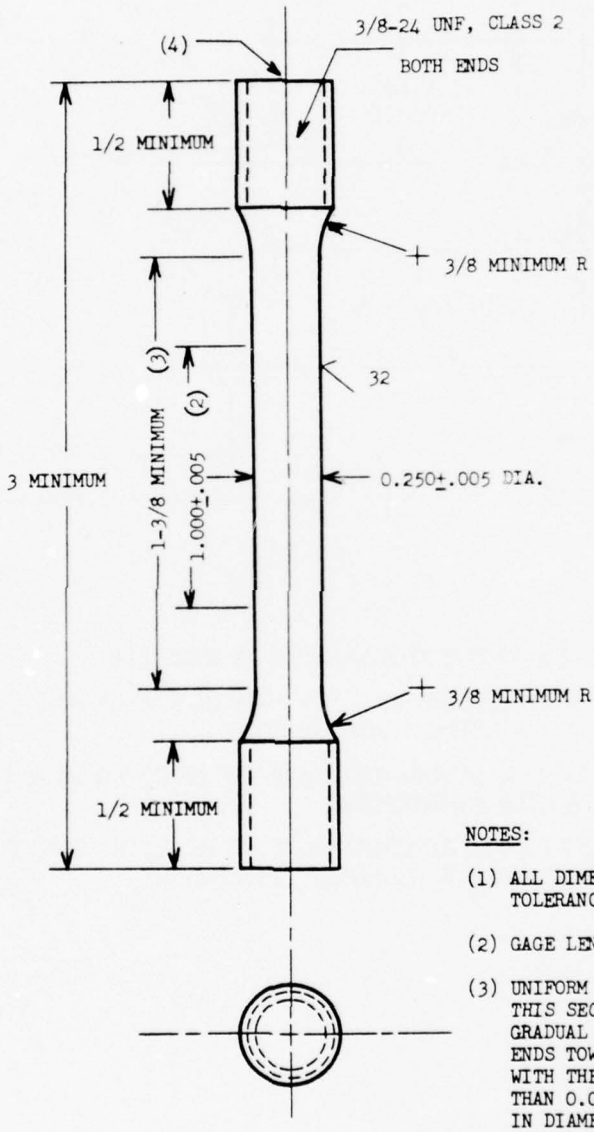

NOTES:

(1) ALL DIMENSIONS AND TOLERANCES IN INCHES.

(2) GAGE LENGTH.

(3) UNIFORM REDUCED SECTION. THIS SECTION MAY HAVE A GRADUAL TAPER FROM THE ENDS TOWARD THE CENTER, WITH THE ENDS NOT MORE THAN 0.0025 IN. LARGER IN DIAMETER THAN THE CENTER.

(4) LATHE CENTER O.K.

Fig. 3 Tensile Specimen

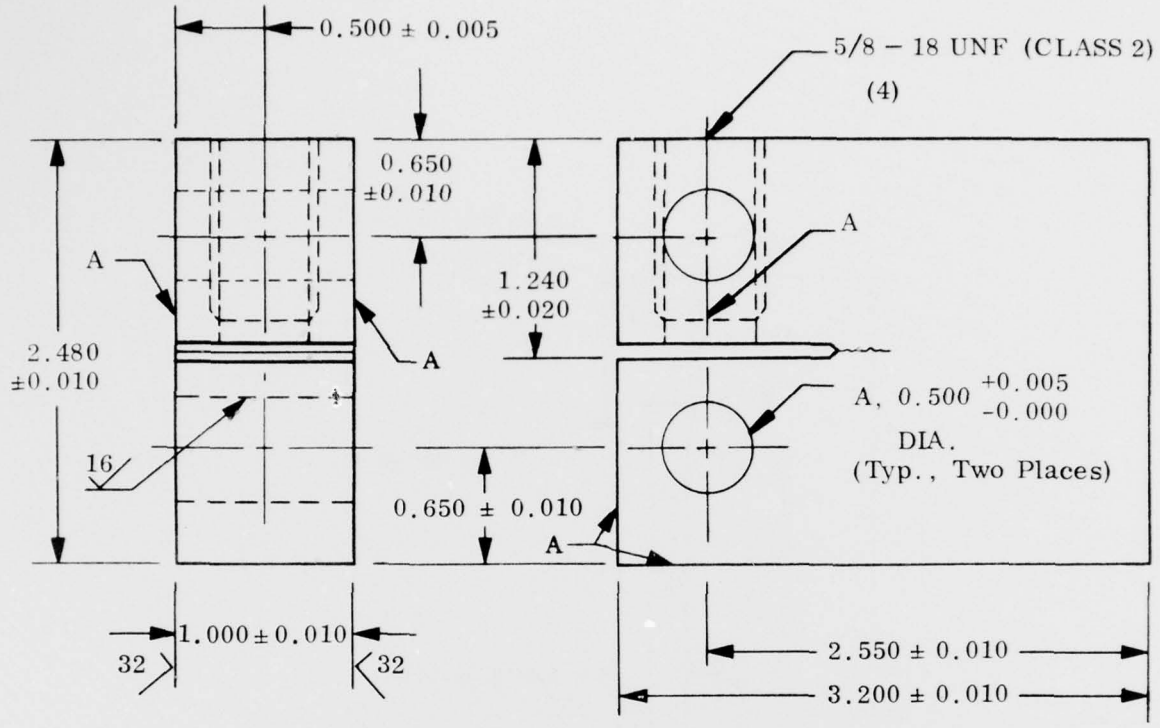

NOTES:

(1) ALL DIMENSIONS AND TOLERANCES IN INCHES.

(2) "A" SURFACES SHALL BE PERPENDICULAR AND PARALLEL AS APPLICABLE TO WITHIN 0.004 IN. TIR.

(3) ROUGHNESS ON ALL SURFACES NOT TO EXCEED 64 RMS UNLESS OTHERWISE SPECIFIED.

(4) HOLE TO BE FULL-THREADED TO 1.00 IN. MIN. DEPTH. HOLE OMITTED IN K_{Ic} AND da/dN SPECIMENS.

Fig. 4 Compact Tension Specimen Used for K_{Ic}, da/dN Versus ΔK, and K_{Iscc} Tests

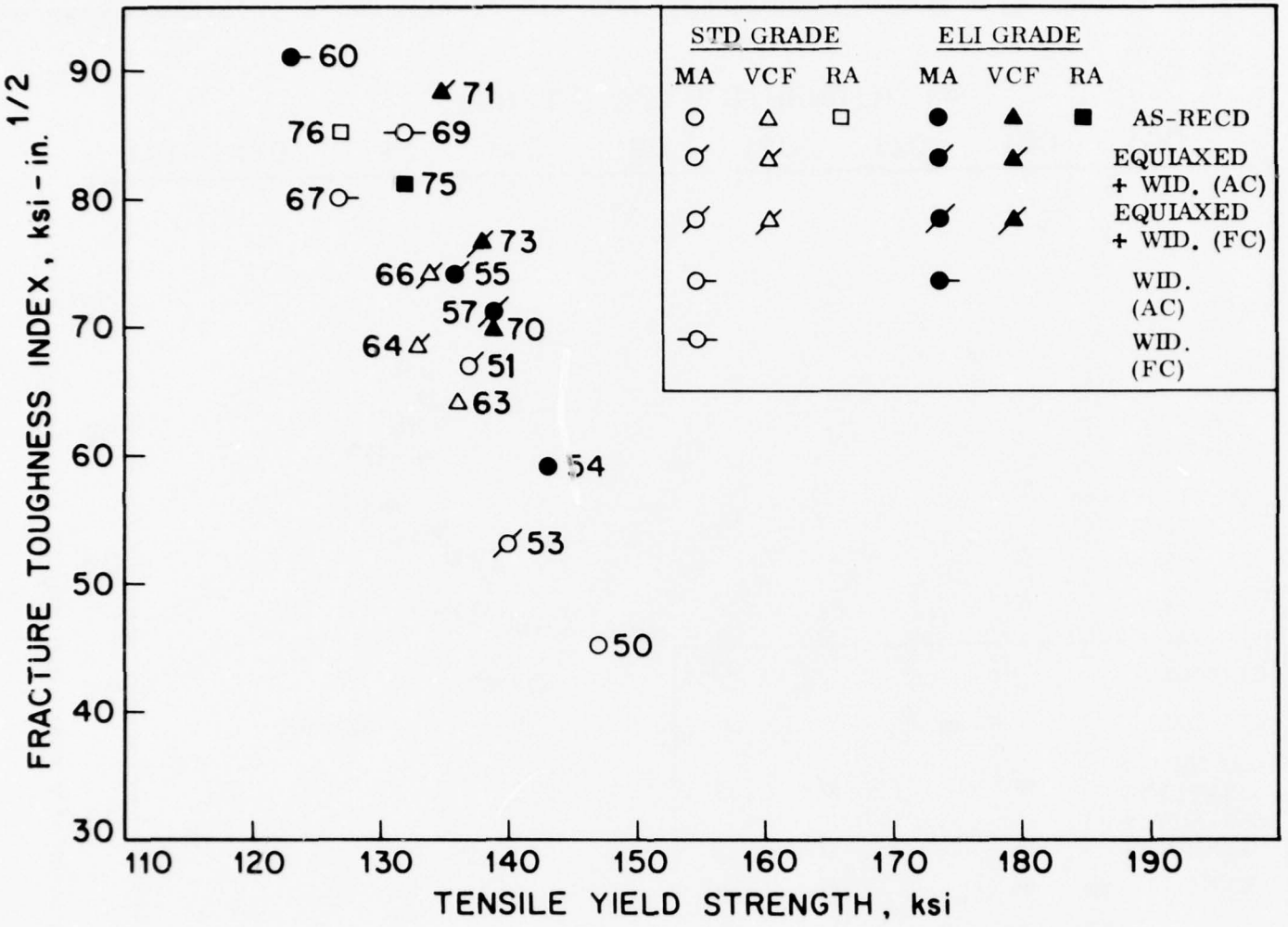

Fig. 5 Fracture Toughness Versus Yield Strength Comparison for the Seventeen Conditions of Ti-6 Al-4V 1-in. Plate

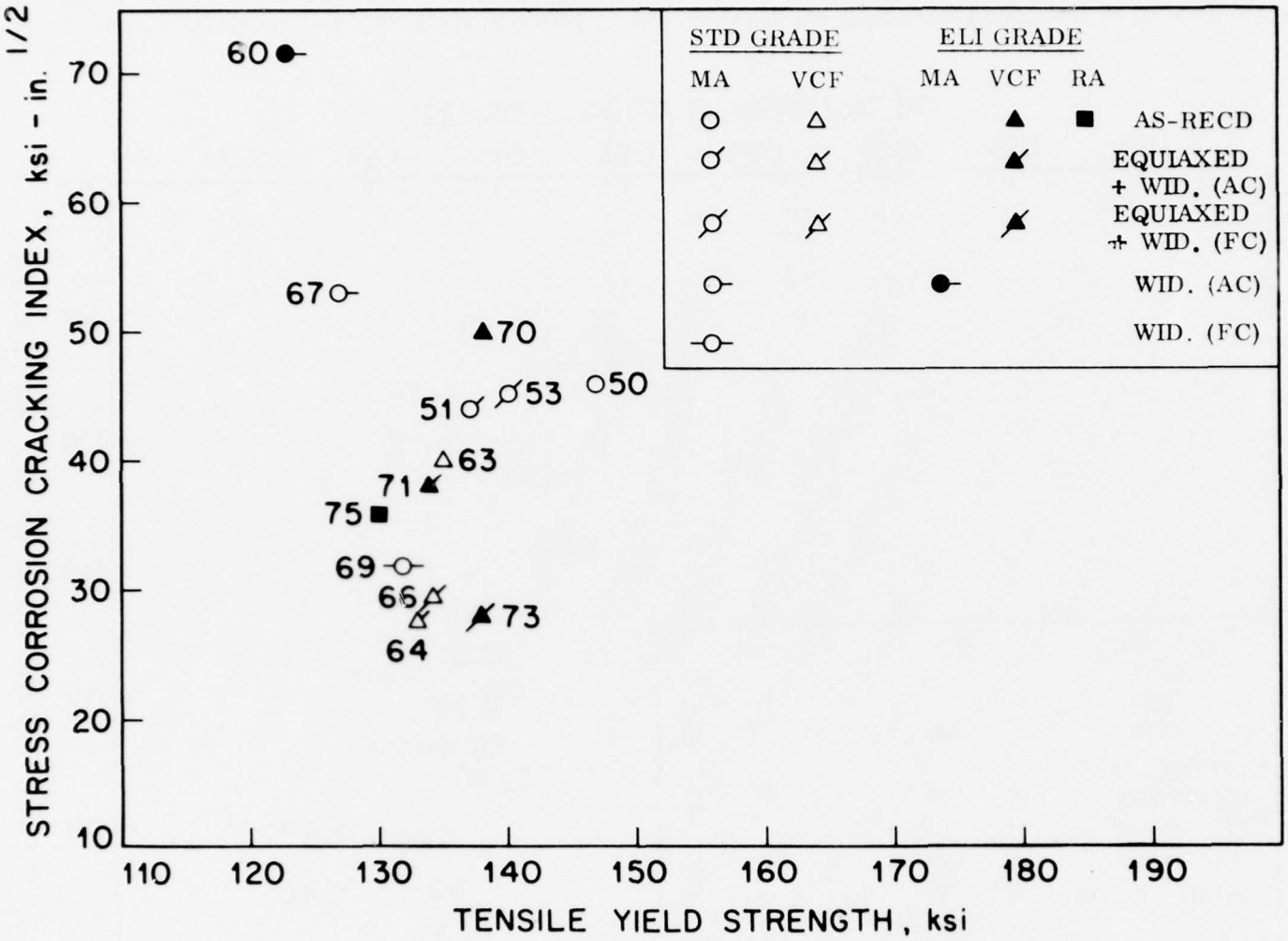

Fig. 6 Stress Corrosion Cracking Index (K_{Iscc}) Versus Yield Strength Comparisons for Thirteen Conditions of Ti-6 Al-4V 1-in. Plate

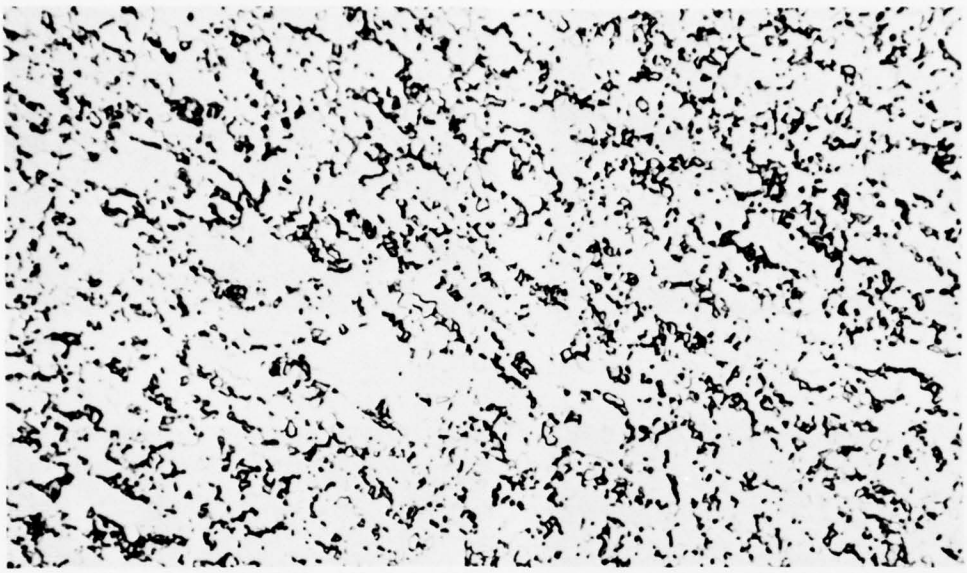

C7739 (a) 500×

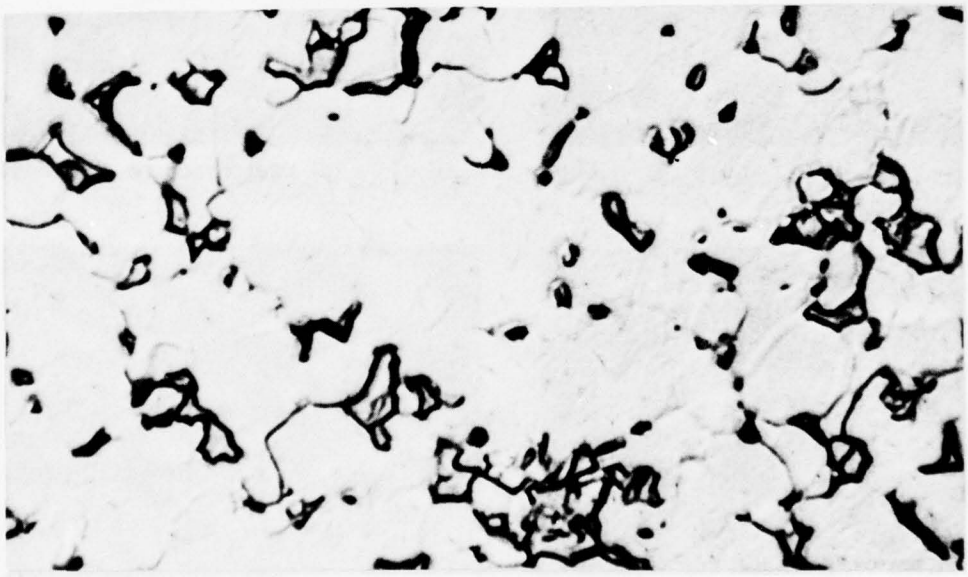

C7740 3000×

Fig. 7 Ti-6 Al-4V Condition 50. Mill annealed, standard grade, 1-in. plate, as-received. K_{Ic} = 45 ksi-in.$^{1/2}$, K_{Iscc} = 45 ksi-in.$^{1/2}$, F_{ty} = 147 ksi

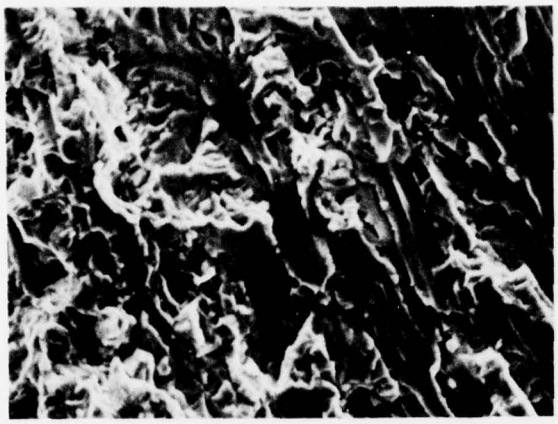

6LHG (a) Fatigue 600×

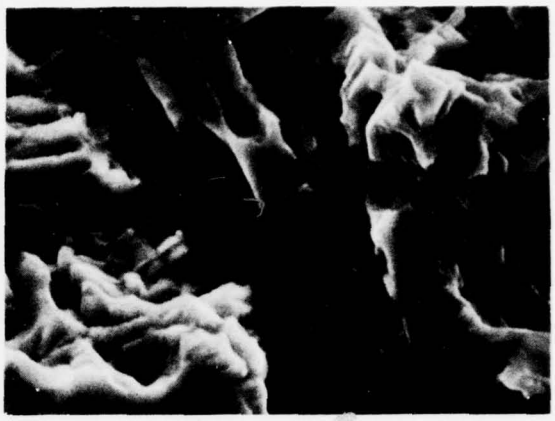

6LHH (b) Fatigue 2400×

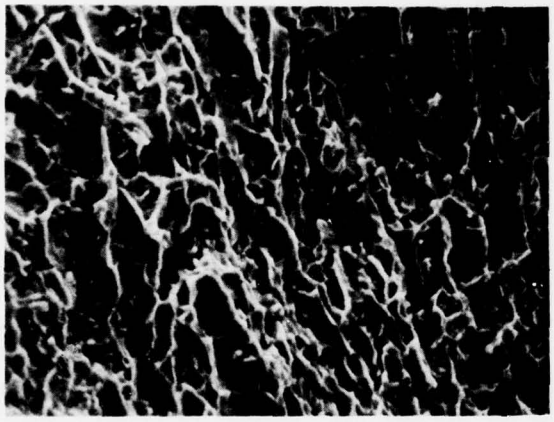

6LHH (c) Fast Fracture 600×

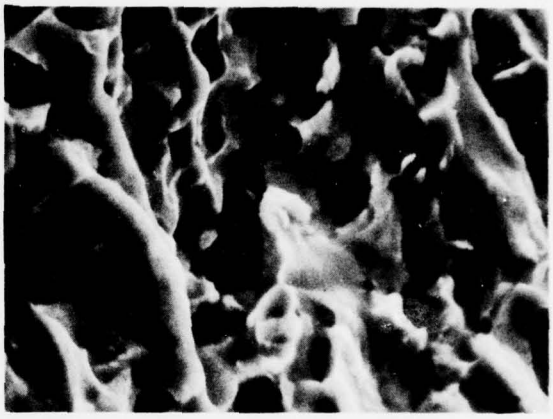

6LHI (d) Fast Fracture 2400×

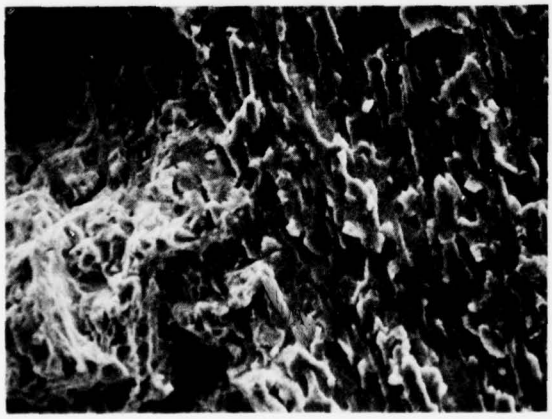

6LMG (e) SCC 540×

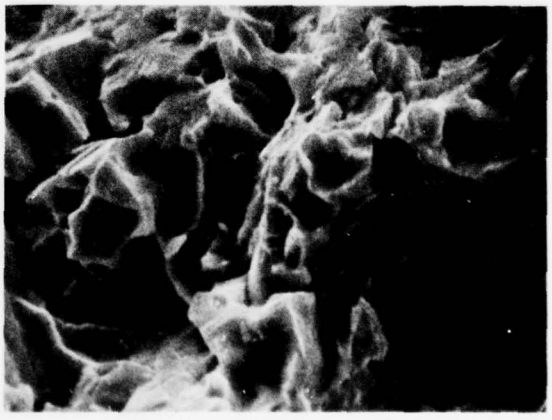

6LMH (f) SCC 2150×

Fig. 8 SEM Fractographs of Ti-6 Al-4V Condition 50

C7761 (a) 500×

C7762 (b) 3000×

Fig. 9 Ti-6 Al-4V Condition 51. Mill annealed, standard grade, 1-in. plate, 1775°F-1/2 h-AC, 1450°F-1h-AC. K_{Ic} = 65 ksi-in.$^{1/2}$, K_{Iscc} = 44 ksi-in.$^{1/2}$, F_{ty} = 137 ksi

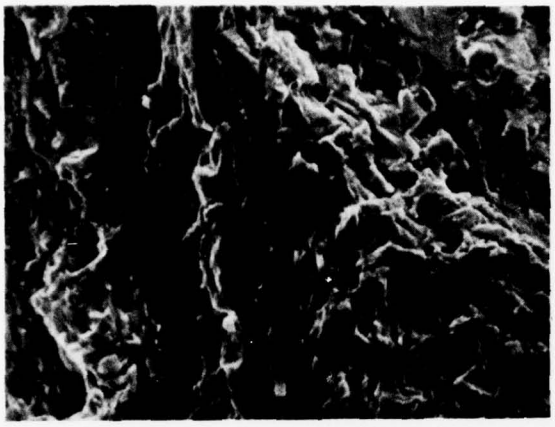

6LHJ (a) Fatigue 575×

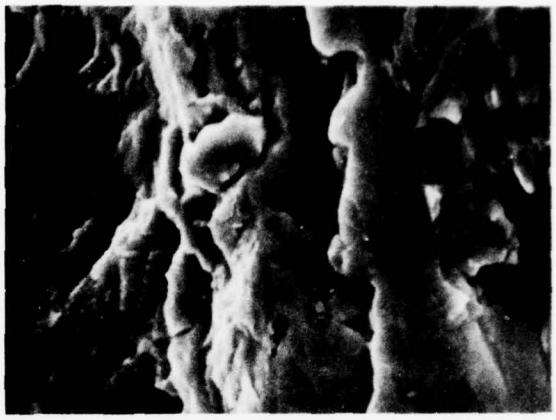

6LHK (b) Fatigue 2300×

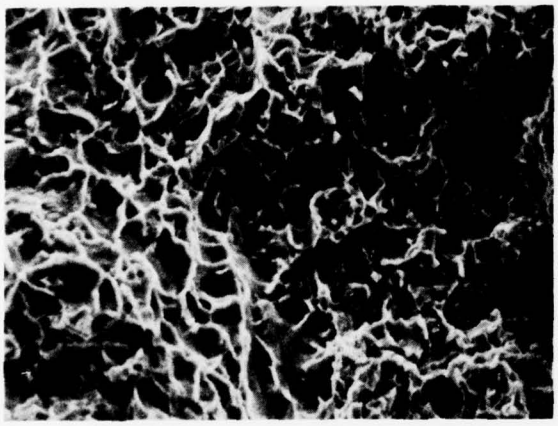

6LHL (c) Fast Fracture 560×

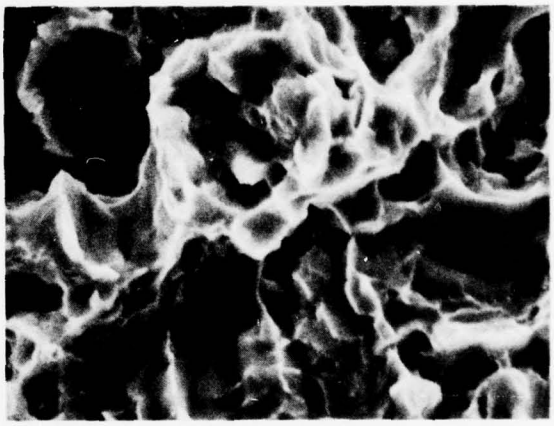

6LHM (d) Fast Fracture 2250×

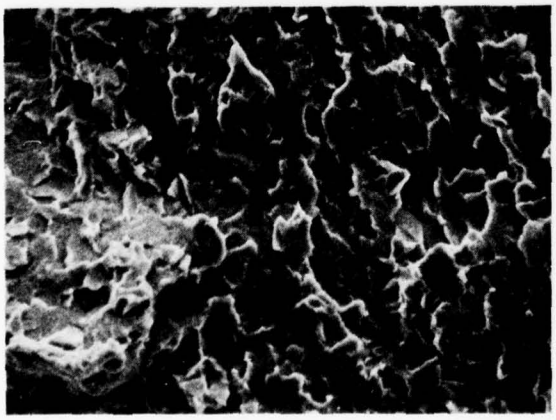

6LMO (e) SCC 550×

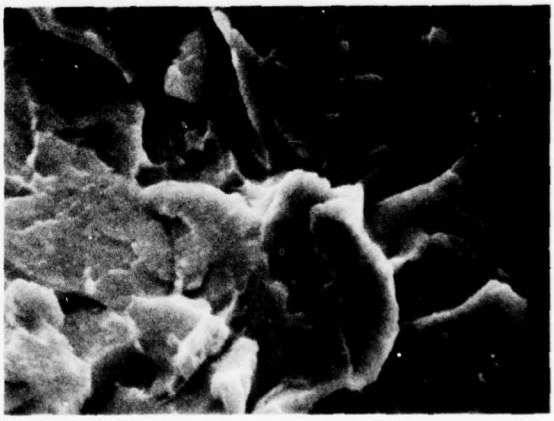

6LMP (f) SCC 2200×

Fig. 10 SEM Fractographs of Ti-6 Al-4V Condition 51

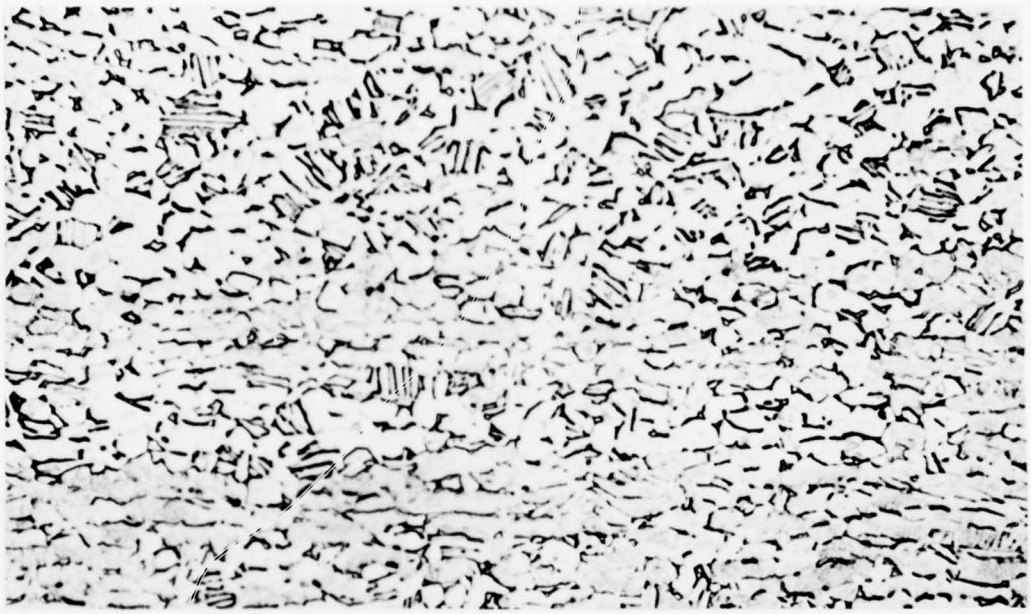

C7759 (a) 500×

C7760 (b) 3000×

Fig. 11 Ti-6Al-4V Condition 53. Mill annealed, standard grade, 1-in. plate, 1775°F-1/2 h-AC, 1450°F-1 h-FC. K_{Ic} = 55 ksi-in.$^{1/2}$, K_{Iscc} = 45 ksi-in.$^{1/2}$, F_{ty} = 140 ksi

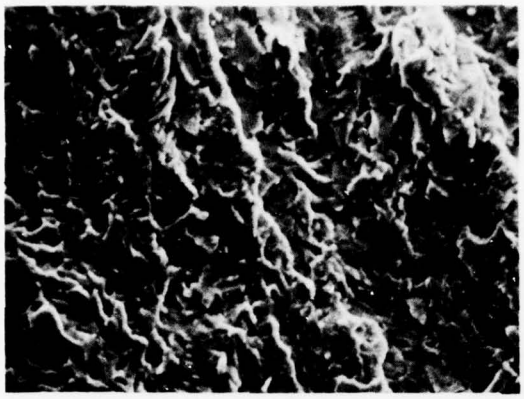

6LHN (a) Fatigue 575×

6LHO (b) Fatigue 2300×

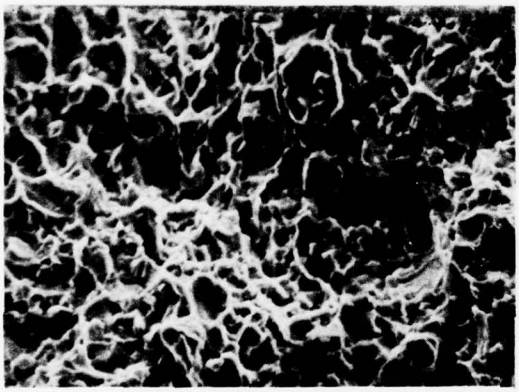

6LHP (c) Fast Fracture 560×

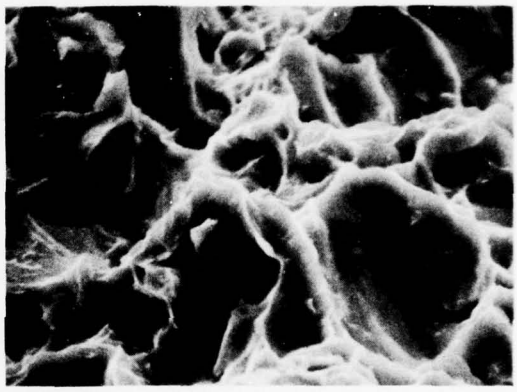

6LHQ (d) Fast Fracture 2250×

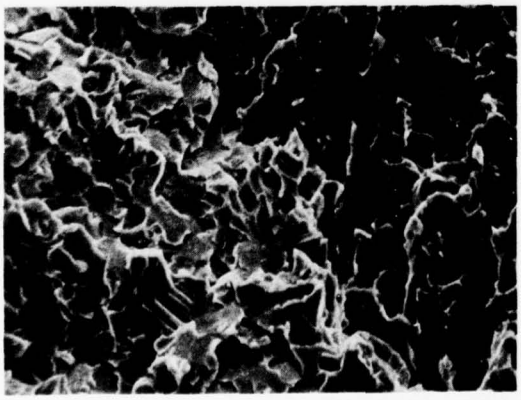

6LMM (e) SCC 500×

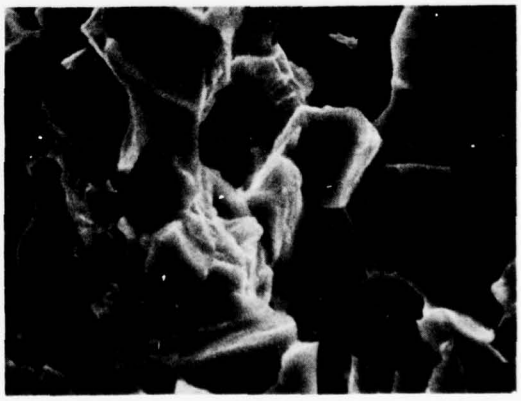

6LMN (f) SCC 2000×

Fig. 12 SEM Fractographs of Ti-6 Al-4V Condition 53

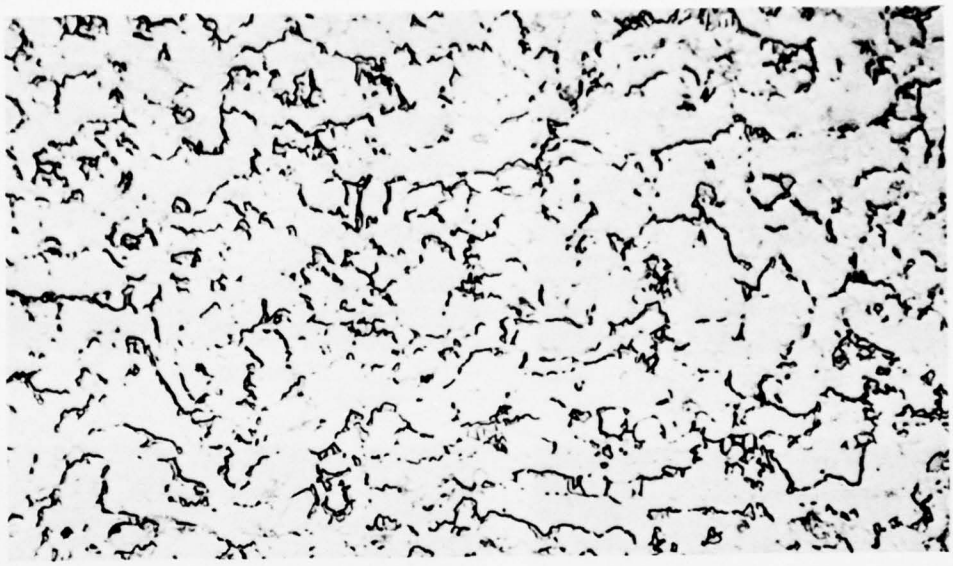

C7749 (a) 500×

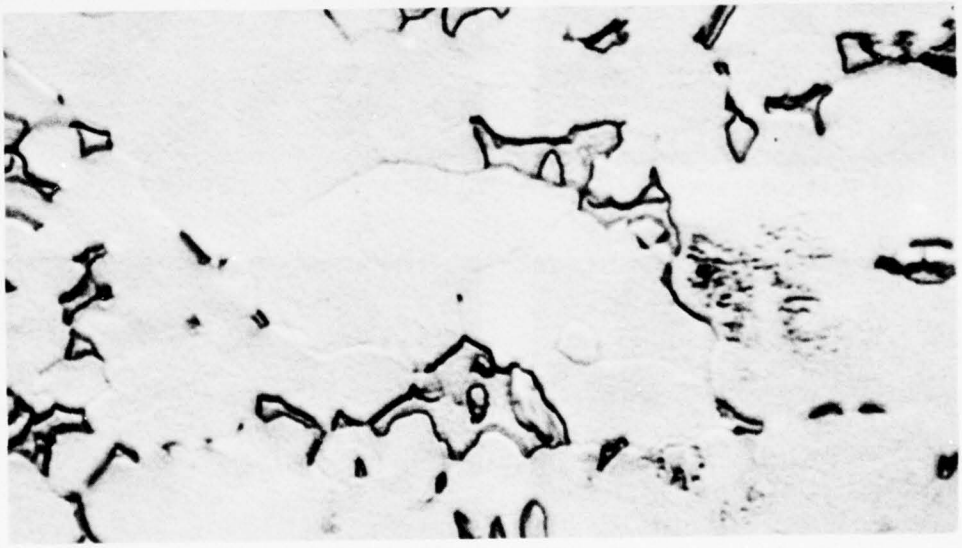

C7750 (b) 3000×

Fig. 13 Ti-6 Al-4V Condition 54. Mill annealed, ELI grade, 1-in. plate, as-received. K_{Ic} = 60 ksi-in.$^{1/2}$, F_{ty} = 144 ksi

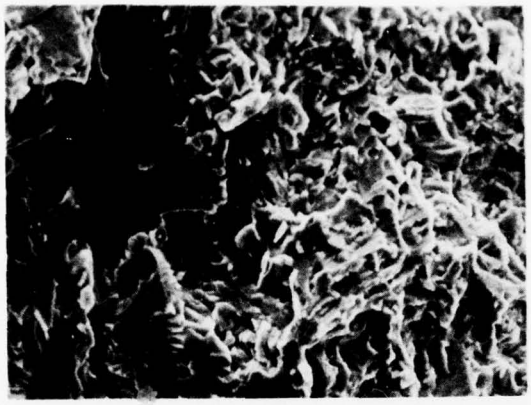

6LHR (a) Fatigue 550×

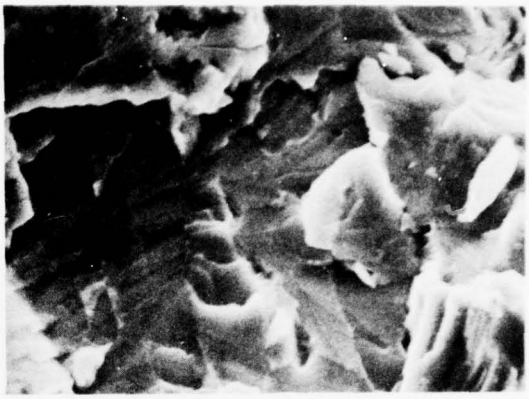

6LHS (b) Fatigue 2200×

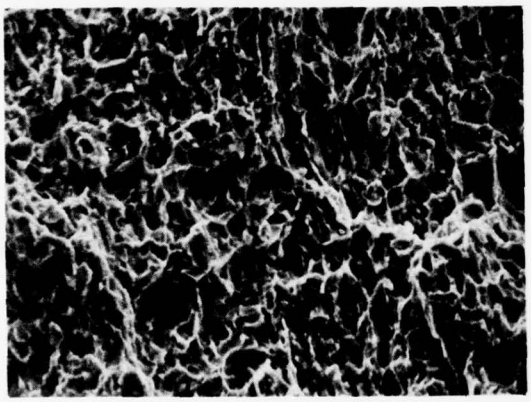

6LHT (c) Fast Fracture 540×

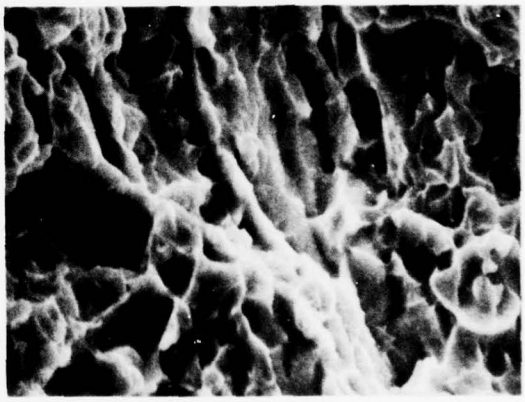

6LHU (d) Fast Fracture 2150×

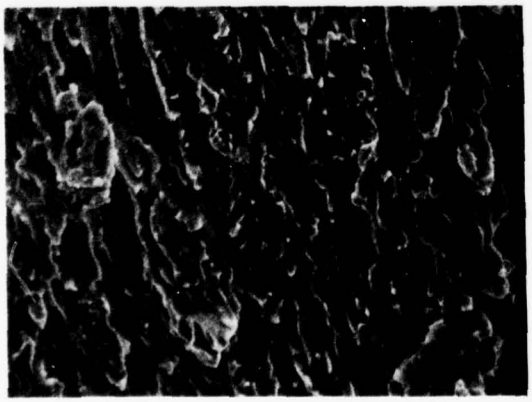

6LME (e) SCC 500×

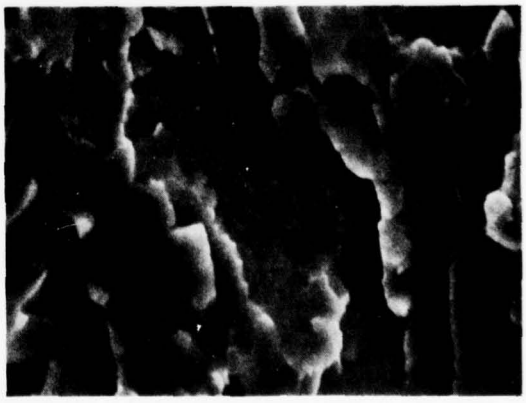

6LMF (f) SCC 2000×

Fig. 14 SEM Fractographs of Ti-6 Al-4V Condition 54

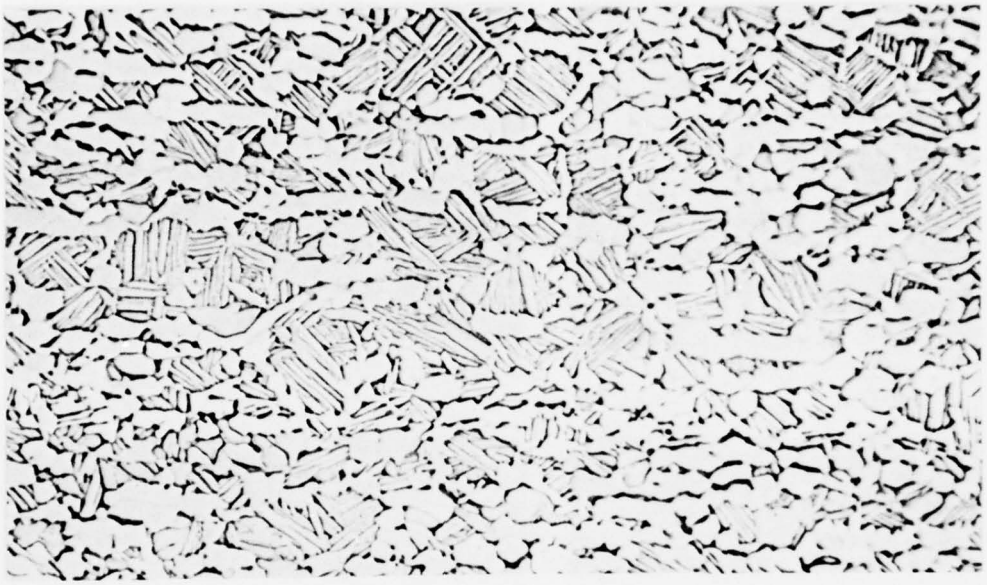

C7737 (a) 500×

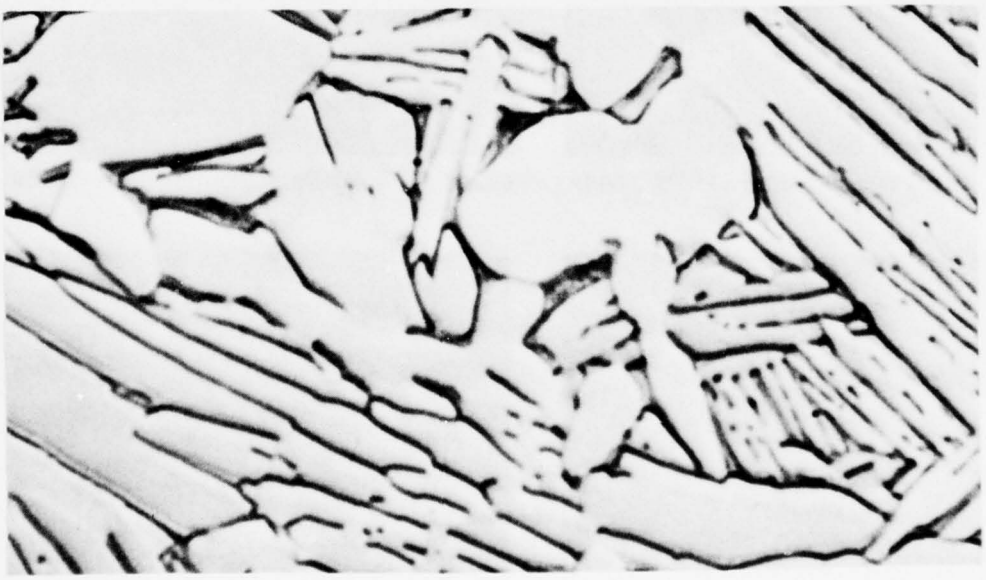

C7738 (b) 3000×

Fig. 15 Ti-6Al-4V Condition 55. Mill annealed, ELI grade, 1-in. plate, 1775°F-1/2 h-AC, 1450°F-1 h-AC. K_{Ic} = 74 ksi-in.$^{1/2}$, F_{ty} = 136 ksi

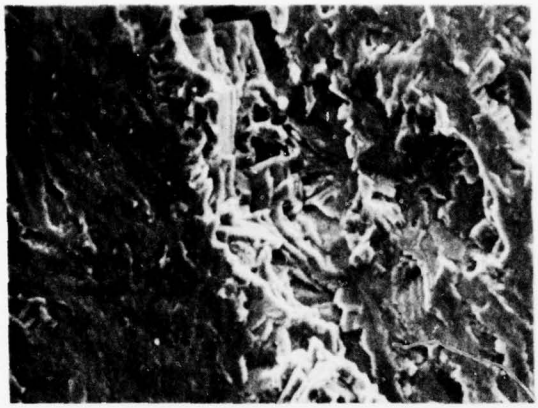

6LHV (a) Fatigue 550×

6LHW (b) Fatigue 2200×

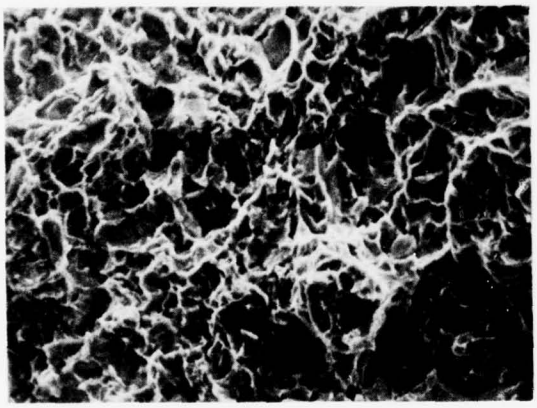

6LHX (c) Fast Fracture 540×

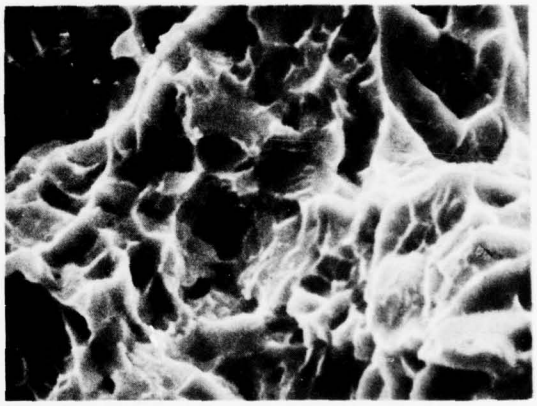

6LHY (d) Fast Fracture 2150×

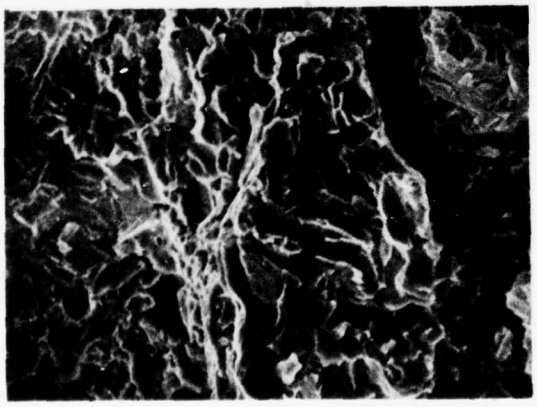

6LML (e) SCC 500×

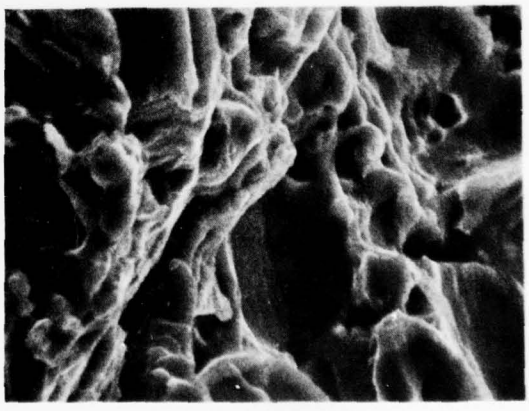

6LMK (f) SCC 2000×

Fig. 16 SEM Fractographs of Ti-6 Al-4V Condition 55

C7757 (a) 500×

C7758 (b) 3000×

Fig. 17 Ti-6 Al-4 V Condition 57. Mill annealed, ELI grade, 1-in. plate, 1775°F-1/2 h-AC, 1450°F - 1 h-FC. K_{Ic} = 72 ksi-in.$^{1/2}$, F_{ty} = 139 ksi

6LID (a) Fatigue 520×

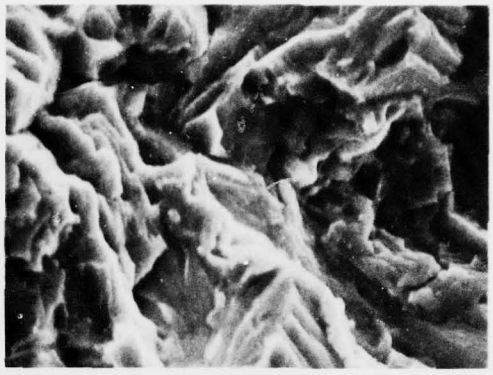

6LIE (b) Fatigue 2050×

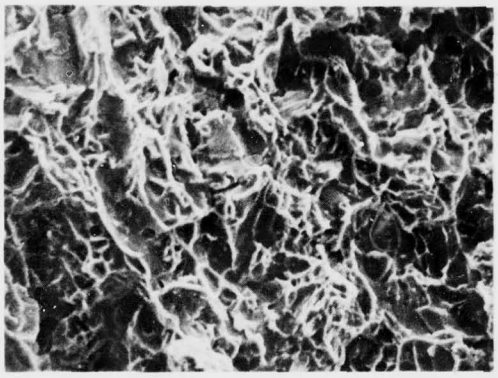

6LIF (c) Fast Fracture 510×

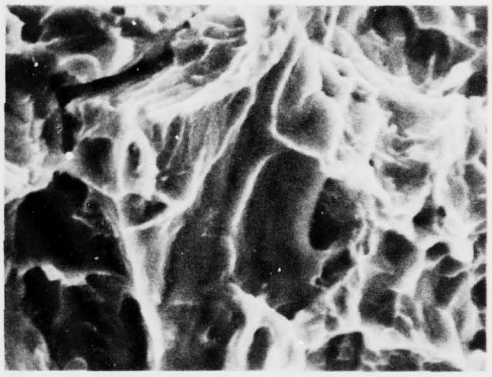

6LIG (d) Fast Fracture 2025×

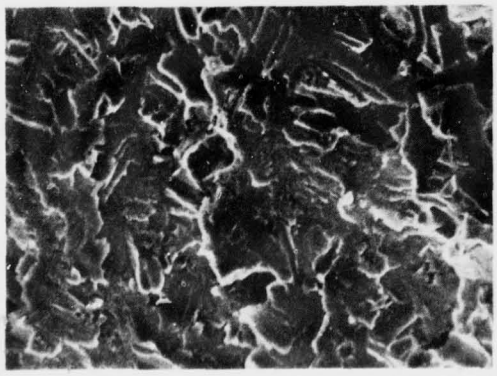

6LMI (e) SCC 550×

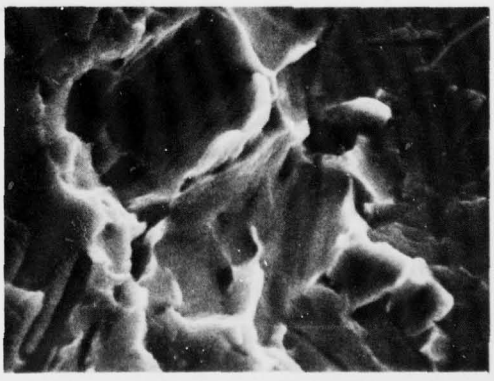

6LMJ (f) SCC 2200×

Fig. 18 SEM Fractographs of Ti-6 Al-4V Condition 57

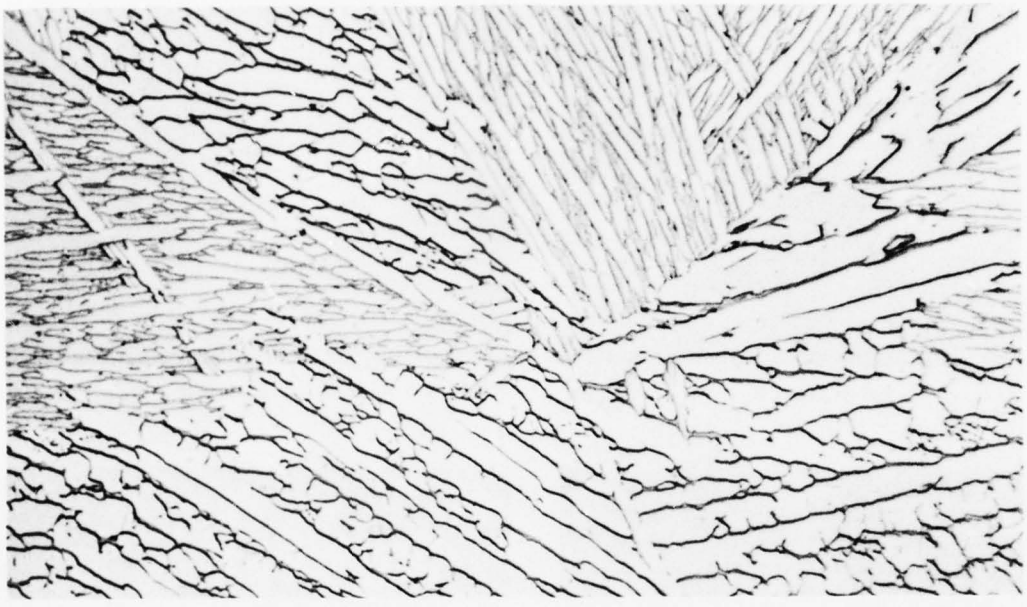

C7735 (a) 500×

C7736 (b) 3000×

Fig. 19 Ti-6 Al-4V Condition 60. Mill annealed, ELI grade, 1-in. plate, 1825°F-1/2 h-AC, 1775°F-1/2 h-AC, 1450°F-1 h-AC. K_Q = 95 ksi-in.$^{1/2}$, K_{Iscc} = 72 ksi-in.$^{1/2}$, F_{ty} = 123 ksi

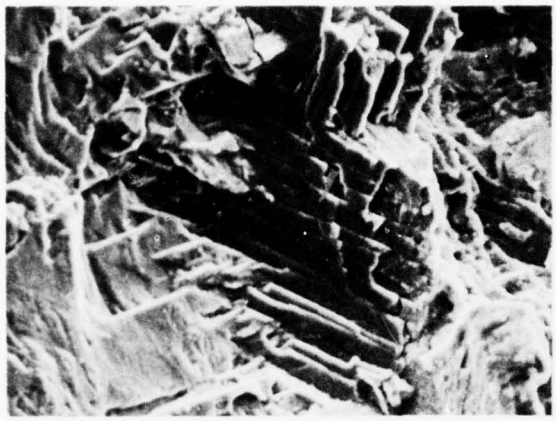

6LHZ (a) Fatigue 610×

6LIA (b) Fatigue 2425×

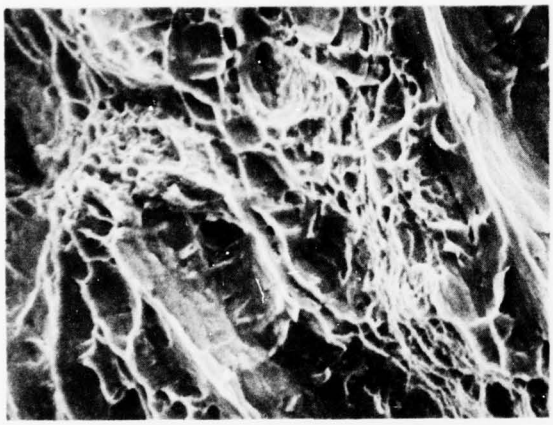

6LIB (c) Fast Fracture 600×

6LIC (d) Fast Fracture 2400×

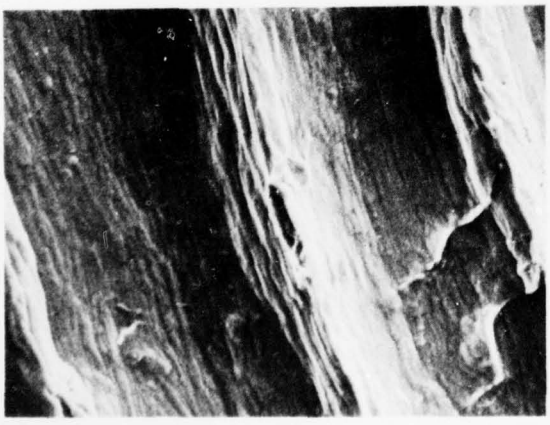

6LMA (e) SCC 550×

6LMB (f) SCC 2250×

Fig. 20 SEM Fractographs of Ti-6 Al-4V Condition 60

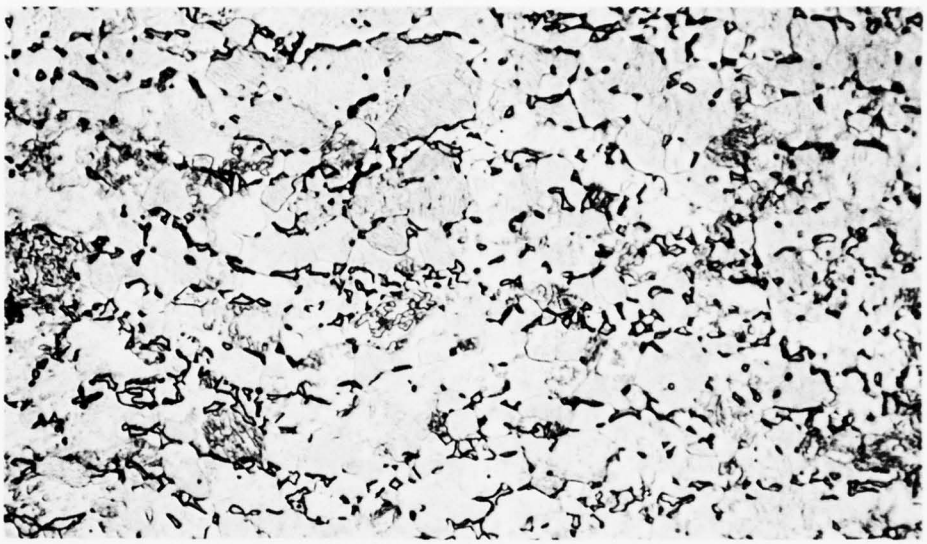

C7767 (a) 500×

C7768 (b) 3000×

Fig. 21 Ti-6 Al-4 V Condition 63. Vacuum creep flattened, standard grade, 1-in. plate, as received. K_{Ic} = 70 ksi-in.$^{1/2}$, K_{Iscc} = 40 ksi-in.$^{1/2}$, F_{ty} = 136 ksi

6LIH (a) Fatigue 600×

6LII (b) Fatigue 2400×

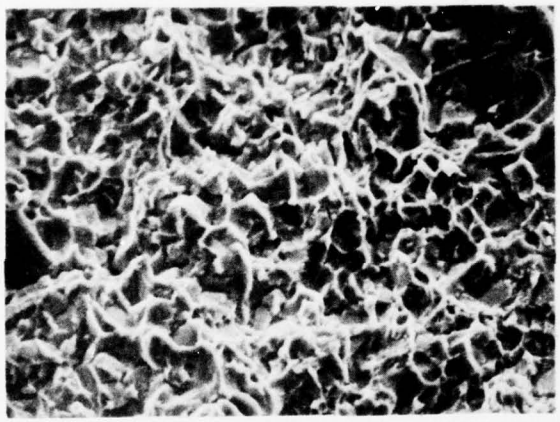

6LIJ (c) Fast Fracture 575×

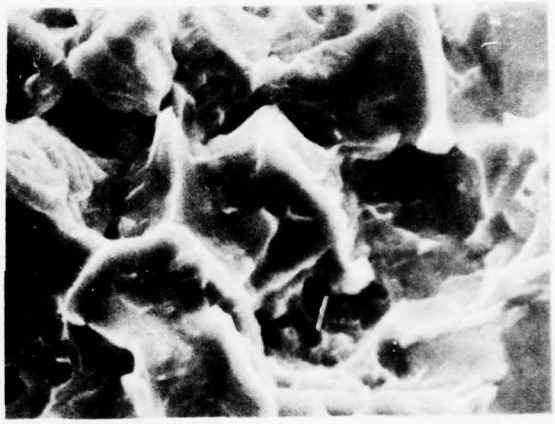

6LIK (d) Fast Fracture 2300×

6LLW (e) SCC 550×

6LLX (f) SCC 2200×

Fig. 22 SEM Fractographs of Ti-6 Al-4V Condition 63

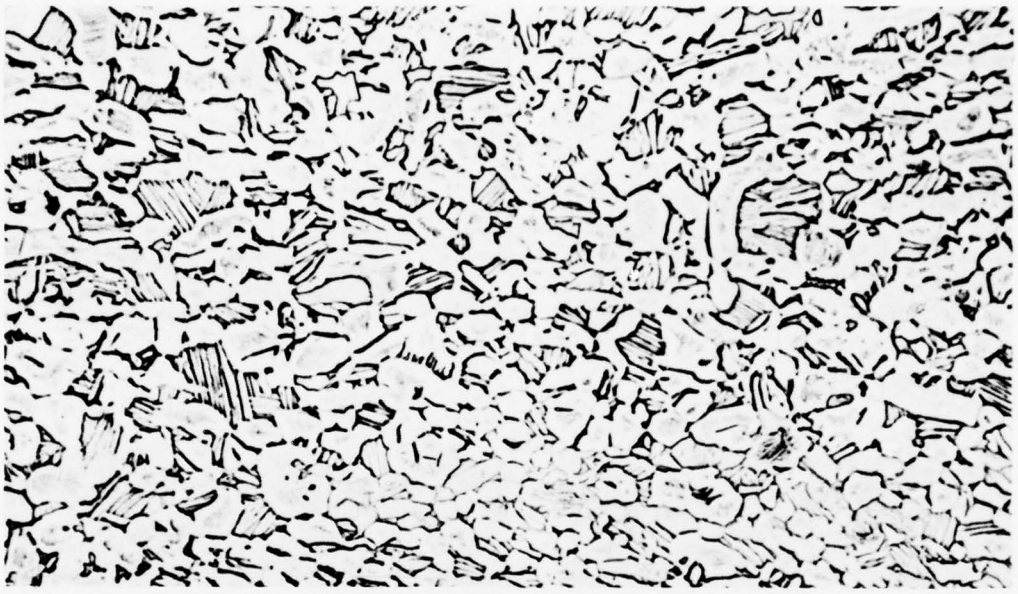

C7745 (a) 500×

C7746 (b) 3000×

Fig. 23 Ti-6 Al-4 V Condition 64. Vacuum creep flattened, standard grade, 1-in. plate, 1775°F-1/2 h-AC, 1450°F-1 h-AC. K_{Ic} = 64 ksi-in.$^{1/2}$, K_{Iscc} = 28 ksi-in.$^{1/2}$, F_{ty} = 133 ksi

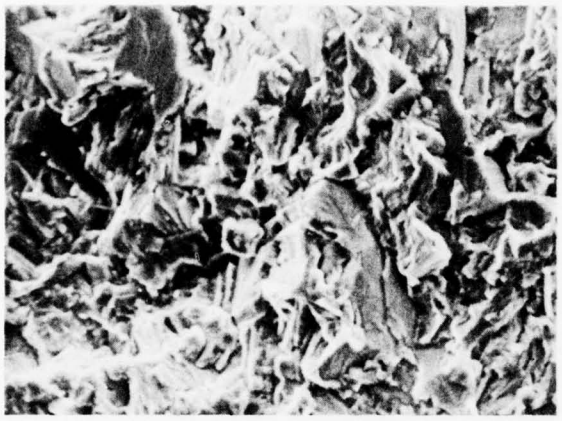

6LJR (a) Fatigue 575×

6LJS (b) Fatigue 2300×

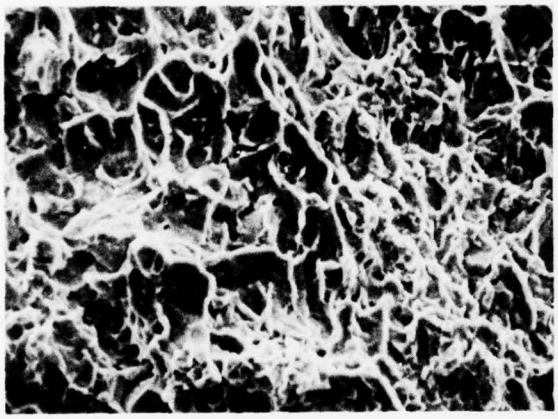

6LJT (c) Fast Fracture 560×

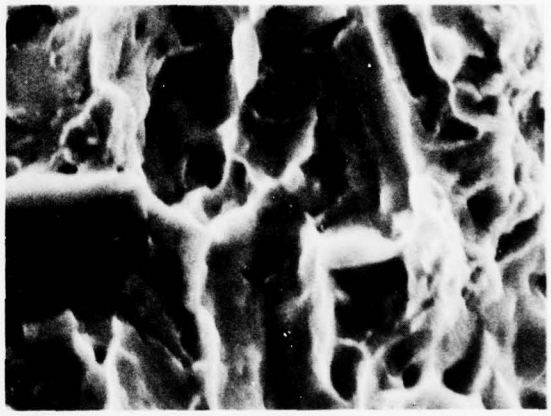

6LJU (d) Fast Fracture 2250×

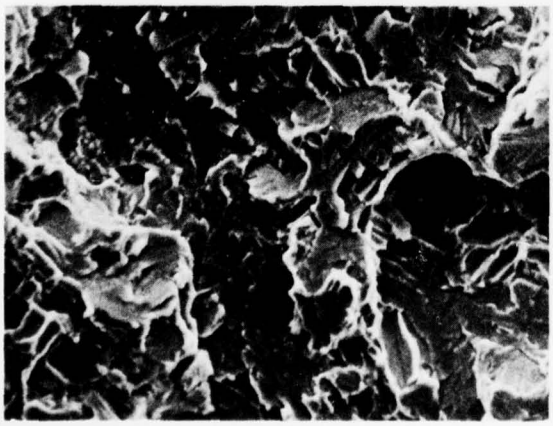

6LLS (e) SCC 575×

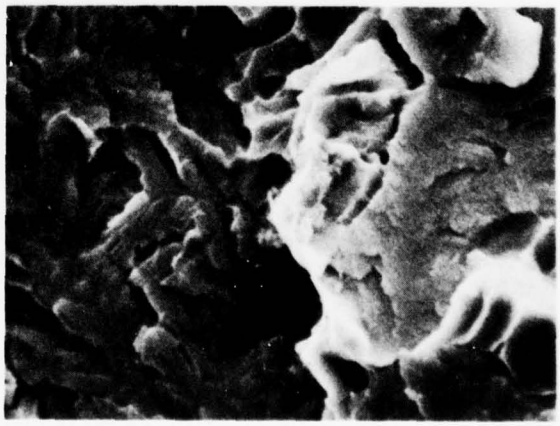

6LLT (f) SCC 2300×

Fig. 24 SEM Fractographs of Ti-6 Al-4V Condition 64

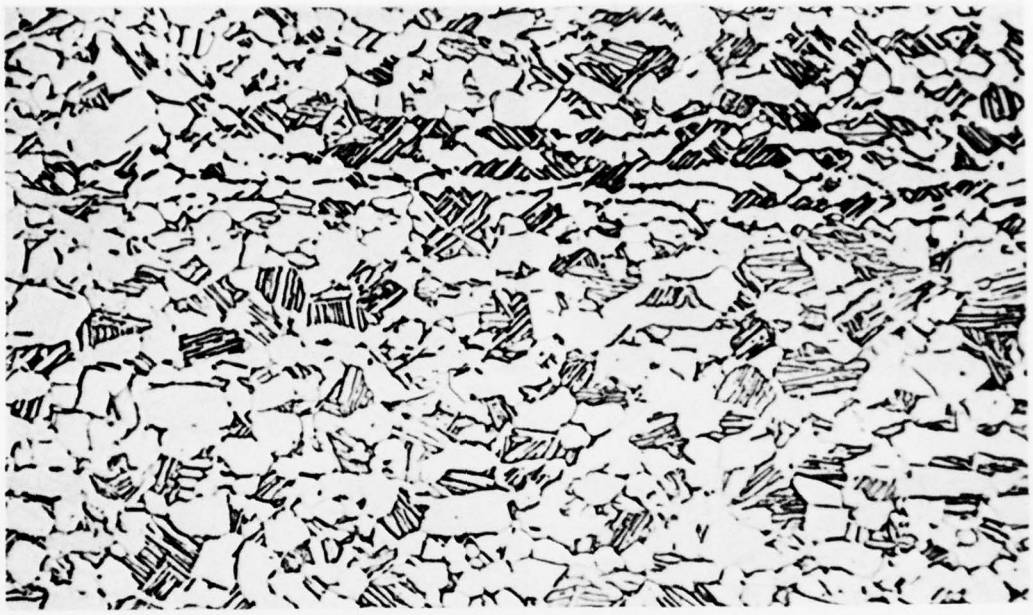

C7741 (a) 500×

C7742 (b) 3000×

Fig. 25 Ti-6 Al-4 V Condition 66. Vacuum creep flattened, standard grade, 1-in. plate, 1775°F-1/2 h-AC, 1450°F-1 h-FC. K_{Ic} = 74 ksi-in.$^{1/2}$, K_{Iscc} = 29 ksi-in.$^{1/2}$, F_{ty} = 134 ksi

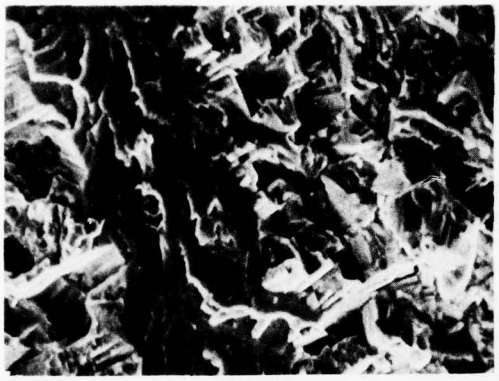

6LIL (a) Fatigue 550×

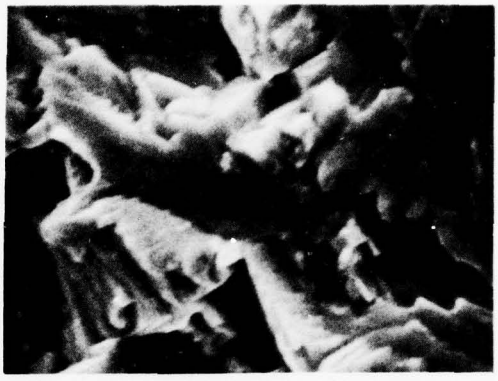

6LIM (b) Fatigue 2350×

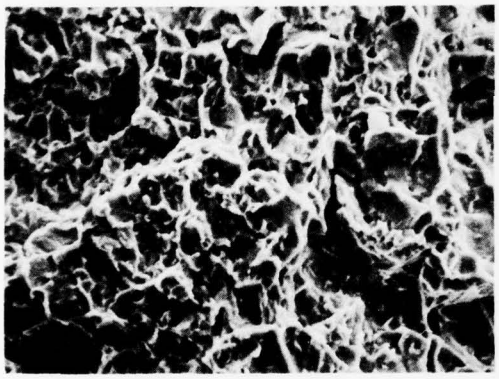

6LIN (c) Fast Fracture 575×

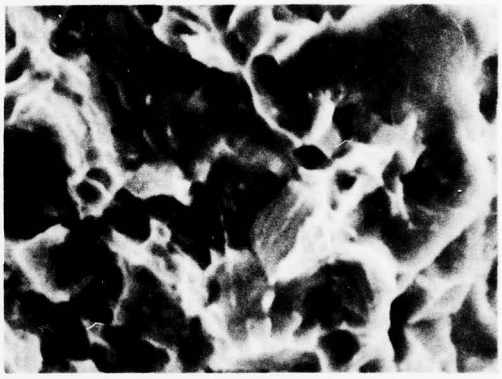

6LIO (d) Fast Fracture 2300×

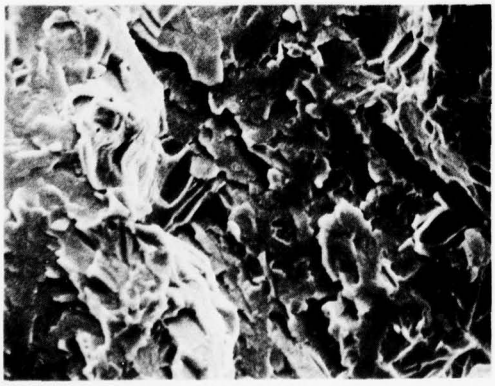

6LLU (e) SCC 625×

6LLV (f) SCC 2450×

Fig. 26 SEM Fractographs of Ti-6 Al-4V Condition 66

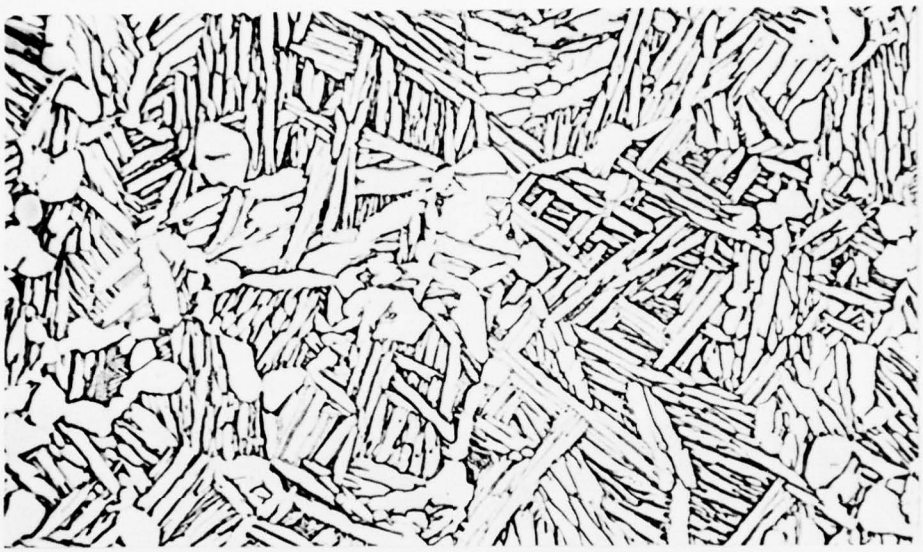

C7743 (a) 500×

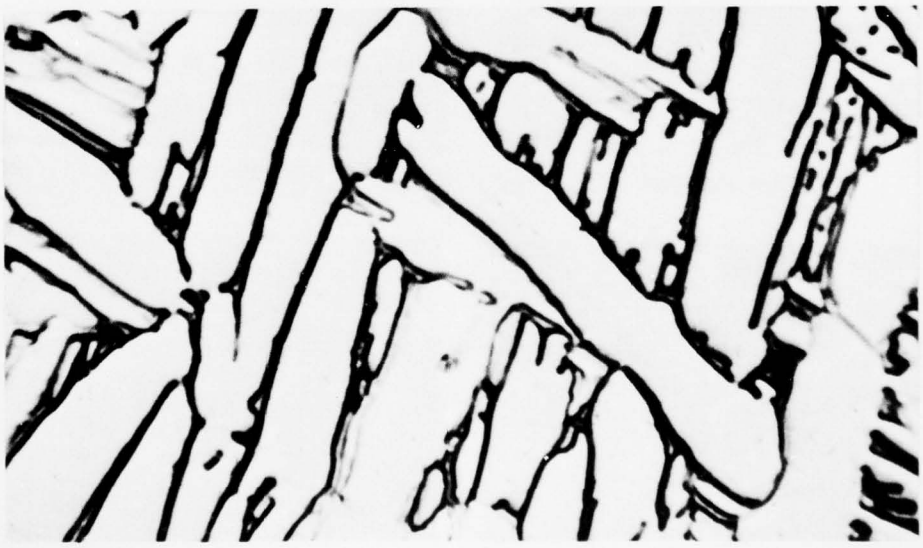

C7744 (b) 3000×

Fig. 27 Ti-6 Al-4 V Condition 67. Vacuum creep flattened, standard grade, 1-in. plate, 1825°F-1/2 h-AC, 1775°F-1/2 h-AC, 1450°F-1 h-AC. K_{Ic} = 80 ksi-in.$^{1/2}$, K_{Iscc} = 54 ksi-in.$^{1/2}$, F_{ty} = 127 ksi

Fig. 14 SEM Fractographs of Ti-6 Al-4V Condition 54

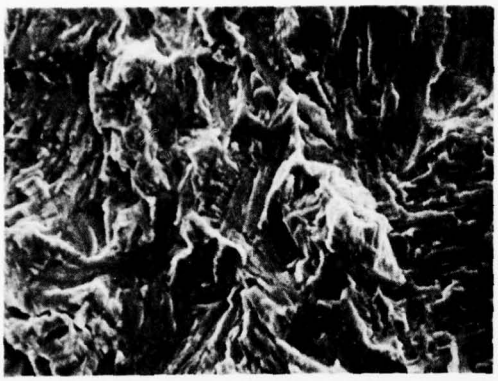

6LIP (a) Fatigue 550×

6LIQ (b) Fatigue 2200×

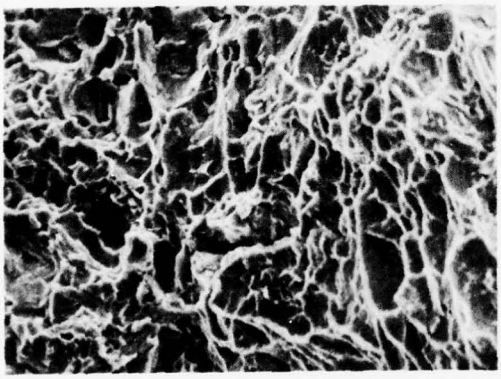

6LIR (c) Fast Fracture 550×

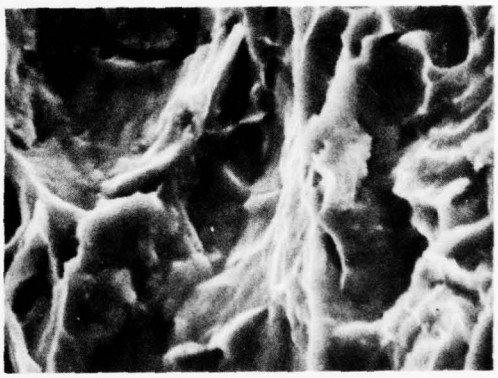

6LIS (d) Fast Fracture 2200×

6LLY (e) SCC 625×

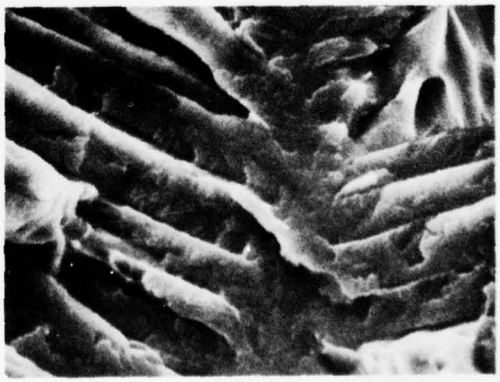

6LLZ (f) SCC 2500×

Fig. 28 SEM Fractographs of Ti-6 Al-4V Condition 67

1775°F-1/2 h-AC, 1450°F-1 h-AC. K_{Ic} = [illegible] ksi-in.$^{1/2}$,
F_{ty} = 136 ksi

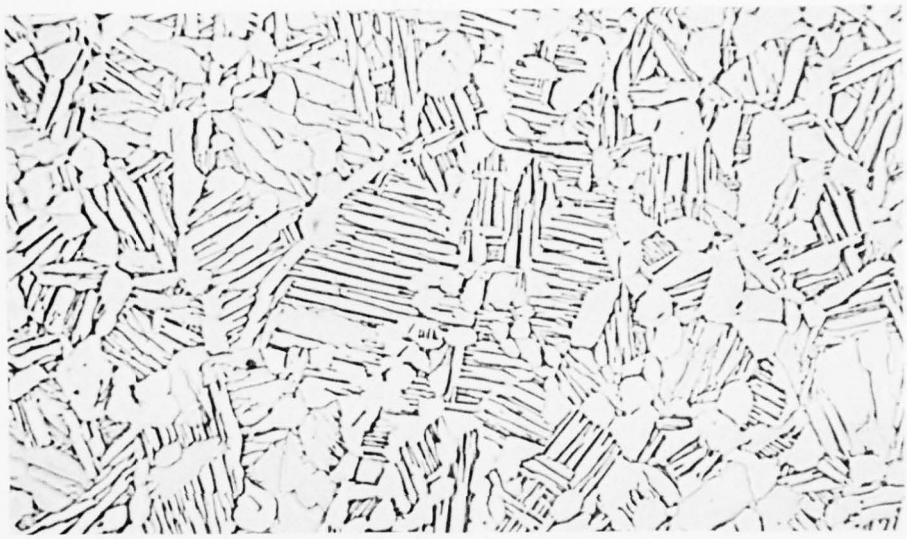

C7733 (a) 500×

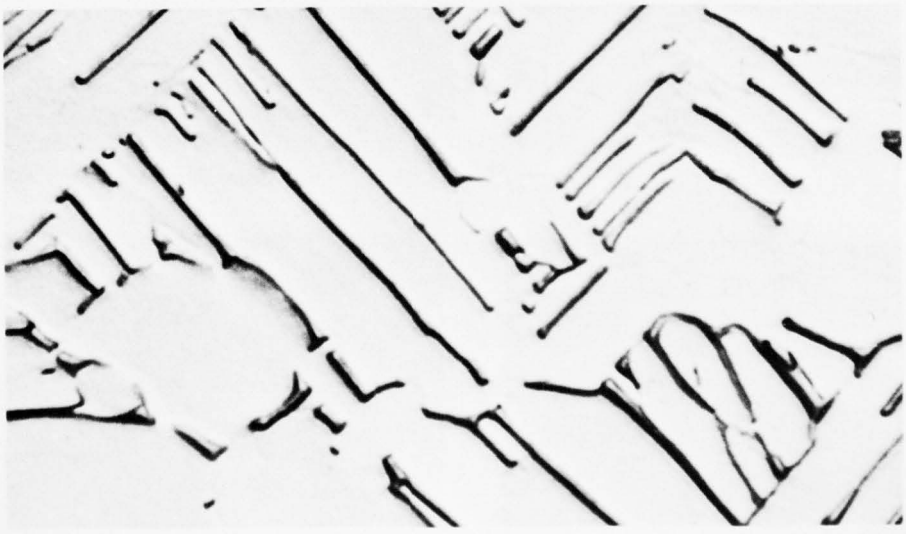

C7734 (b) 3000×

Fig. 29 Ti-6 Al-4 V Condition 69. Vacuum creep flattened, standard grade, 1-in. plate, 1825°F-1/2 h-AC, 1775°F-1/2 h-AC, 1450°F- 1 h-FC. K_{Ic} = 82 ksi-in.$^{1/2}$, K_{Iscc} = 32 ksi-in.$^{1/2}$, F_{ty} = 132 ksi

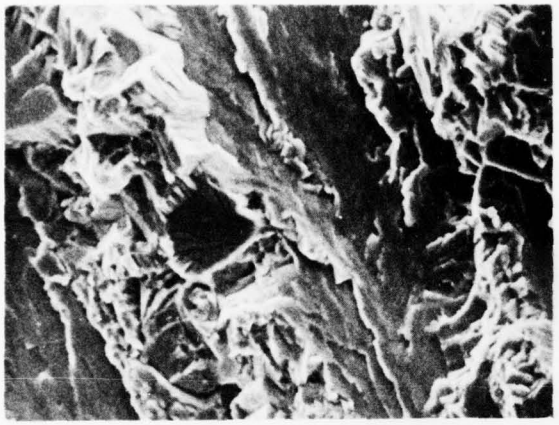

6LIX (a) Fatigue 575×

6LIY (b) Fatigue 2300×

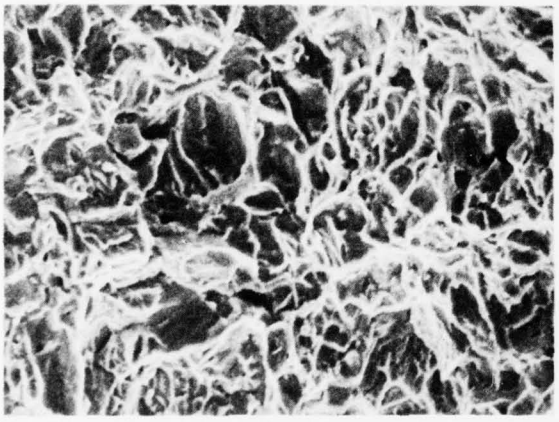

6LIV (c) Fast Fracture 525×

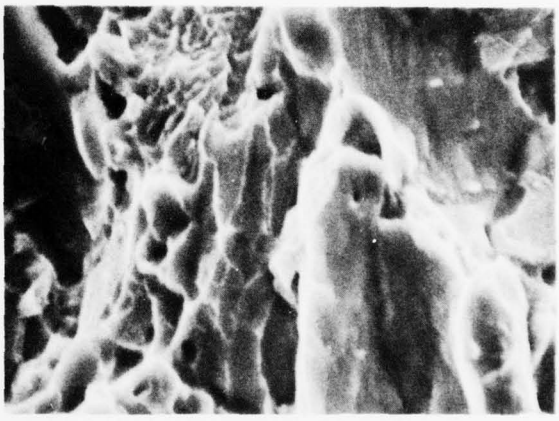

6LIW (d) Fast Fracture 2100×

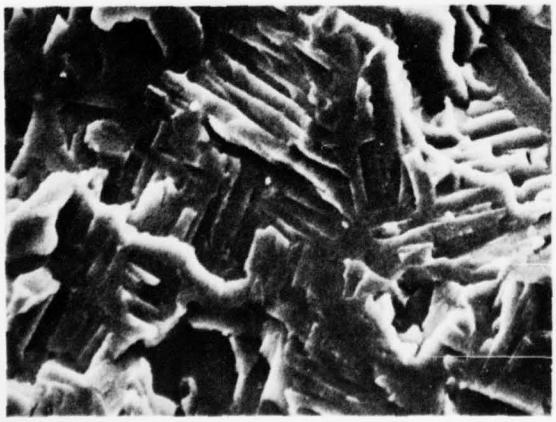

6LLO (e) SCC 625×

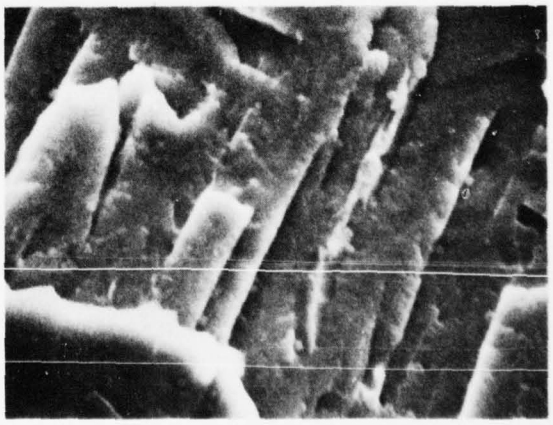

6LLP (f) SCC 2500×

Fig. 30 SEM Fractographs of Ti-6 Al-4V Condition 69

C7763 (a) 500×

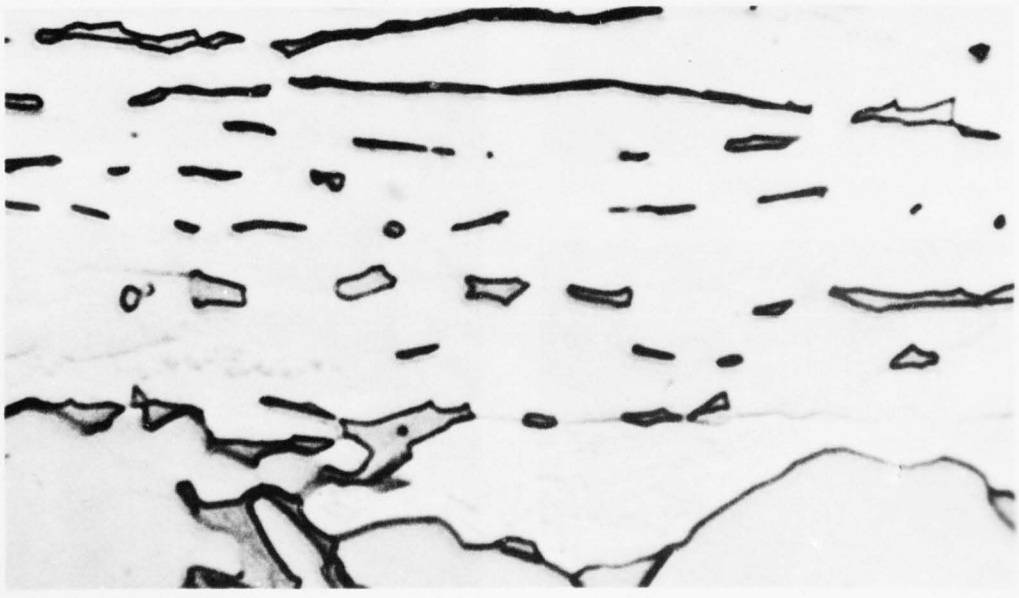

C7764 (b) 3000×

Fig. 31 Ti-6 Al-4V Condition 70. Vacuum creep flattened. ELI grade, 1-in. plate, as received. K_{Ic} = 71 ksi-in.$^{1/2}$, K_{Iscc} = 50 ksi-in.$^{1/2}$, F_{ty} = 138 ksi

AD-A043 741 LOCKHEED MISSILES AND SPACE CO INC PALO ALTO CALIF PA--ETC F/G 11/6
CORRELATION OF MICROSTRUCTURE WITH FRACTURE TOUGHNESS PROPERTIE--ETC(U)
JAN 77 R E LEWIS, F A CROSSLEY N00019-75-C-0378
UNCLASSIFIED LMSC-D555813 NL

2 OF 2
AD
A043 741

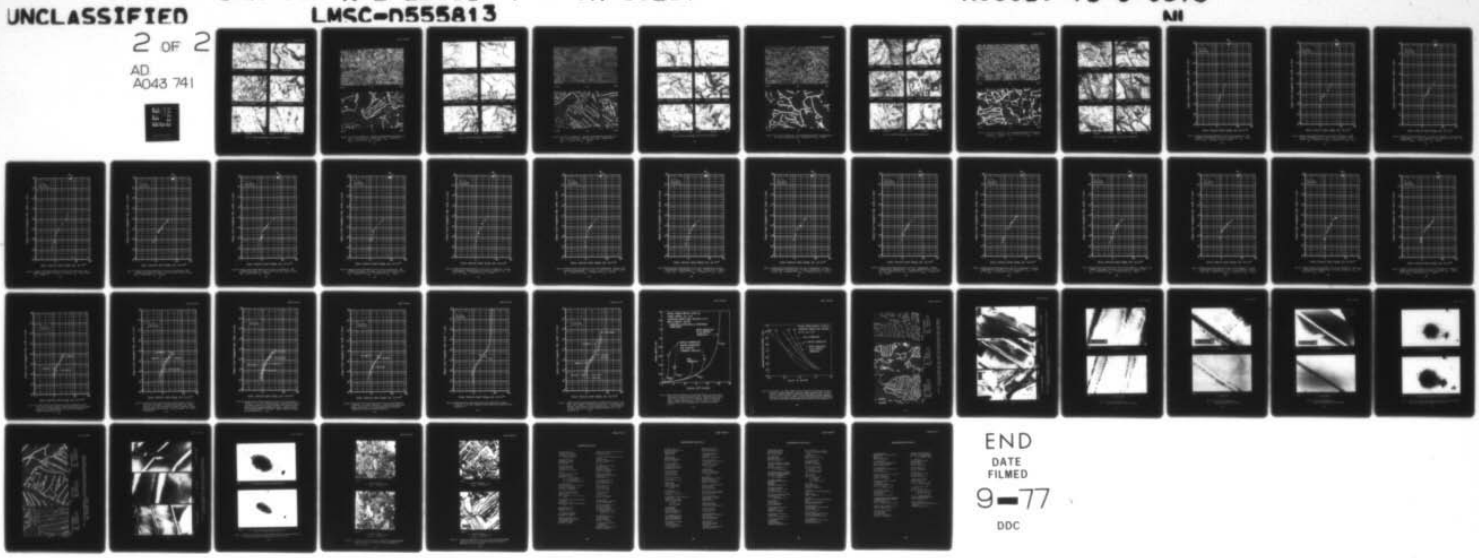

END
DATE
FILMED
9-77
DDC

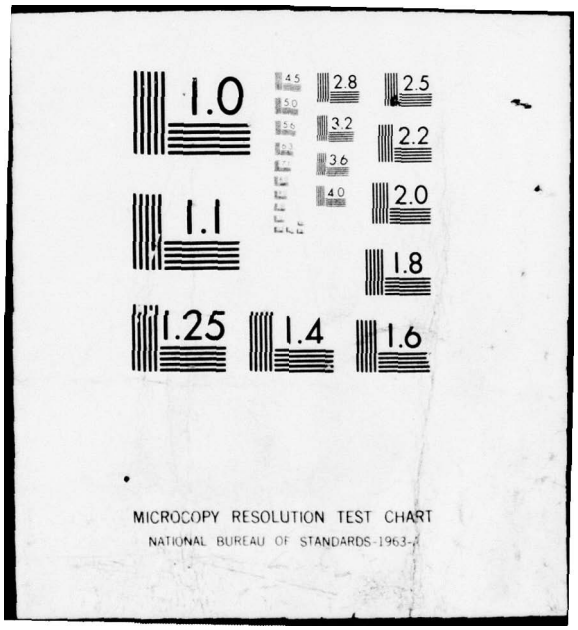
1.0
1.1
1.25
1.4
1.6
1.8
2.0
2.2
2.5
2.8
3.2
3.6
4.0
4.5
5.0
5.6
MICROCOPY RESOLUTION TEST CHART
NATIONAL BUREAU OF STANDARDS-1963-A

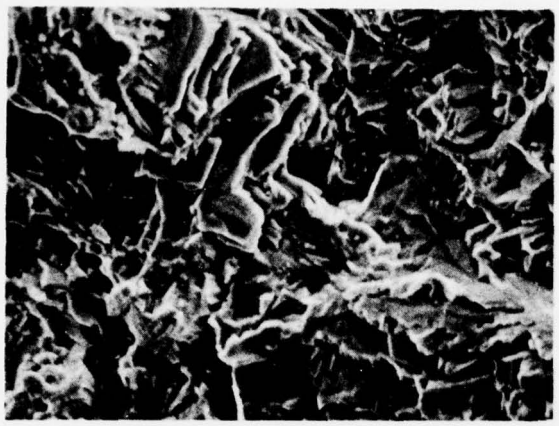

6LIT (a) Fatigue 540×

6LIU (b) Fatigue 2150×

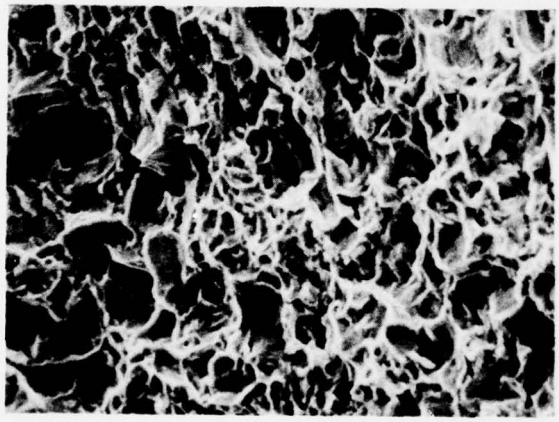

6LMZ (c) Fast Fracture 560×

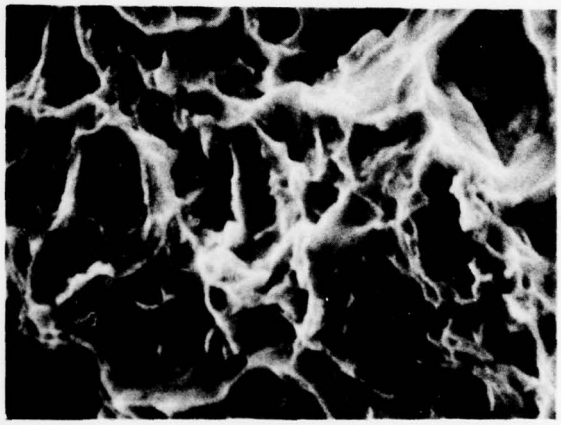

6LJA (d) Fast Fracture 2250×

6LLH (e) SCC 560×

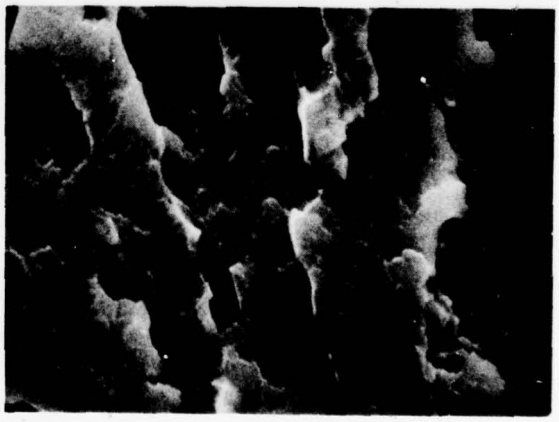

6LLI (f) SCC 2250×

Fig. 32 SEM Fractographs of Ti-6 Al-4V Condition 70

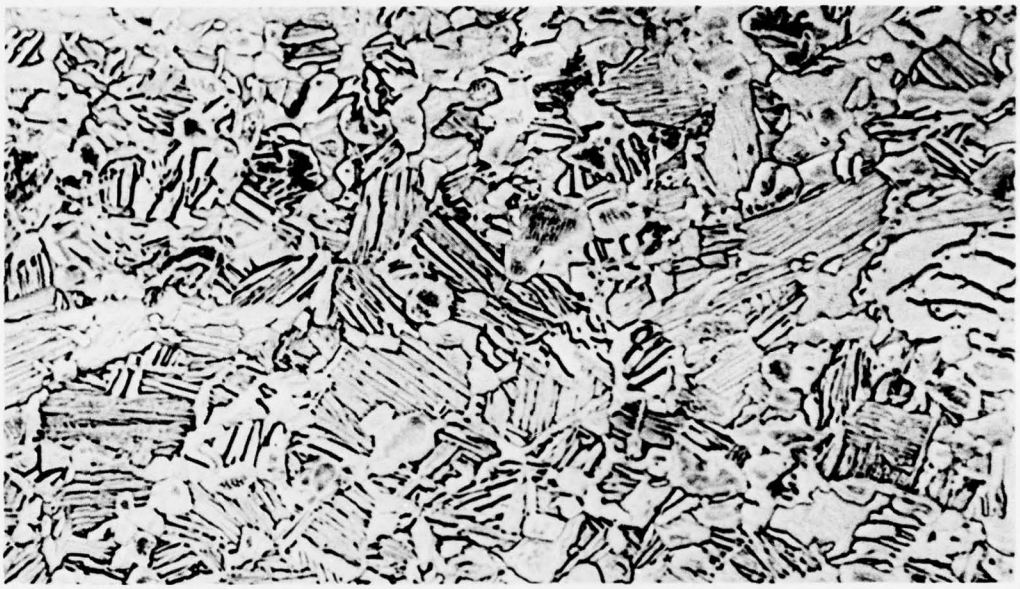

C7747 (a) 500×

C7748 (b) 3000×

Fig. 33 Ti-6 Al-4 V Condition 71. Vacuum creep flattened, ELI grade, 1-in. plate, 1775°F-1/2 h-AC, 1450°F-1 h-AC. K_{Ic} = 84 ksi-in.$^{1/2}$, K_{Iscc} = 38 ksi-in.$^{1/2}$, F_{ty} = 134 ksi

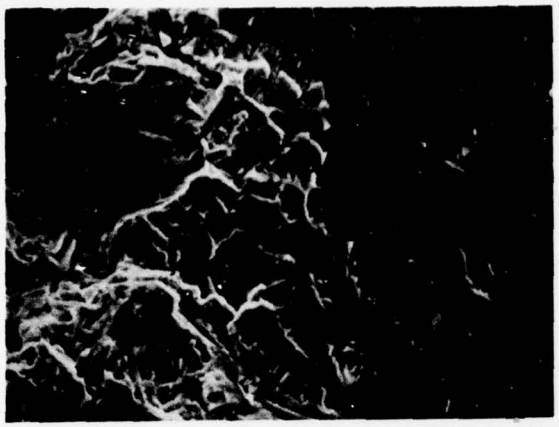

6LJB (a) Fatigue 540×

6LJC (b) Fatigue 2150×

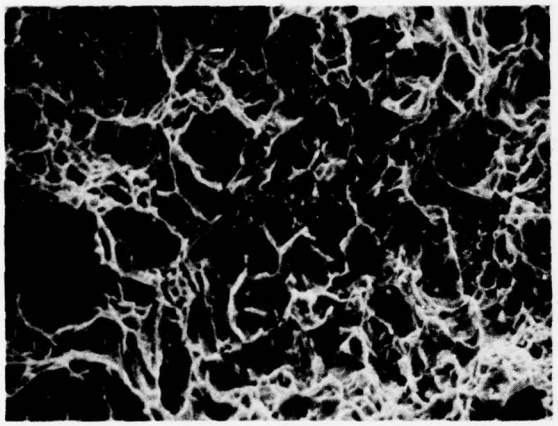

6LJD (c) Fast Fracture 525×

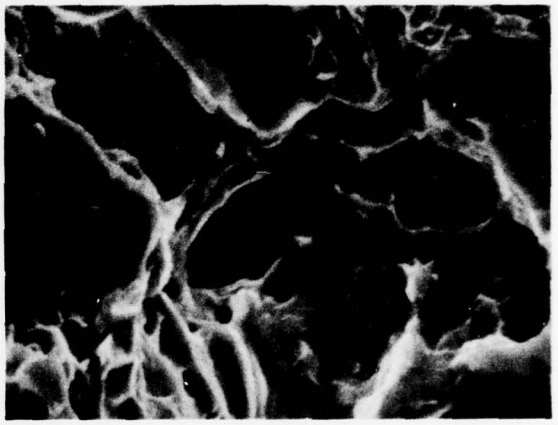

6LJE (d) Fast Fracture 2100×

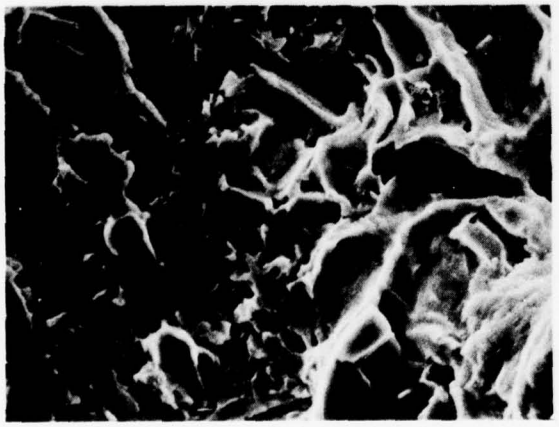

6LLF (e) SCC 590×

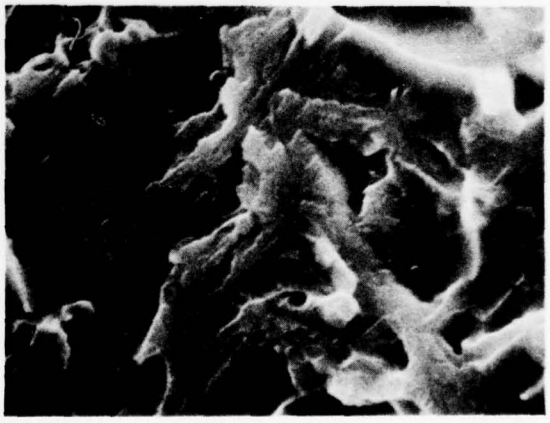

6LLG (f) SCC 2350×

Fig. 34 SEM Fractographs of Ti-6 Al-4V Condition 71

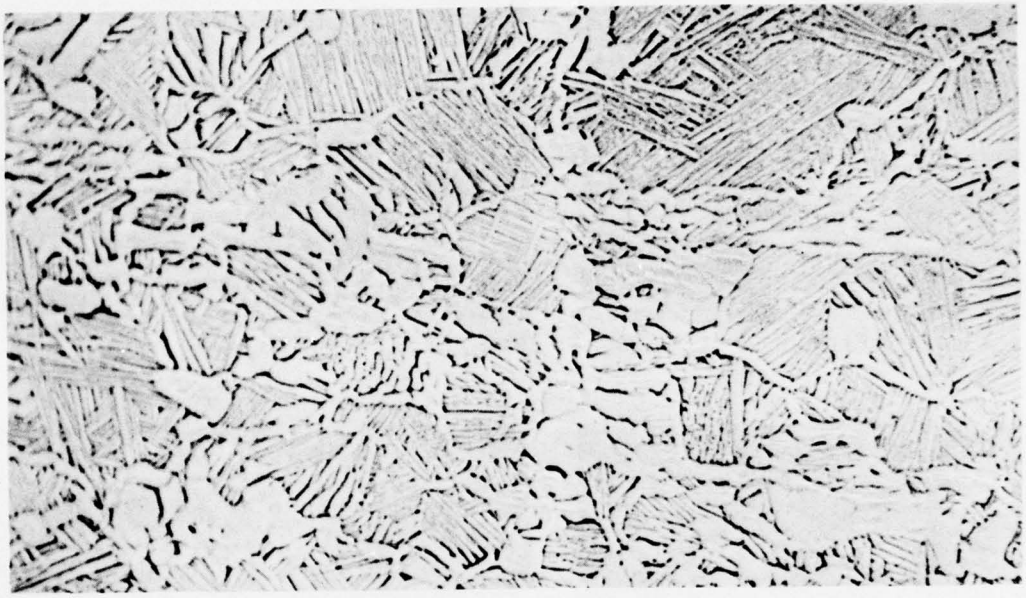

C7765 (a) 500×

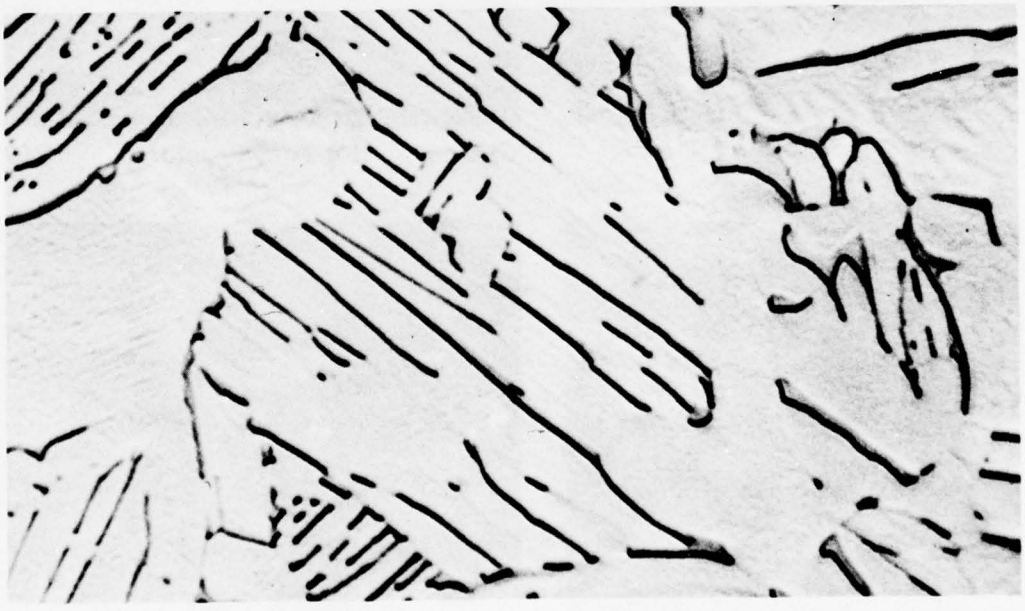

C7766 (b) 3000×

Fig. 35 Ti-6 Al-4 V Condition 73. Vacuum creep flattened, ELI grade, 1-in. plate, 1775°F-1/2 h-AC, 1450°F-1 h-FC. K_{Ic} = 76 ksi-in.$^{1/2}$, K_{Iscc} = 28 ksi-in.$^{1/2}$, F_{ty} = 138 ksi

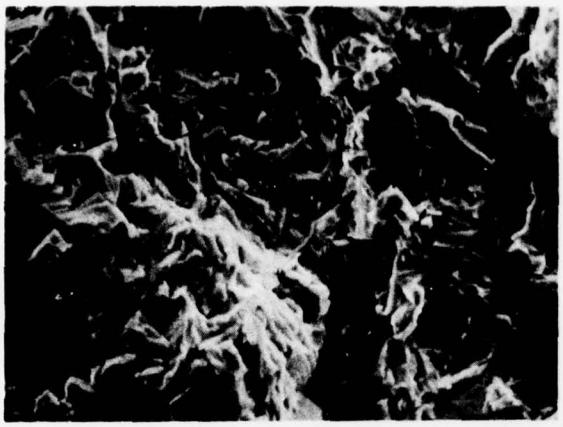

6LJF (a) Fatigue 600×

6LJG (b) Fatigue 2400×

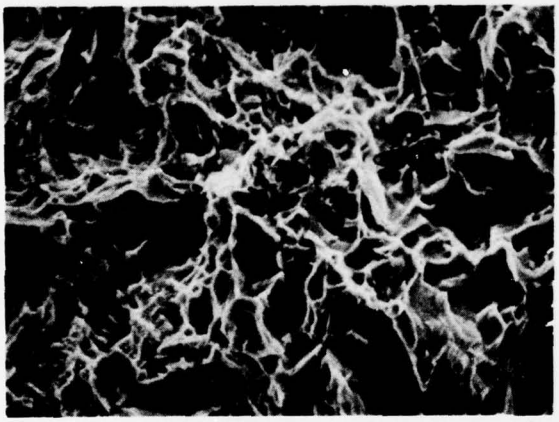

6LJH (c) Fast Fracture 600×

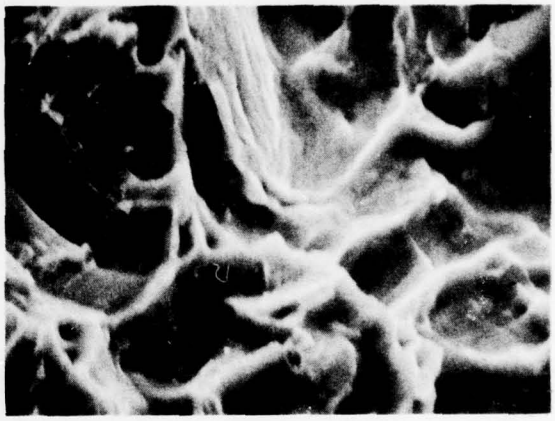

6LJI (d) Fast Fracture 2400×

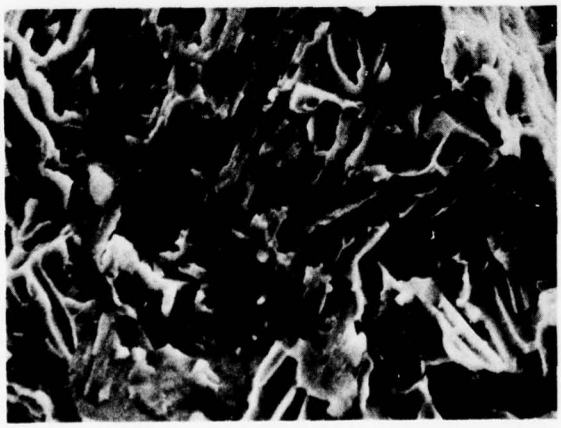

6LLM (e) SCC 590×

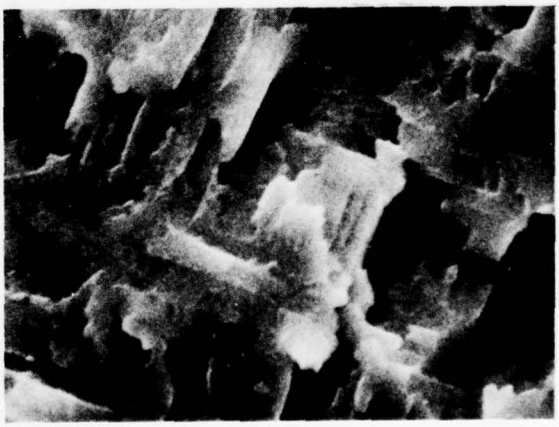

6LLN (f) SCC 2375×

Fig. 36 SEM Fractographs of Ti-6 Al-4V Condition 73

C7753 (a) 500×

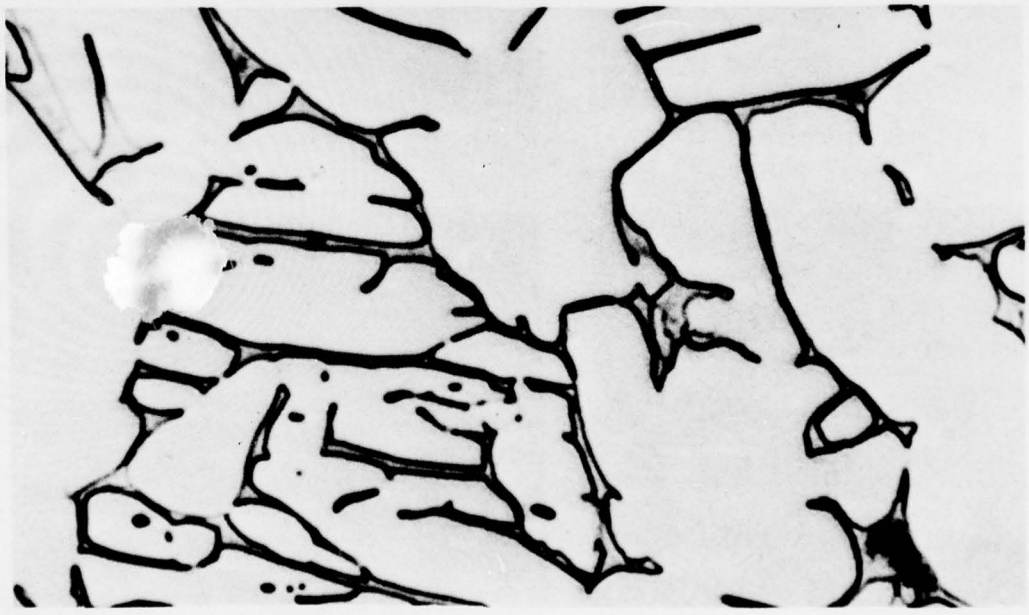

C7754 (b) 3000×

Fig. 37 Ti-6 Al-4 V Condition 76. Recrystallization annealed, standard grade, 1-in. plate, as-received. K_Q = 85 ksi-in.$^{1/2}$, F_{ty} = 127 ksi

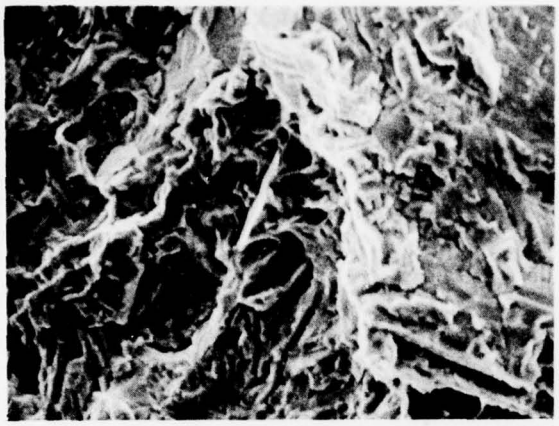

6LJN (a) Fatigue 575×

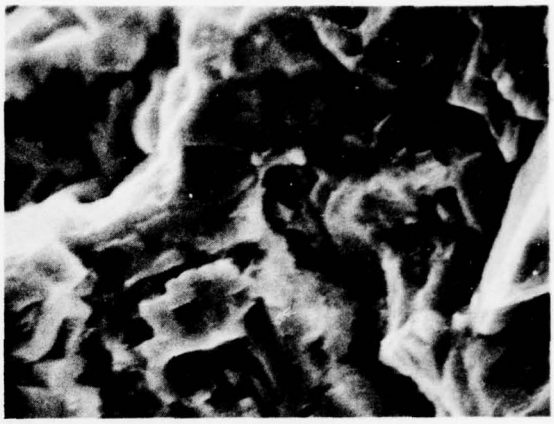

6LJO (b) Fatigue 2300×

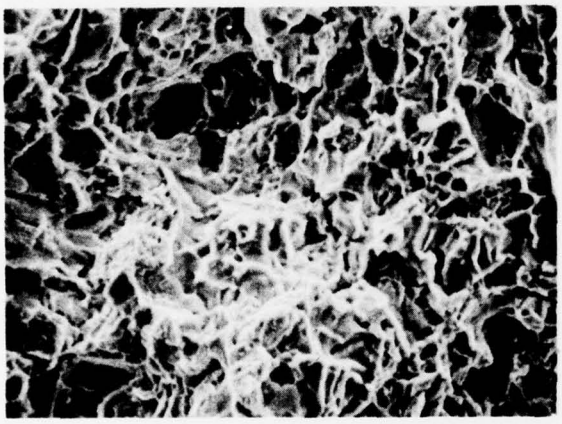

6LJP (c) Fast Fracture 575×

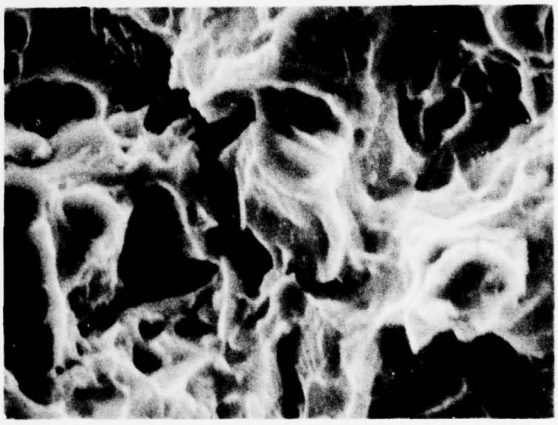

6LJQ (d) Fast Fracture 2300×

6LLJ (e) SCC 525×

6LLL (f) SCC 2100×

Fig. 38 SEM Fractographs of Ti-6 Al-4V Condition 76

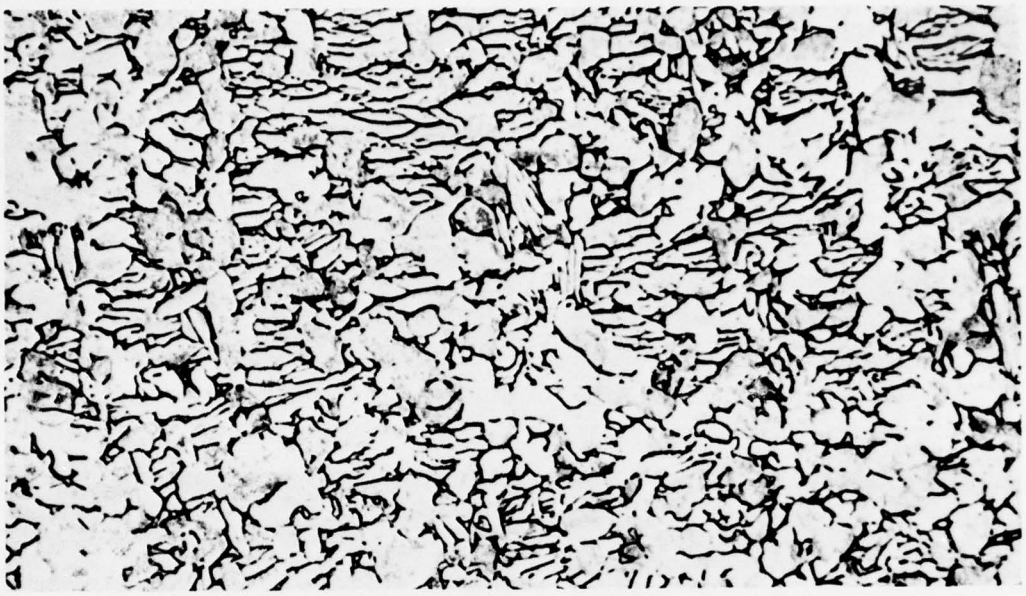

C7755 (a) 500×

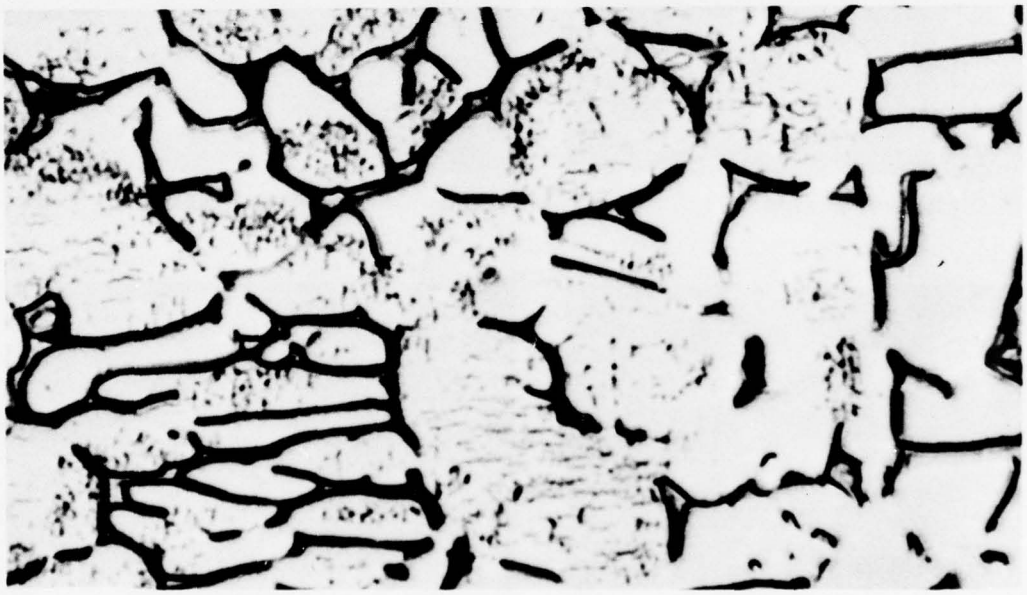

C7756 (b) 3000×

Fig. 39 Ti-6 Al-4 V Condition 75. Recrystallization annealed, ELI grade, 1-in. plate, as-received. K_{Ic} = 82 ksi-in.$^{1/2}$, K_{Iscc} = 36 ksi-in.$^{1/2}$, F_{ty} = 132 ksi

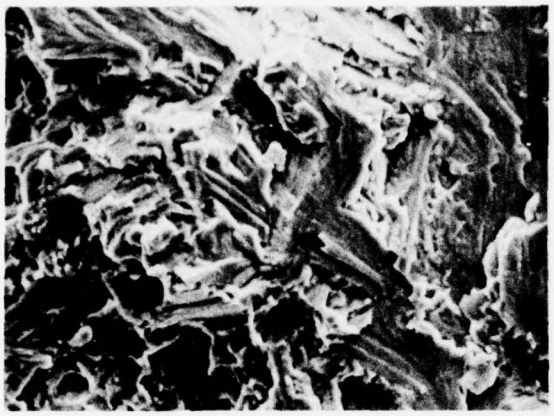

6LJJ (a) Fatigue 575×

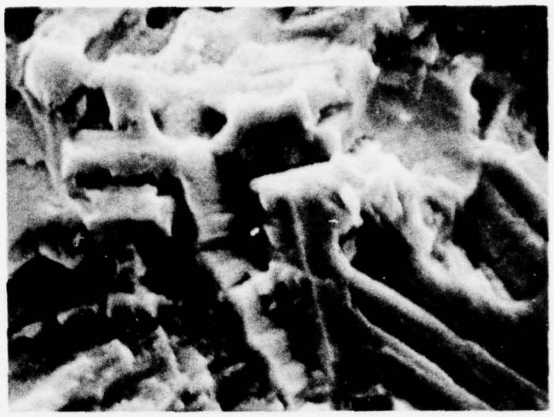

6LJK (b) Fatigue 2300×

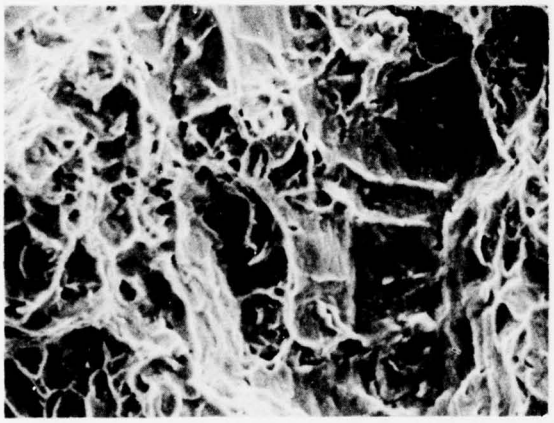

6LJL (c) Fast Fracture 560×

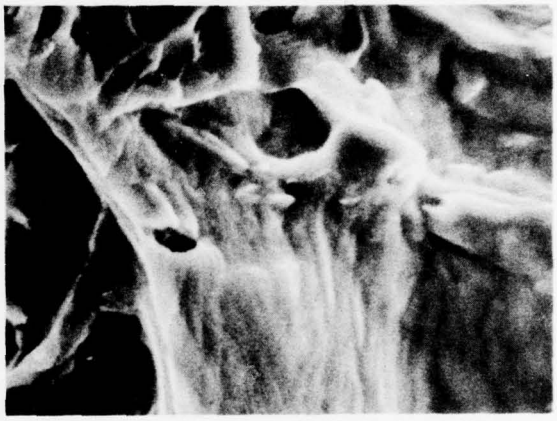

6LJM (d) Fast Fracture 2250×

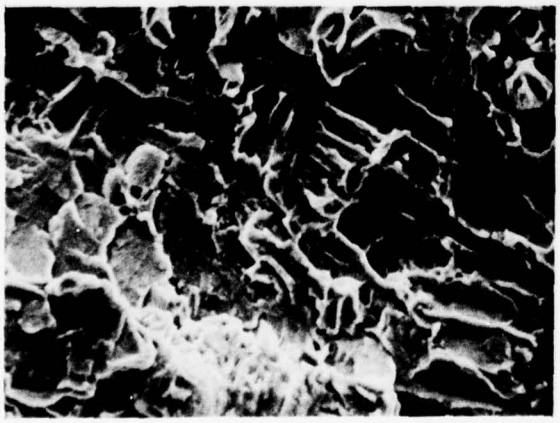

6LLQ (e) SCC 590×

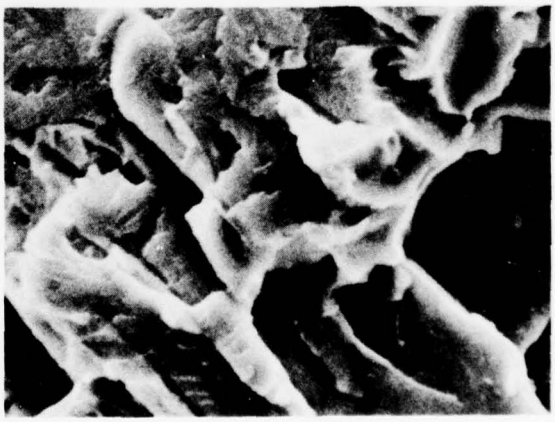

6LLR (f) SCC 2350×

Fig. 40 SEM Fractographs of Ti-6 Al-4V Condition 75

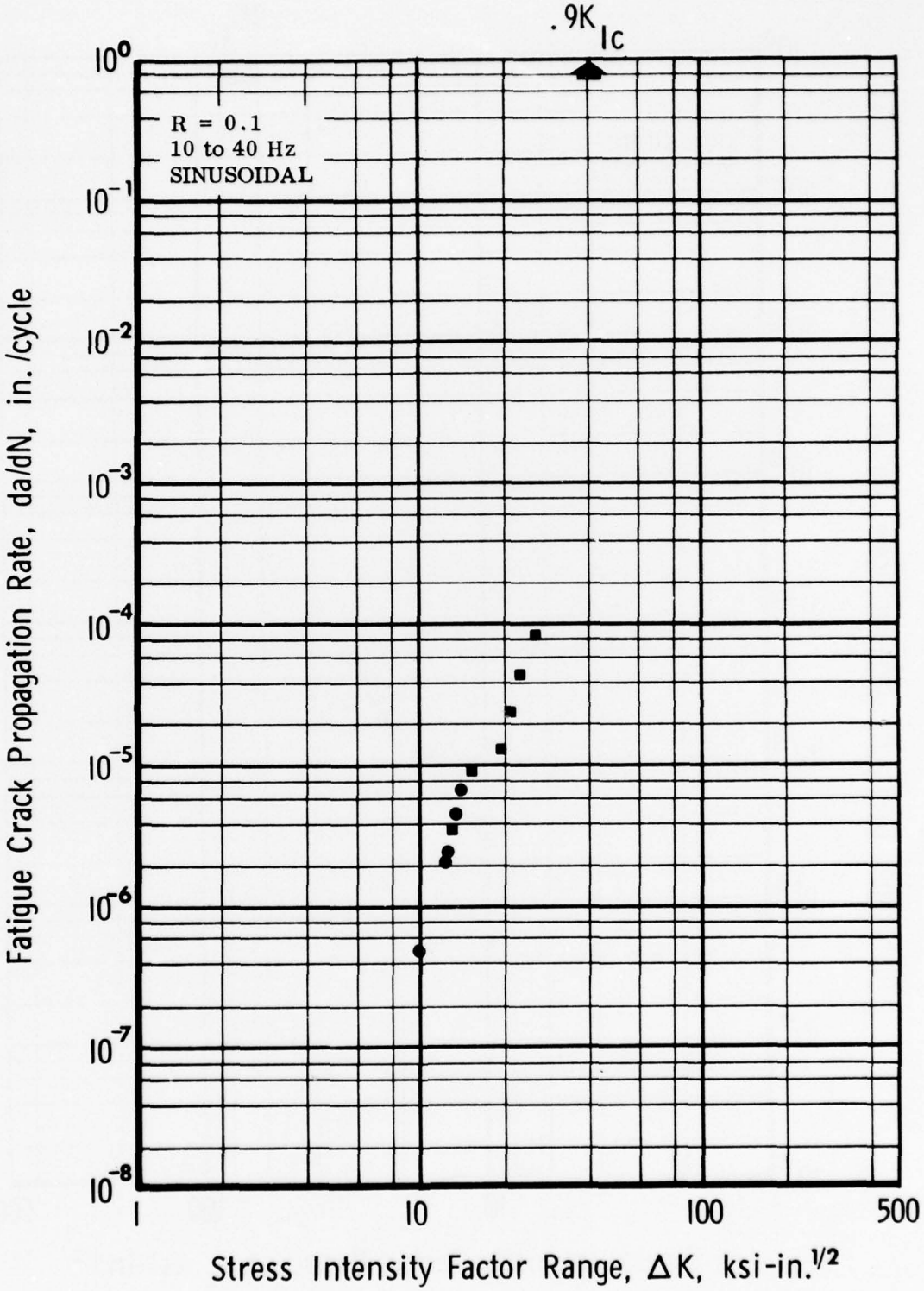

Fig. 41 Fatigue Crack Growth Behavior in Ti-6 Al-4 V Condition 50. Mill annealed, standard grade, 1-in. plate, as-received. K_{Ic} = 45 ksi-in.$^{1/2}$, K_{Iscc} = 45 ksi-in.$^{1/2}$, F_{ty} = 147 ksi

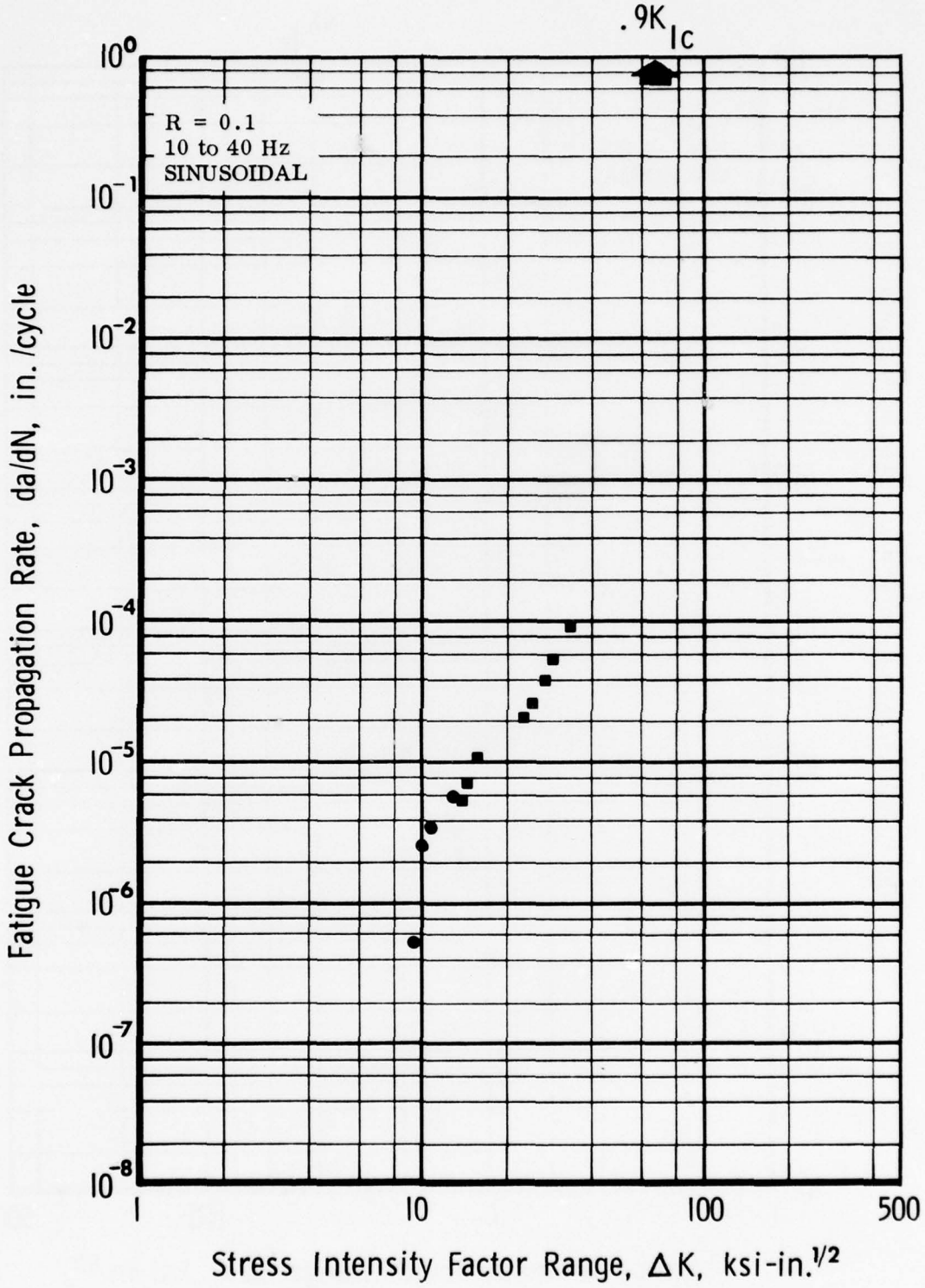

Fig. 42 Fatigue Crack Growth Behavior in Ti-6 Al-4 V Condition 51. Mill annealed, standard grade, 1-in. plate, 1775°F-1/2 h-AC, 1450°F-1 h-AC. K_{Ic} = 65 ksi-in.$^{1/2}$, K_{Iscc} = 44 ksi-in.$^{1/2}$, F_{ty} = 137 ksi

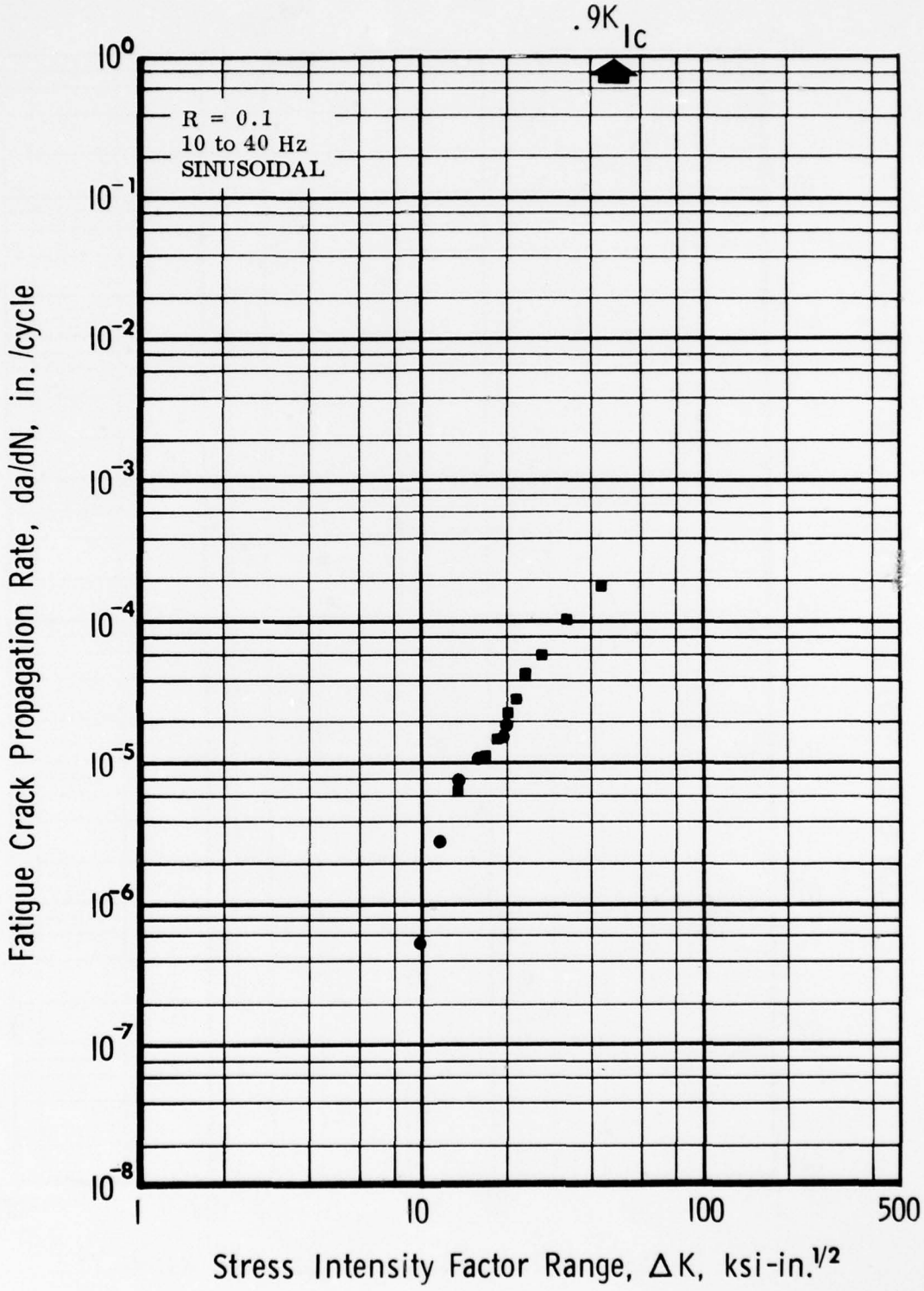

Fig. 43 Fatigue Crack Growth Behavior in Ti-6 Al-4 V Condition 53. Mill annealed, standard grade, 1-in. plate, 1775°F-1/2 h-AC, 1450°F-1 h-FC. K_{Ic} = 55 ksi-in.$^{1/2}$, K_{Iscc} = 45 ksi-in.$^{1/2}$, F_{ty} = 140 ksi

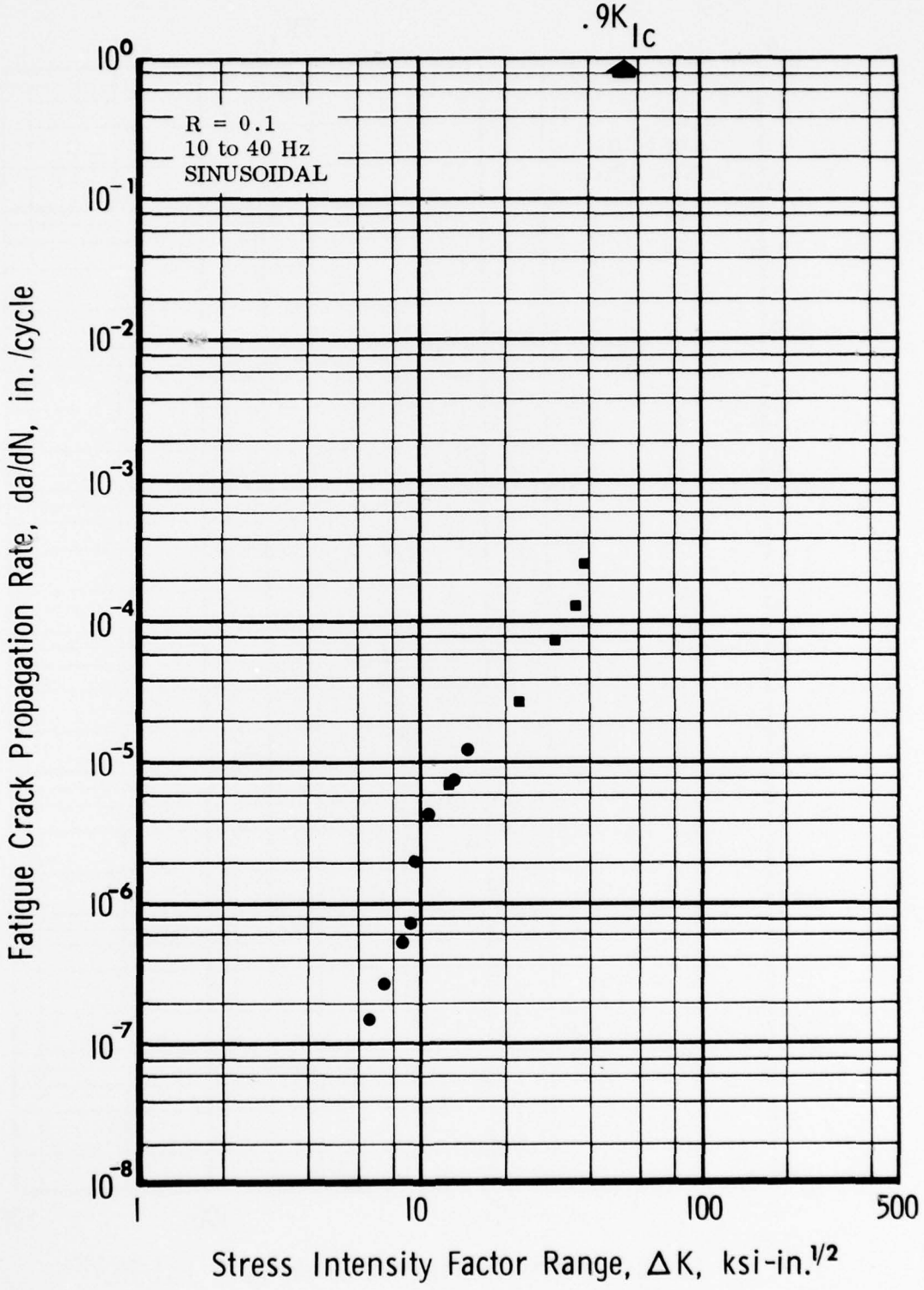

Fig. 44 Fatigue Crack Growth Behavior in Ti-6 Al-4 V Condition 54. Mill annealed, ELI grade, 1-in. plate, as-received. K_{Ic} = 60 ksi-in.$^{1/2}$, F_{ty} = 144 ksi

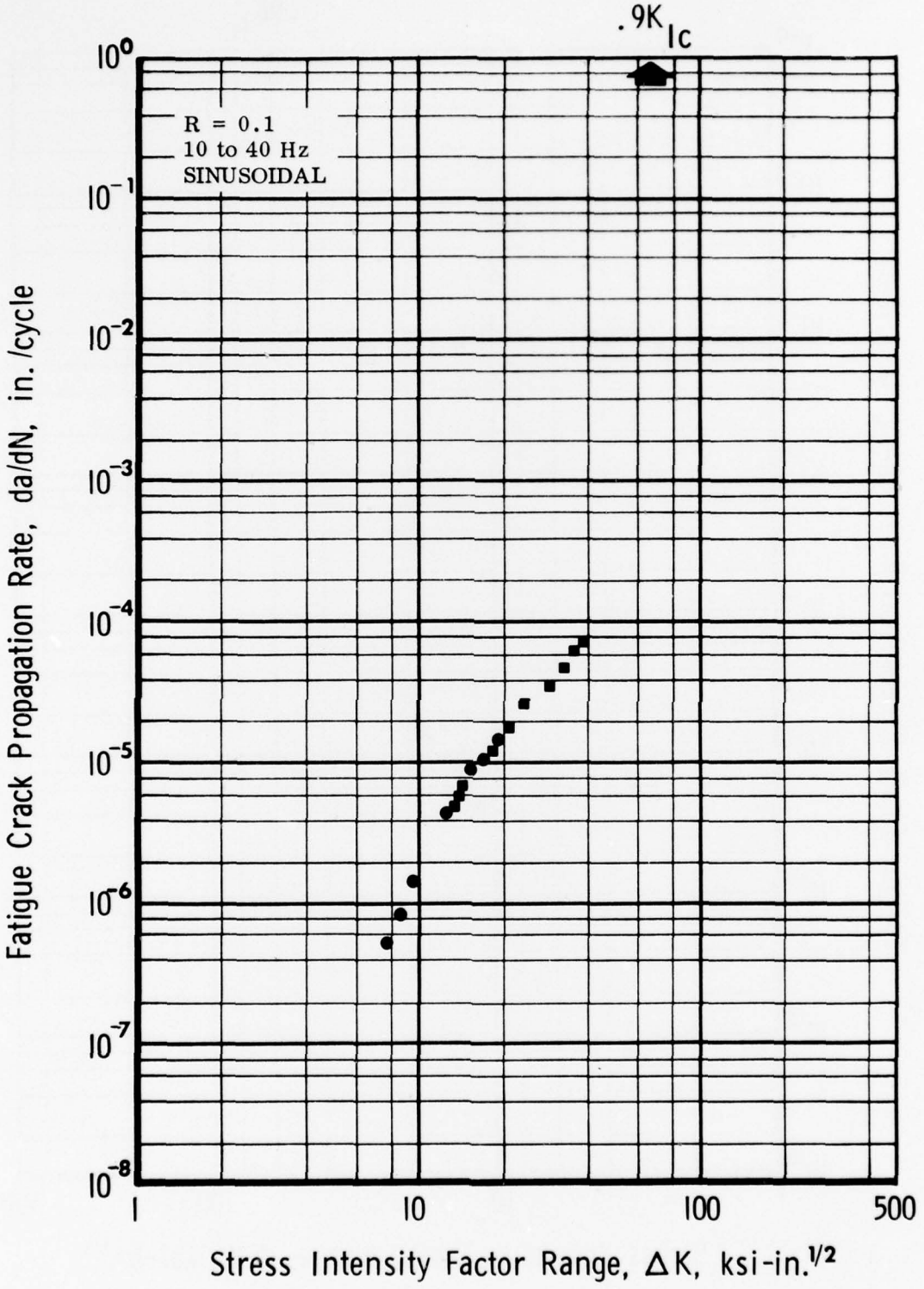

Fig. 45 Fatigue Crack Growth Behavior in Ti-6 Al-4 V Condition 55. Mill annealed, ELI grade, 1-in. plate, 1775°F-1/2 h-AC, 1450°F-1 h-AC. K_{Ic} = 74 ksi-in.$^{1/2}$, F_{ty} = 136 ksi

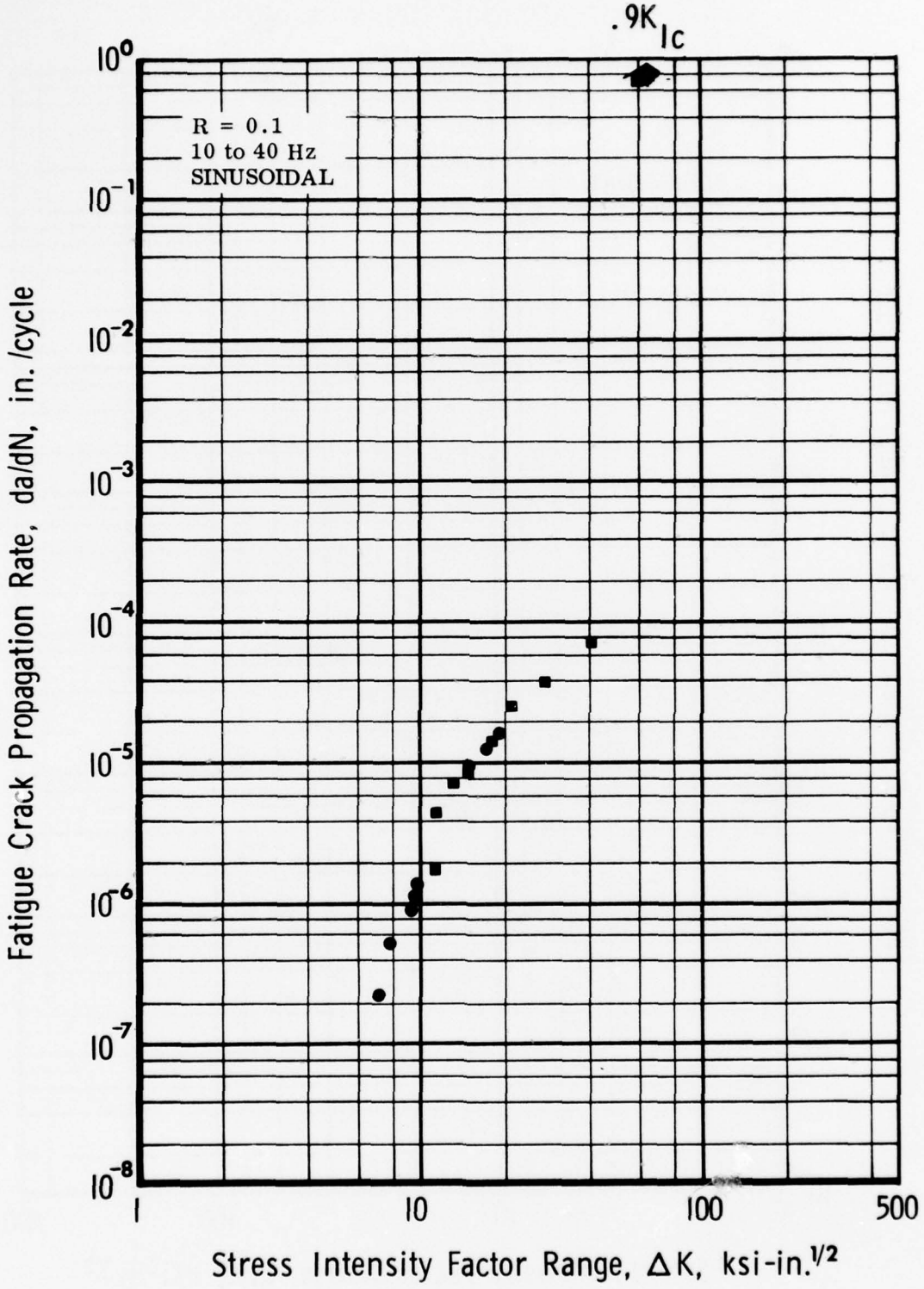

Fig. 46 Fatigue Crack Growth Behavior in Ti-6 Al-4 V Condition 57. Mill annealed, ELI grade, 1-in. plate, 1775°F-1/2 h-AC, 1450°F-1 h-FC. K_{Ic} = 72 ksi-in.$^{1/2}$, F_{ty} = 139 ksi

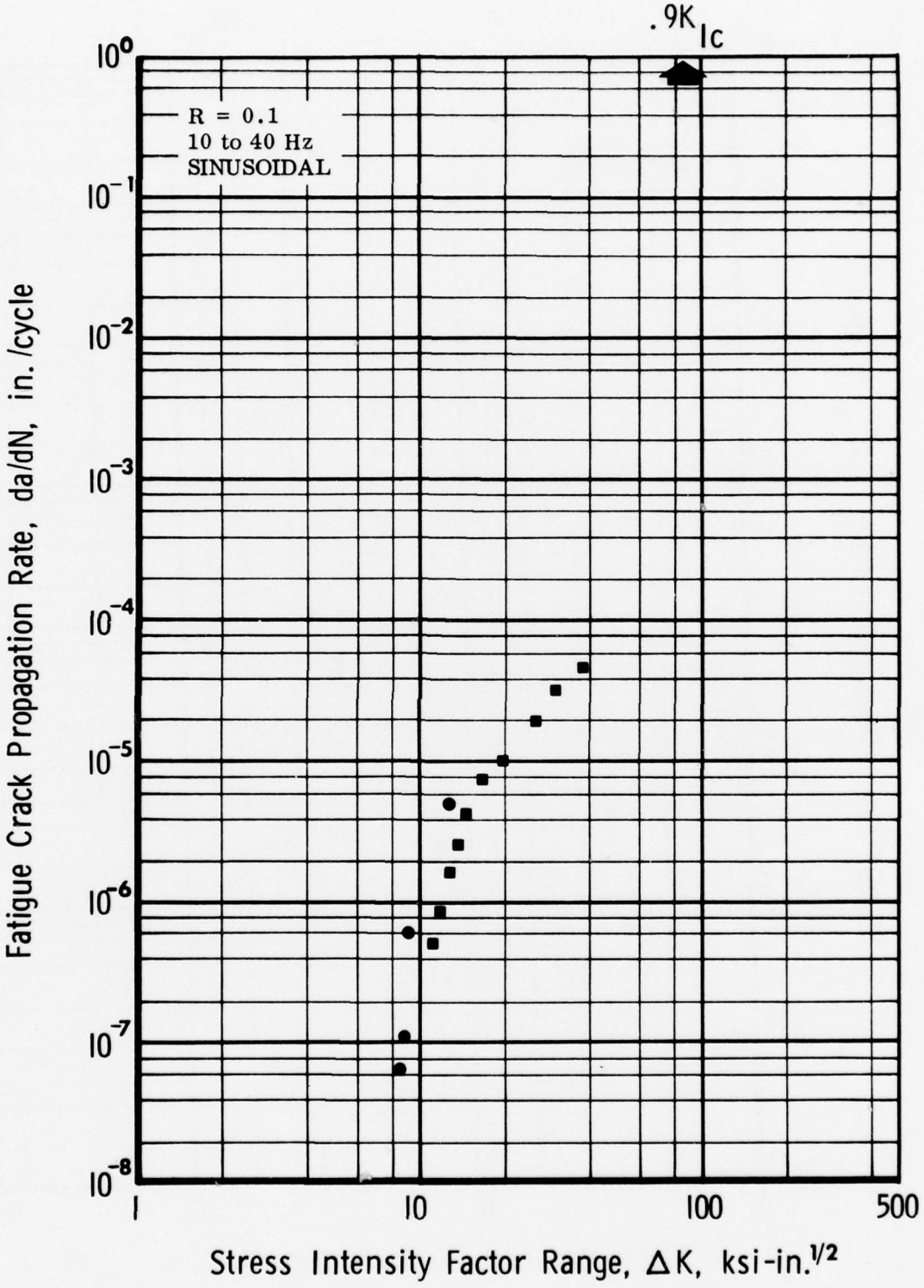

Fig. 47 Fatigue Crack Growth Behavior in Ti-6 Al-4 V Condition 60. Mill annealed, ELI grade, 1-in. plate, 1825°F-1/2 h-AC, 1450°F-1 h-AC. K_Q = 95 ksi-in.$^{1/2}$, K_{Iscc} = 72 ksi-in.$^{1/2}$, F_{ty} = 123 ksi

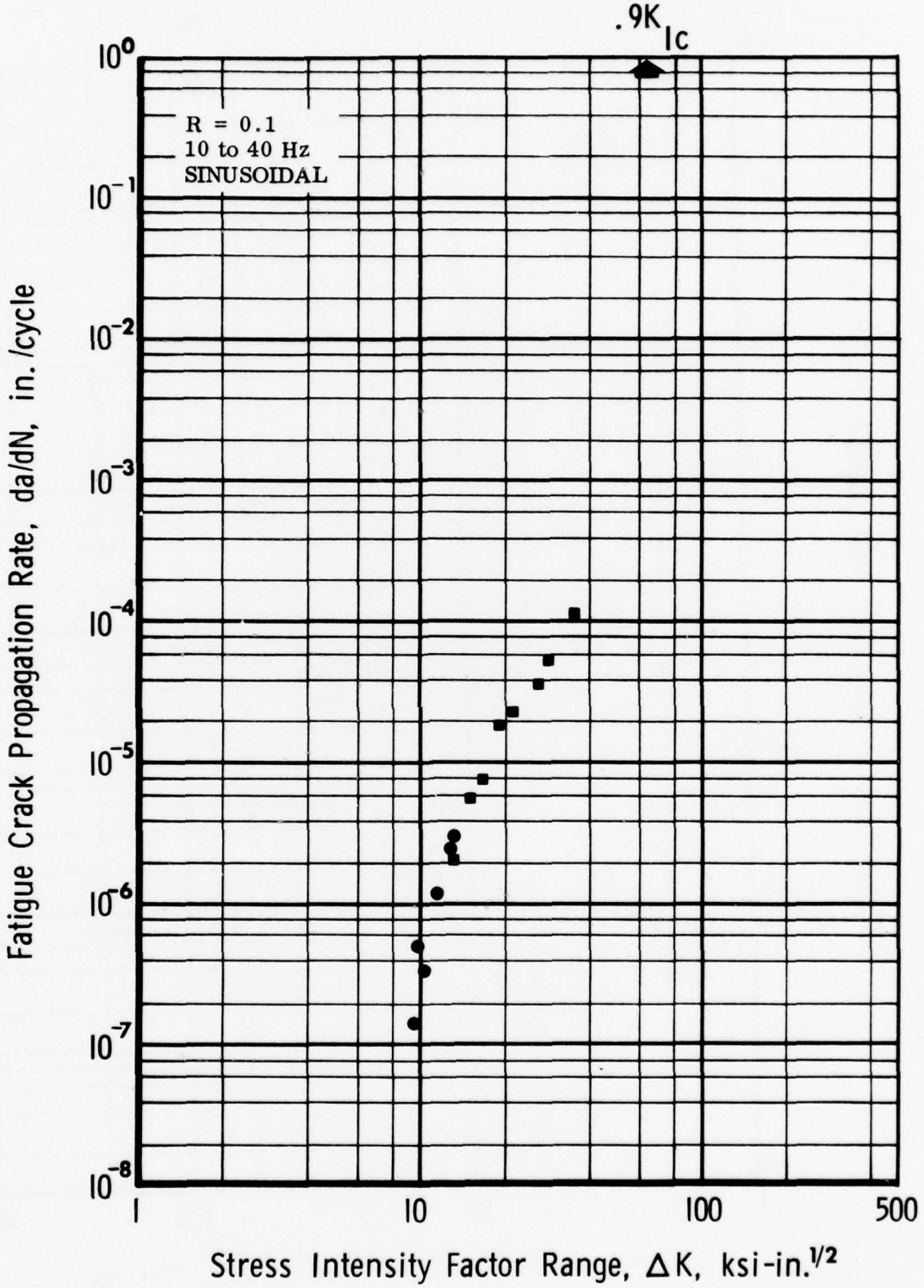

Fig. 48 Fatigue Crack Growth Behavior in Ti-6 Al-4 V Condition 63. Vacuum creep flattened, standard grade, 1-in. plate, as received. K_{Ic} = 70 ksi-in.$^{1/2}$, K_{Iscc} = 40 ksi-in.$^{1/2}$, F_{ty} = 136 ksi

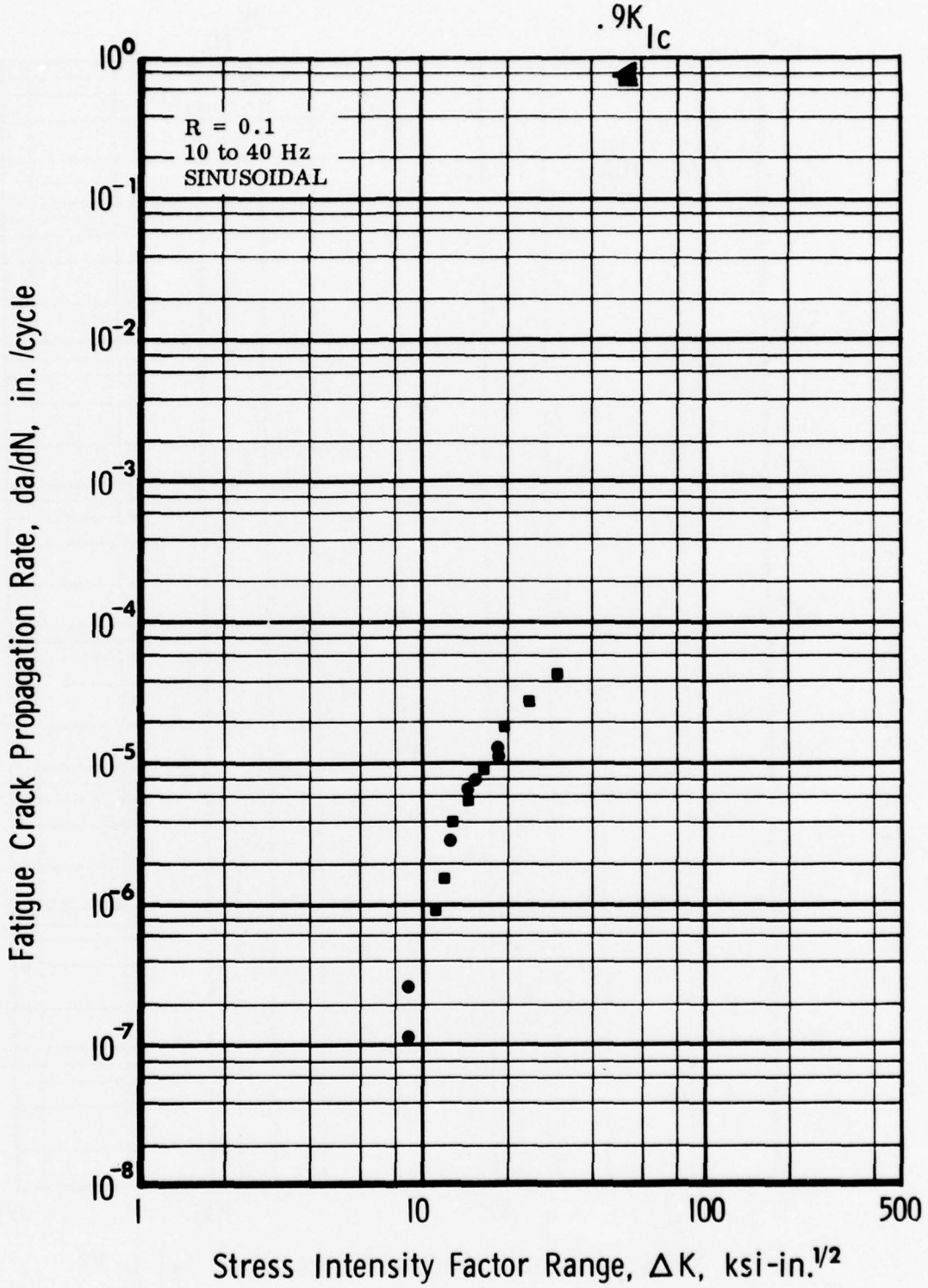

Fig. 49 Fatigue Crack Growth Behavior Ti-6 Al-4 V Condition 64. Vacuum creep flattened, standard grade, 1-in. plate, 1775°F-1/2 h-AC, 1450°F-1 h-AC. K_{Ic} = 64 ksi-in.$^{1/2}$, K_{Iscc} = 28 ksi-in.$^{1/2}$, F_{ty} = 133 ksi

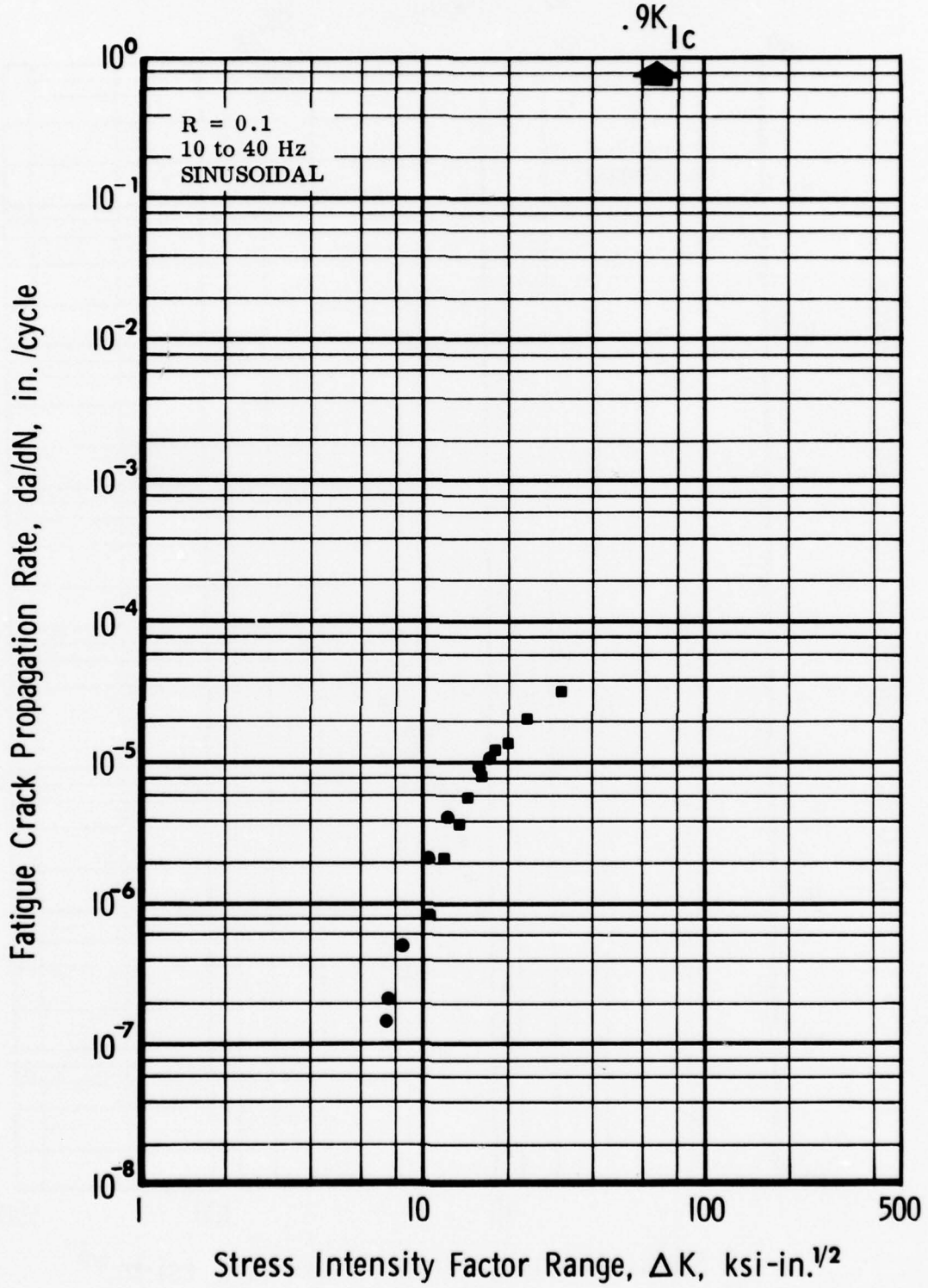

Fig. 50 Fatigue Crack Growth Behavior in Ti-6 Al-4 V Condition 66. Vacuum creep flattened, standard grade, 1-in. plate, 1775°F-1/2 h-AC, 1450°F-1 h-FC. K_{Ic} = 74 ksi-in.$^{1/2}$, K_{Iscc} = 29 ksi-in.$^{1/2}$, F_{ty} = 134 ksi

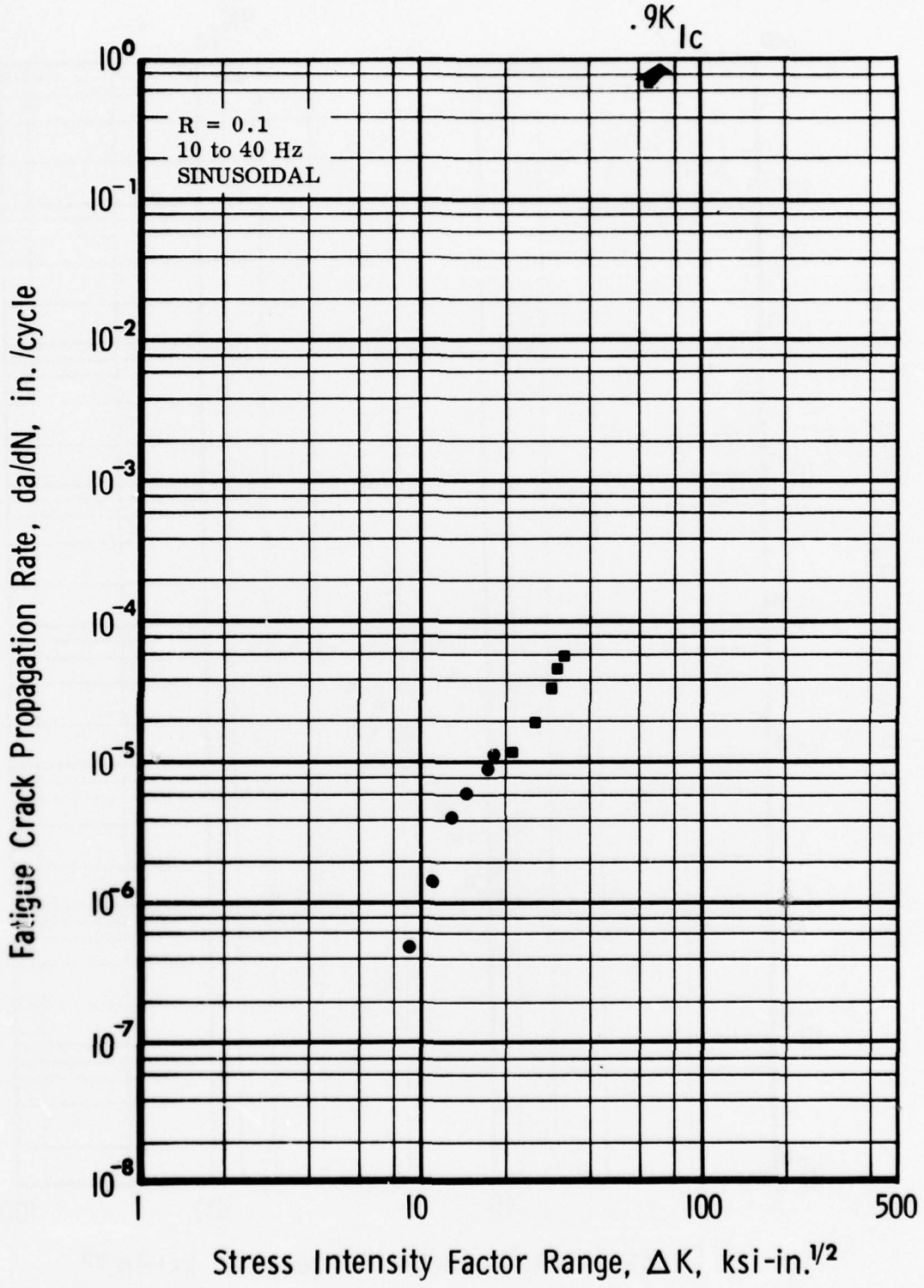

Fig. 51 Fatigue Crack Growth Behavior in Ti-6 Al-4 V Condition 67. Vacuum creep flattened, standard grade, 1-in. plate, 1825°F-1/2 h-AC, 1775°F-1 h-AC. K_{Ic} = 80 ksi-in.$^{1/2}$, K_{Iscc} = 54 ksi-in.$^{1/2}$, F_{ty} = 127 ksi

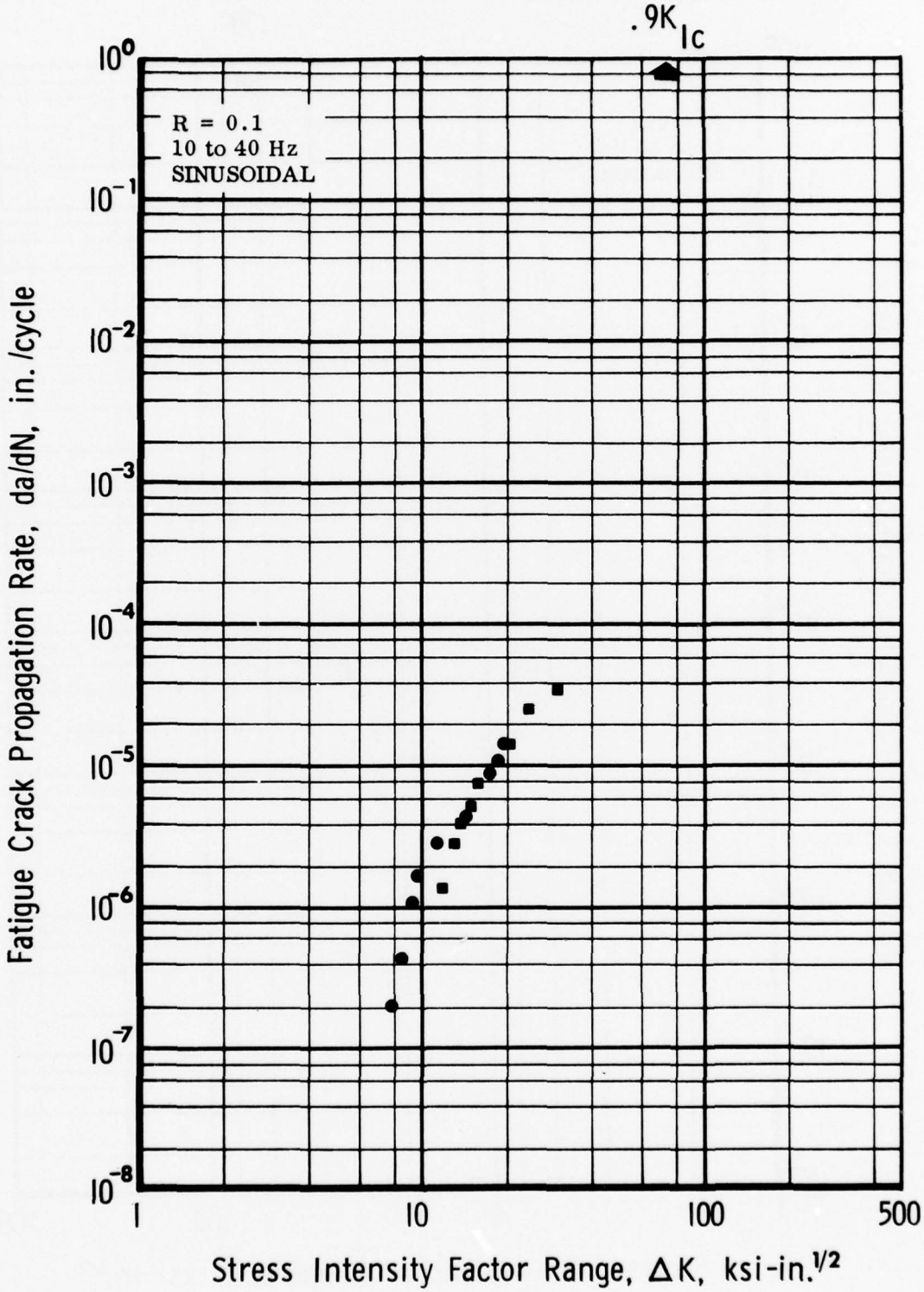

Fig. 52 Fatigue Crack Growth Behavior in Ti-6 Al-4 V Condition 69. Vacuum creep flattened, standard grade, 1-in. plate, 1825°F-1/2 h-AC, 1775°F-1/2 h-AC, 1450°F-1 h-FC. K_{Ic} = 82 ksi-in.$^{1/2}$, K_{Iscc} = 32 ksi-in.$^{1/2}$, F_{ty} = 132 ksi

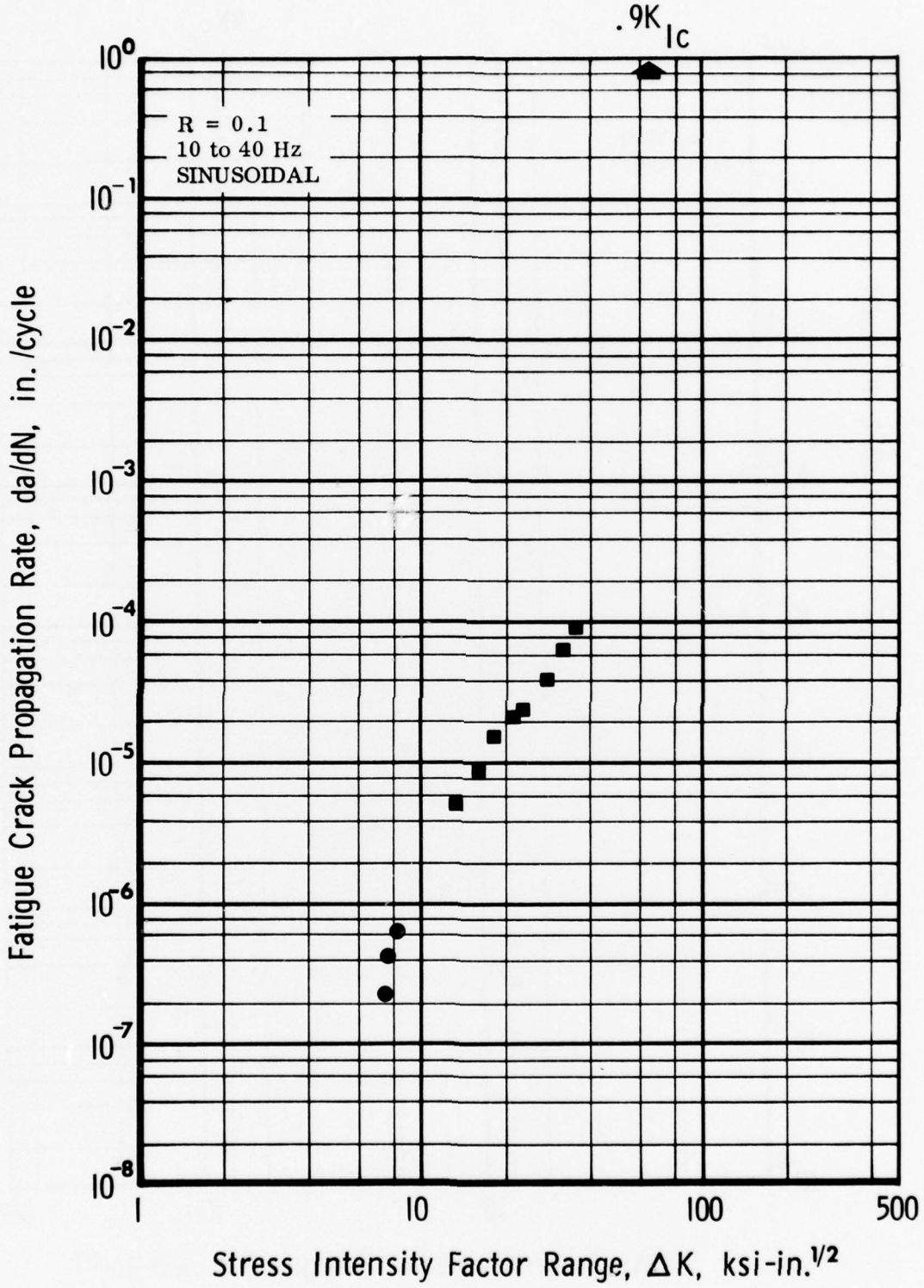

Fig. 53 Fatigue Crack Growth Behavior in Ti-6 Al-4 V Condition 70. Vacuum creep flattened, ELI grade, 1-in. plate, as received. K_{Ic} = 71 ksi-in.$^{1/2}$, K_{Iscc} = 50 ksi-in.$^{1/2}$, F_{ty} = 138 ksi

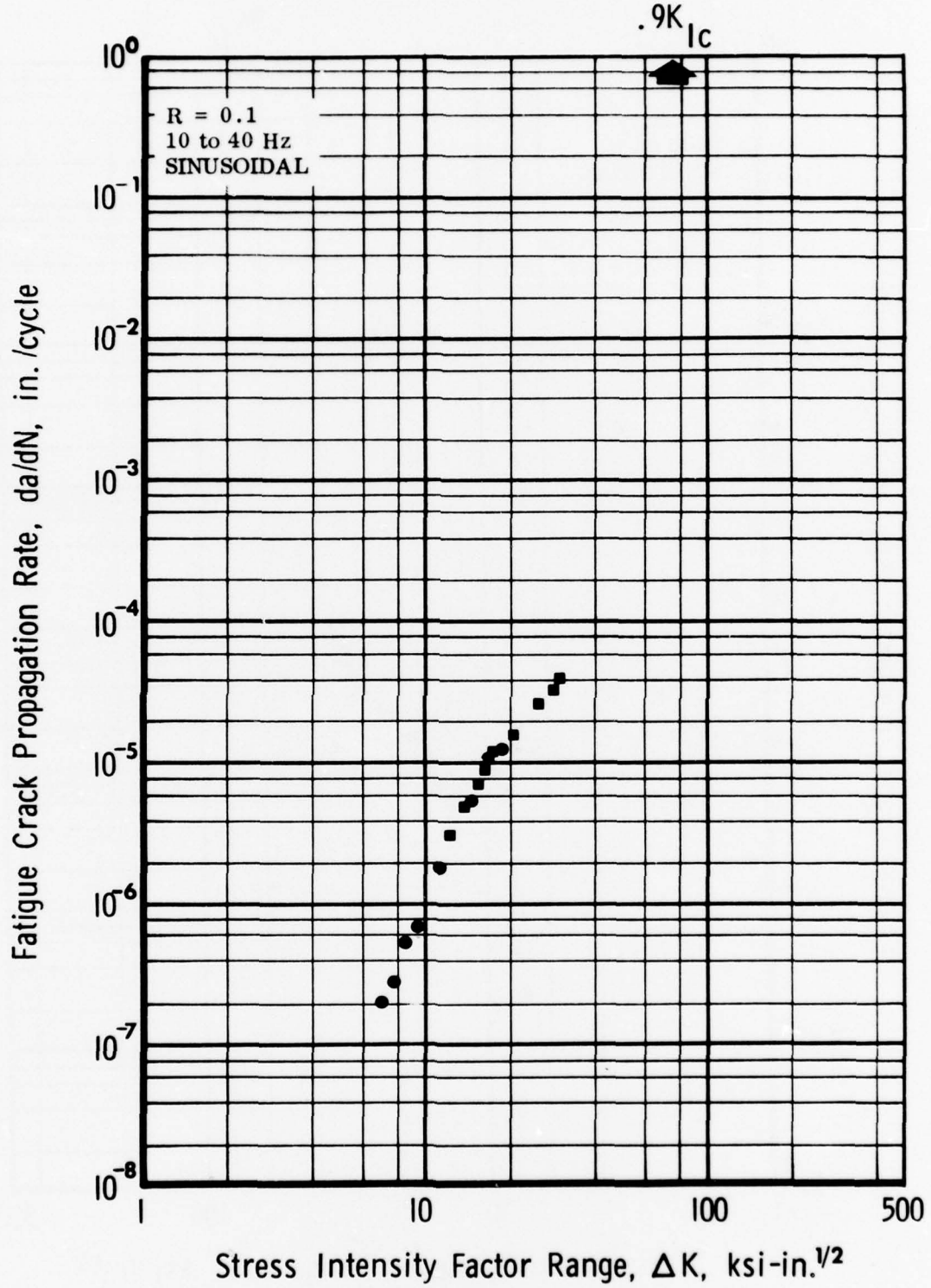

Fig. 54 Fatigue Crack Growth Behavior in Ti-6 Al-4V Condition 71. Vacuum creep flattened, ELI grade, 1-in. plate, 1775°F-1/2 h-AC, 1450°F-1 h-AC. K_{Ic} = 84 ksi-in.$^{1/2}$, K_{Iscc} = 38 ksi-in.$^{1/2}$, F_{ty} = 134 ksi

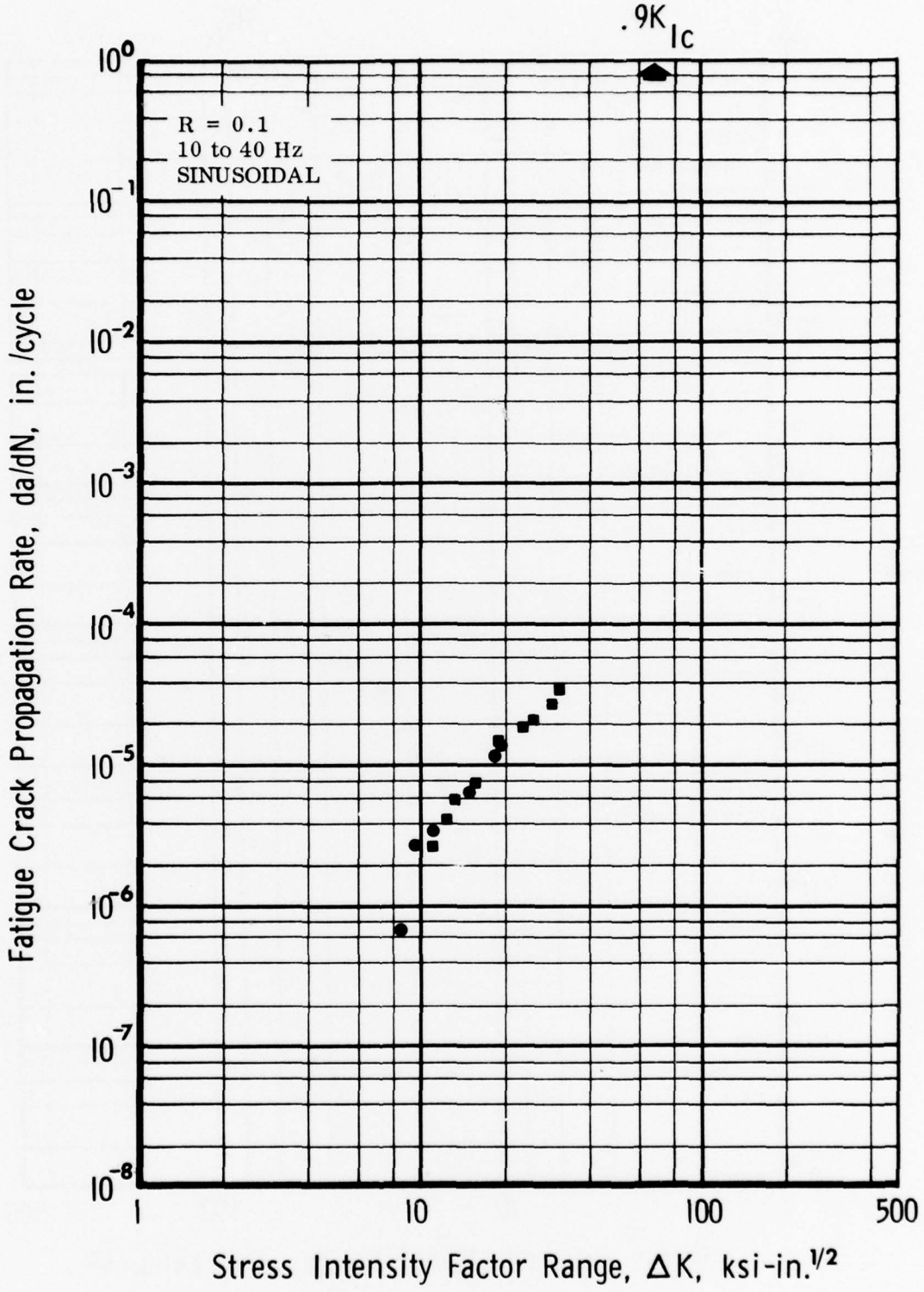

Fig. 55 Fatigue Crack Growth Behavior in Ti-6 Al-4 V Condition 73. Vacuum creep flattened, ELI grade, 1-in. plate, 1775°F-1/2 h-AC, 1450°F-1 h-FC. K_{Ic} = 76 ksi-in.$^{1/2}$, K_{Iscc} = 28 ksi-in.$^{1/2}$, F_{ty} = 138 ksi

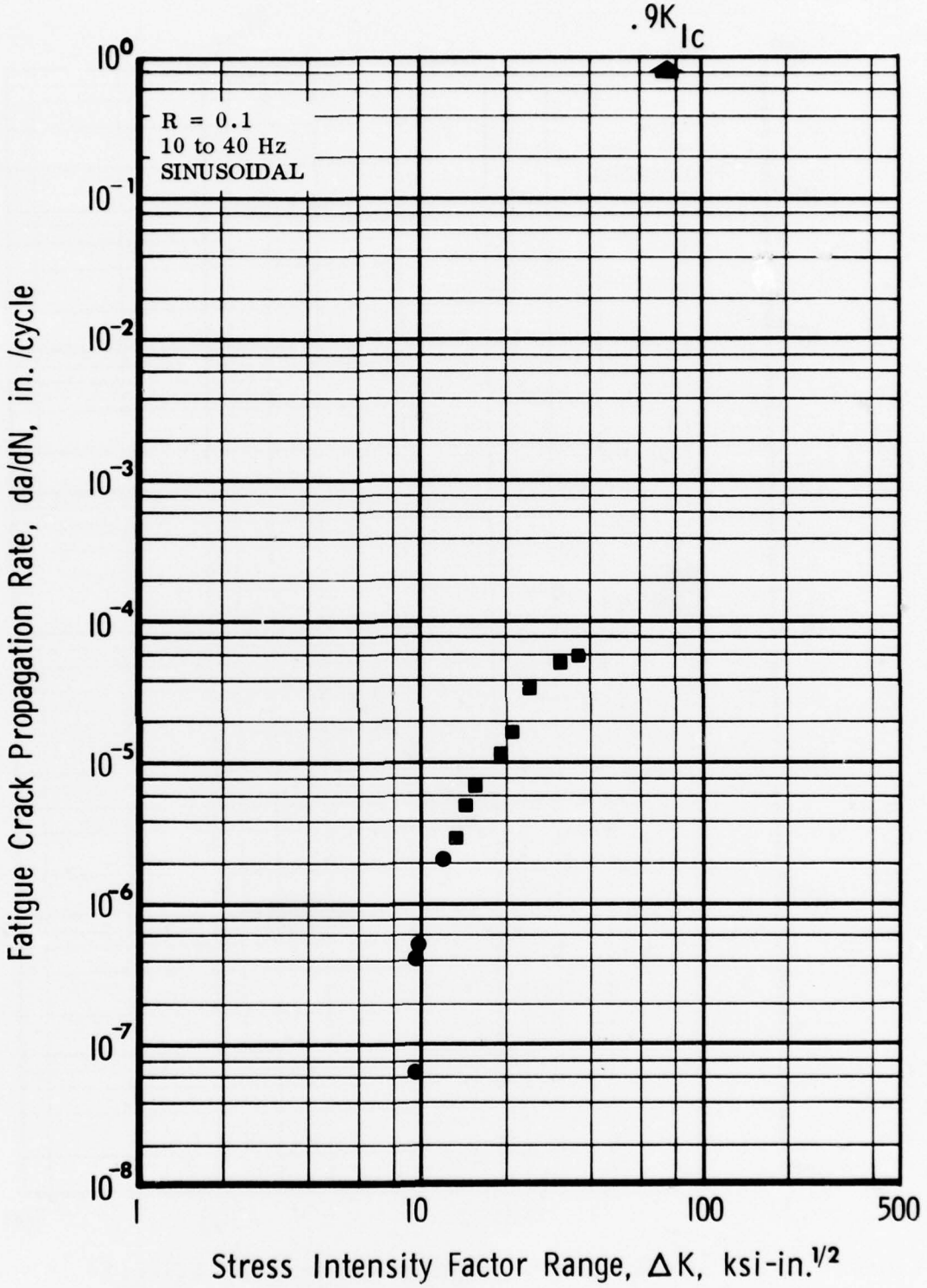

Fig. 56 Fatigue Crack Growth Behavior in Ti-6 Al-4 V Condition 76. Recrystallization annealed, standard grade, 1-in. plate, as-received. K_Q = 85 ksi-in.$^{1/2}$, F_{ty} = 127 ksi

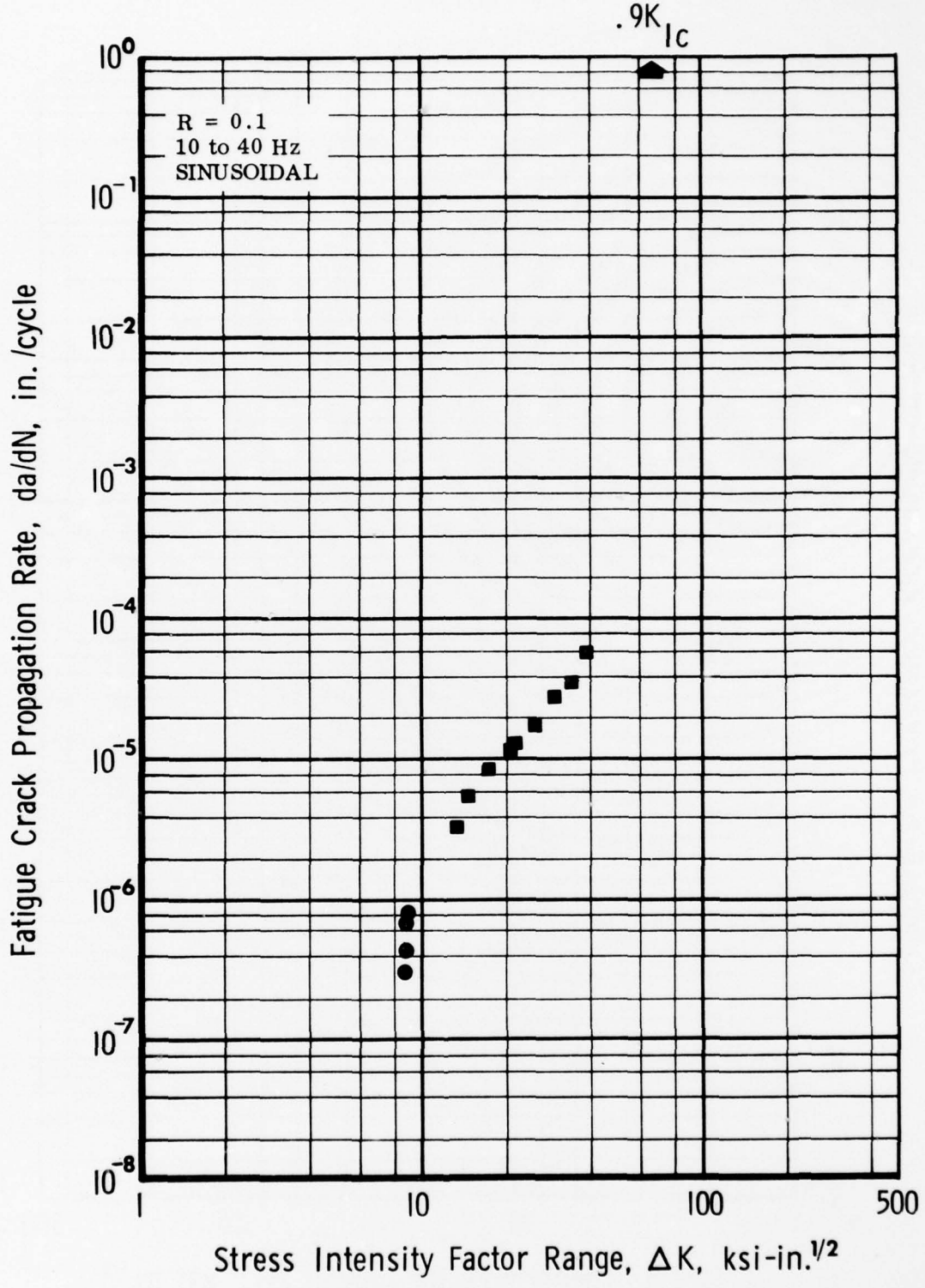

Fig. 57 Fatigue Crack Growth Behavior in Ti-6 Al-4 V Condition 75. Recrystallization annealed, ELI grade, 1-in. plate, as-received. K_{Ic} = 82 ksi-in.$^{1/2}$, K_{Iscc} = 36 ksi-in.$^{1/2}$, F_{ty} = 132 ksi

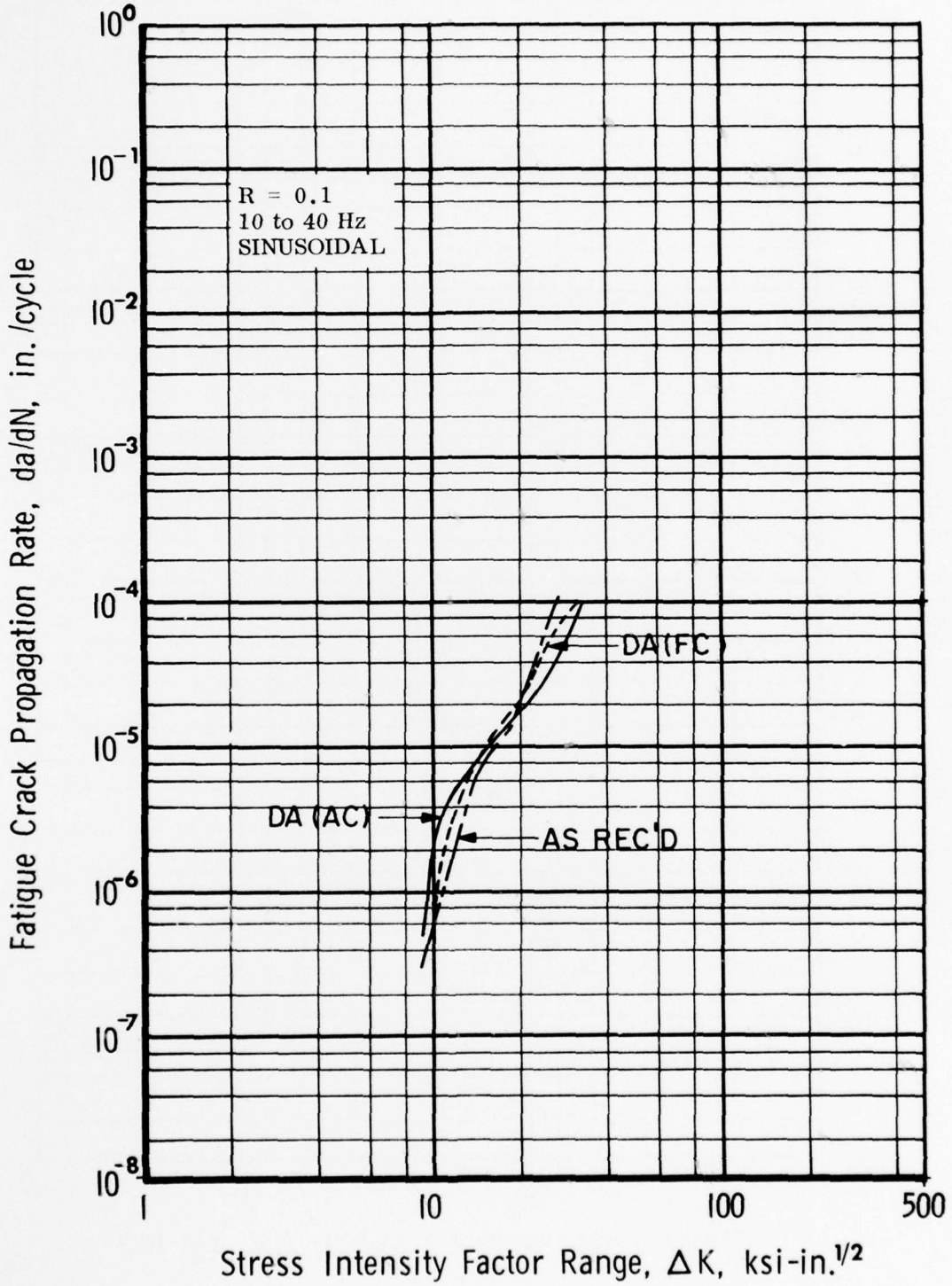

Fig. 58 Fatigue Crack Growth Comparison of Mill Annealed Ti-6Al-4V 1-in. Plate, Standard Grades: As-Received (Condition 50); Duplex Annealed, Air Cooled (Condition 51); and Duplex Annealed, Furnace Cooled (Condition 53)

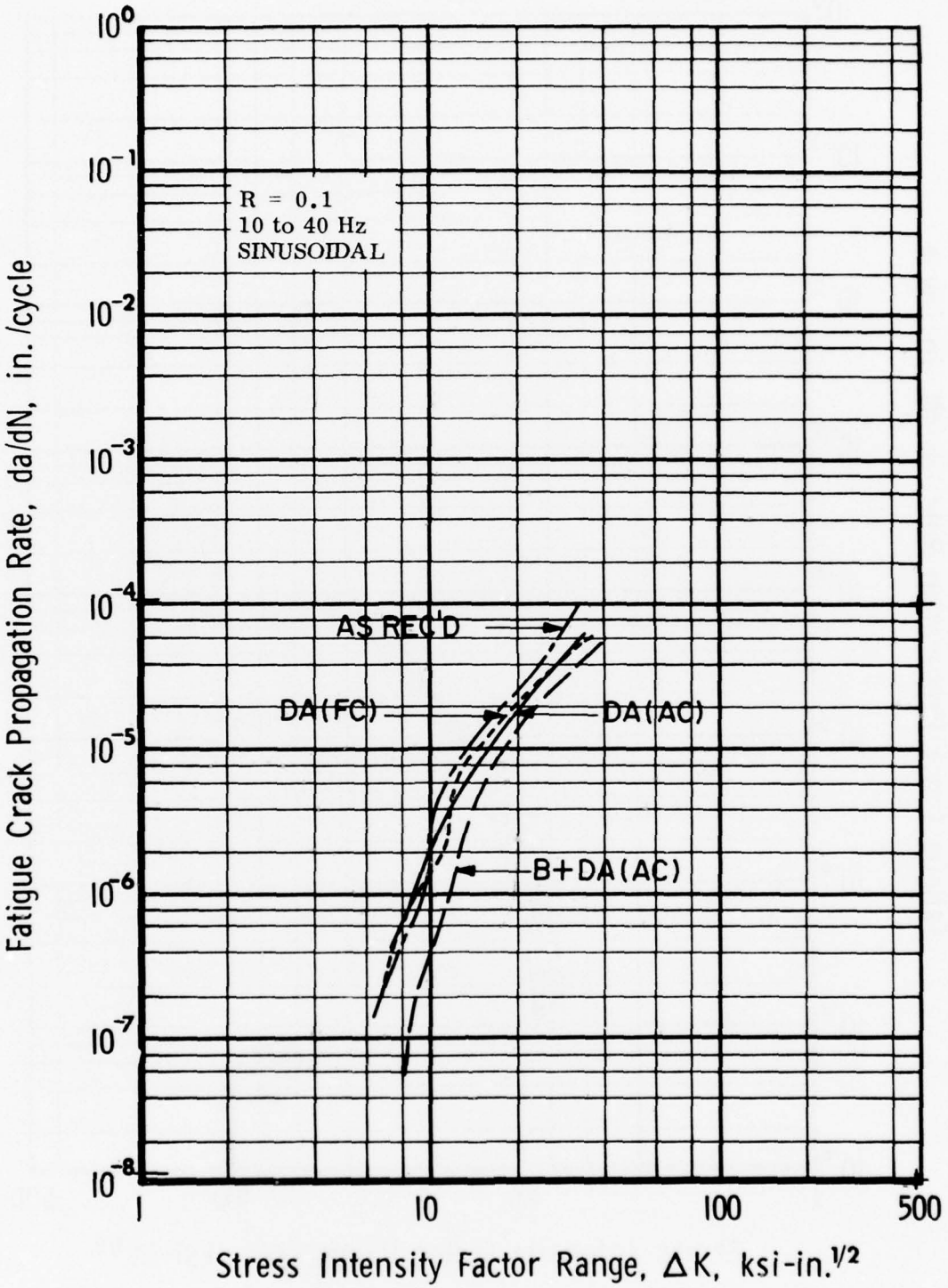

Fig. 59 Fatigue Crack Growth Comparison of Mill Annealed Ti-6Al-4V 1-in. Plate, ELI Grades: As-Received (Condition 54); Duplex Annealed, Air Cooled (Condition 55); Duplex Annealed, Furnace Cooled (Condition 57); and Beta + Duplex Annealed, Air Cooled (Condition 60)

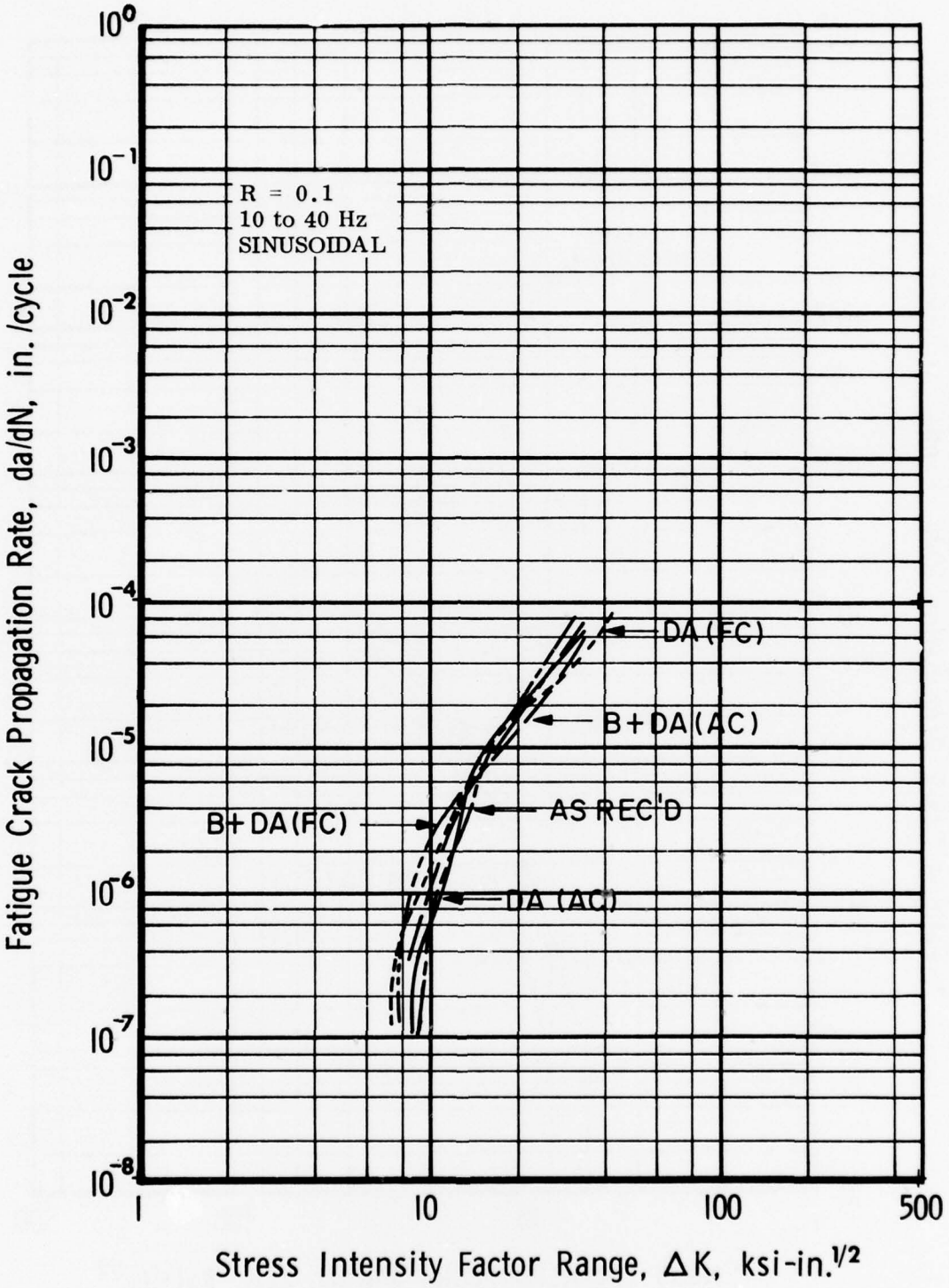

Fig. 60 Fatigue Crack Growth Comparison of Vacuum Creep Flattened Ti-6Al-4V, 1-in. Plate, Standard Grades: As-Received (Condition 63); Duplex Annealed, Air Cooled (Condition 64); Duplex Austenitized, Furnace Cooled (Condition 66); Beta + Duplex Annealed, Air Cooled (Condition 67); and Beta + Duplex Annealed, Furnace Cooled (Condition 69)

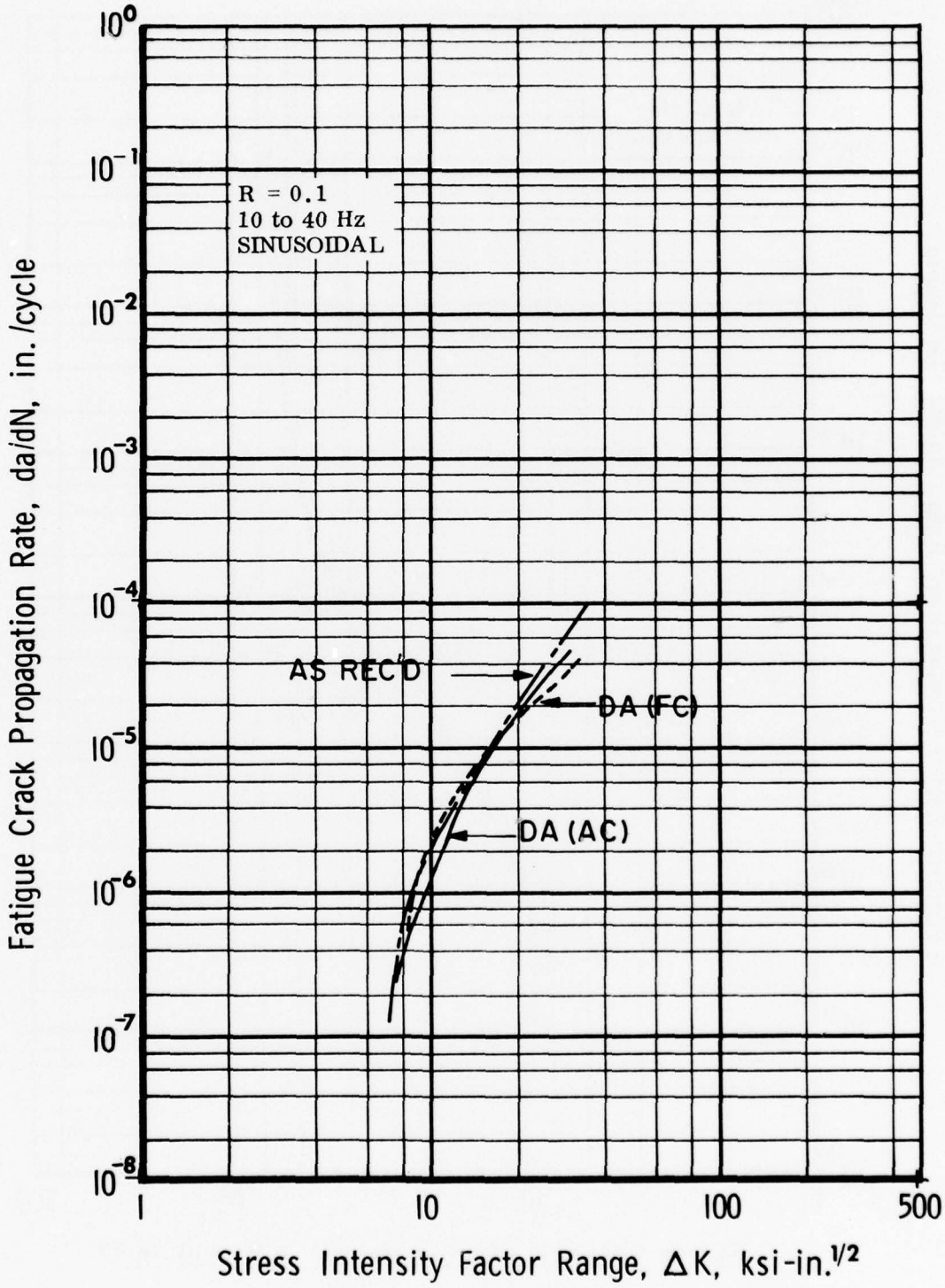

Fig. 61 Fatigue Crack Growth Comparison of Vacuum Creep Flattened Ti-6Al-4V, 1-in. Plate, ELI Grade: As-Received (Condition 70); Duplex Austenitized, Air Cooled (Condition 71); and Duplex Austenitized, Furnace Cooled (Condition 73)

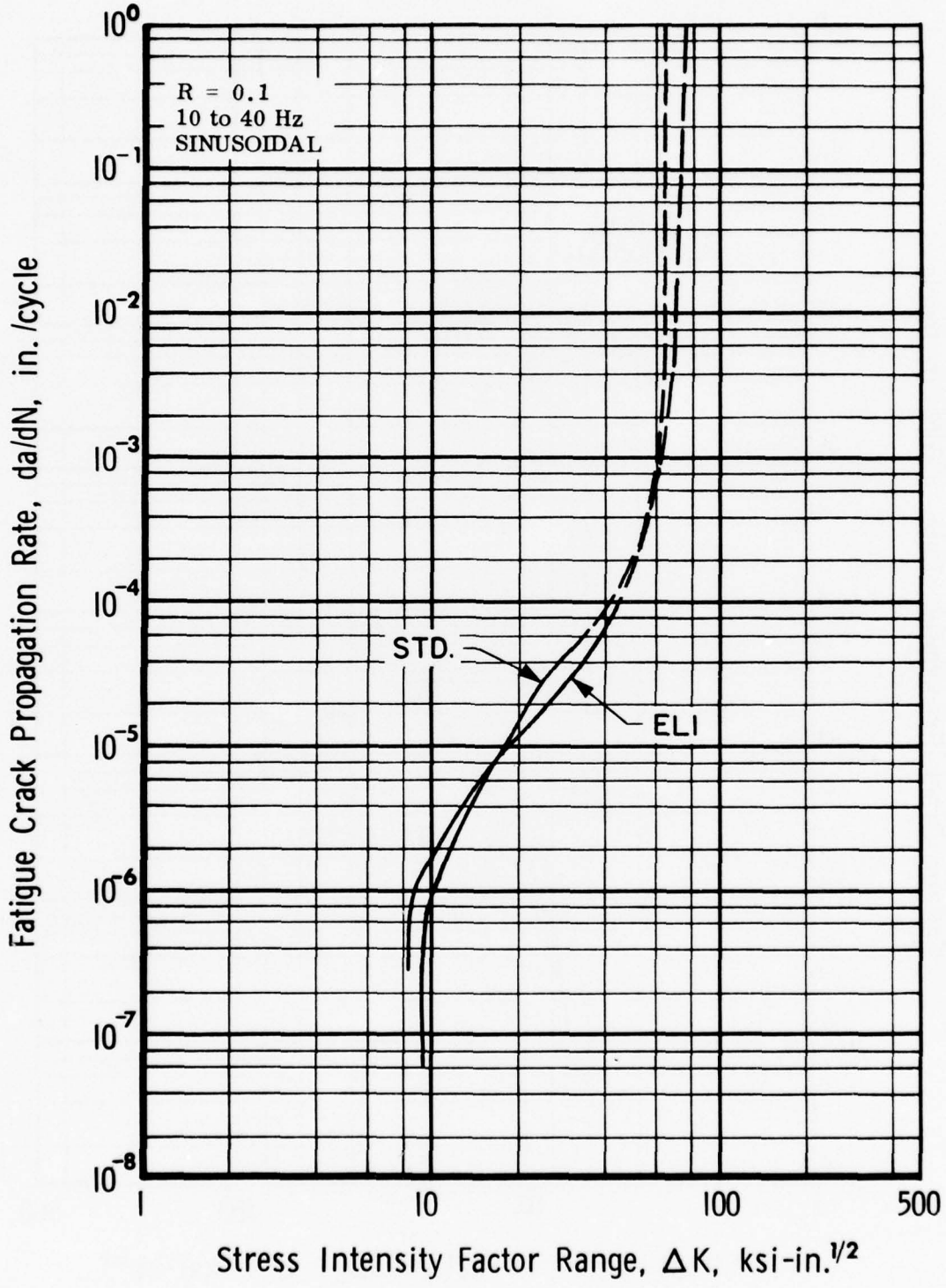

Fig. 62 Fatigue Crack Growth Comparison of Recrystallization Annealed Ti-6Al-4V, 1-in. Plate, Standard Grade (Condition 76) and ELI Grade (Condition 75)

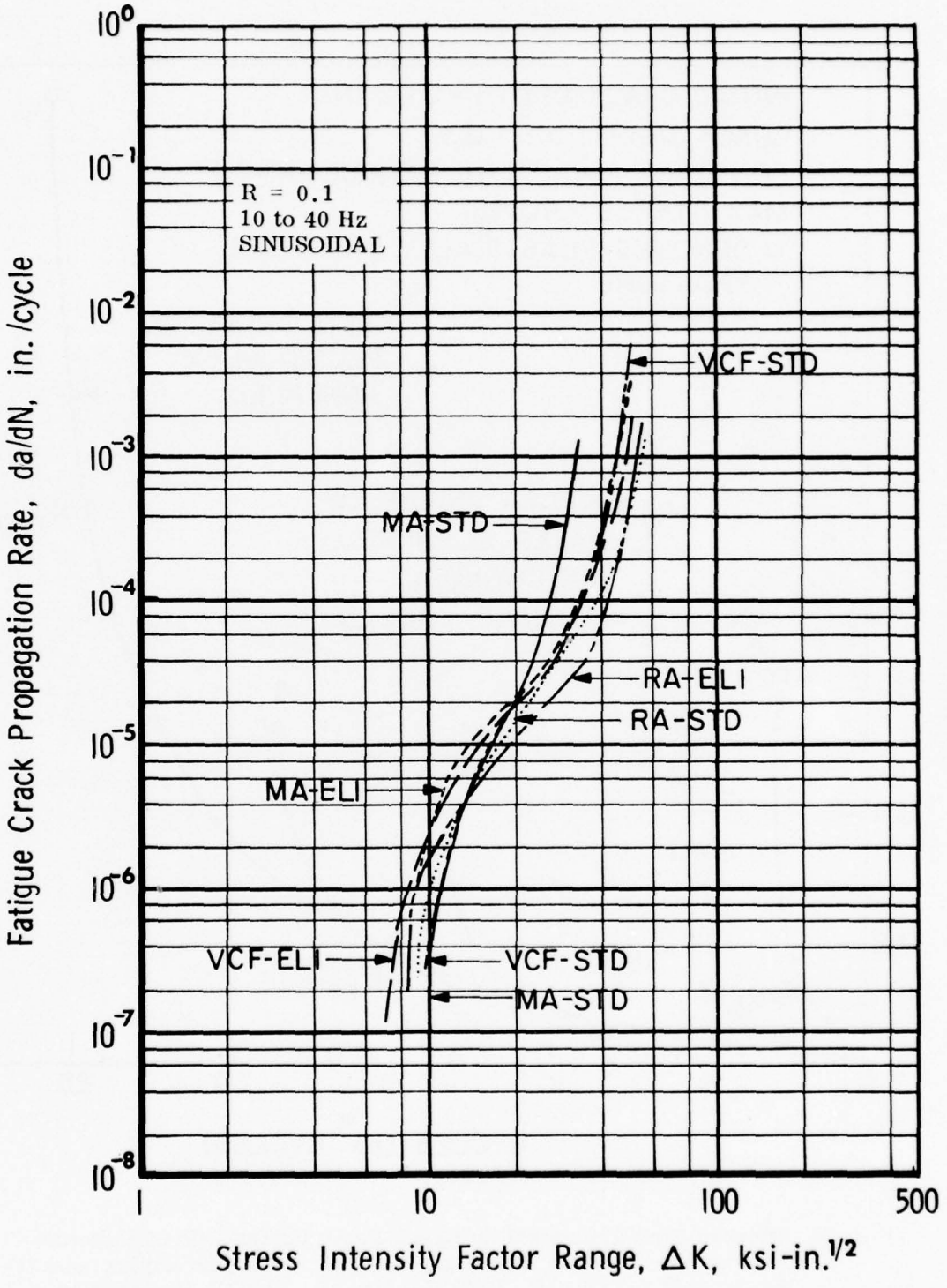

Fig. 63 Fatigue Crack Growth Comparisons of As-Received Ti-6Al-4V, 1-in. Plate: Mill Annealed – Standard (Condition 50), – ELI (Condition 54); Vacuum Creep Flattened – Standard (Condition 63), – ELI (Condition 70); Recrystallization Annealed – Standard (Condition 76), – ELI (Condition 75)

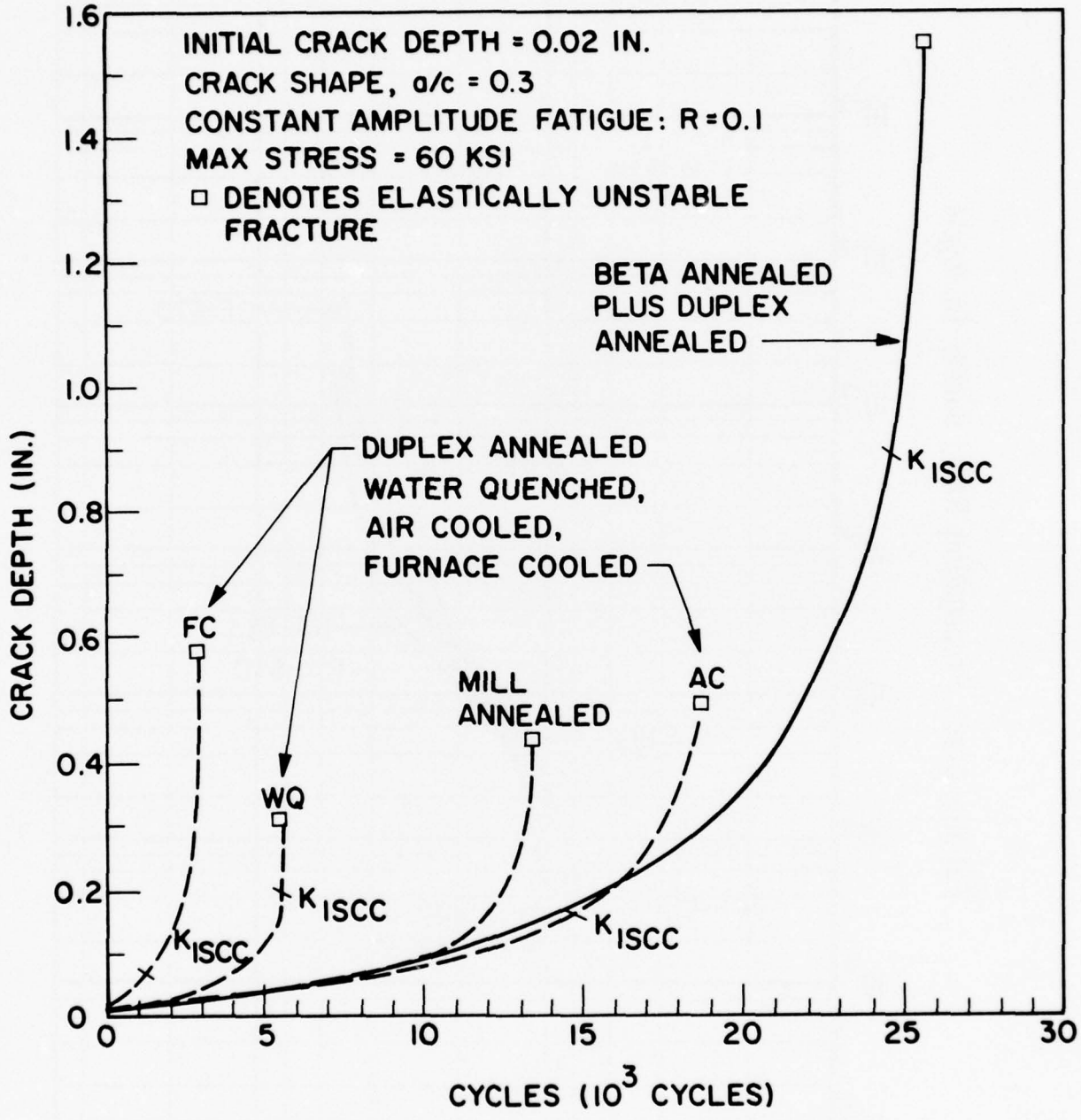

Fig. 64 Effect of Heat Treatment on Crack Depth During Life of Structure Subjected to Constant Amplitude Fatigue. Beta plus duplex annealing is 1825°F-1/2h-AC, 1775°F-1/2h-AC, 1450°F-1h-AC (this study). Duplex annealing cycle is 1775°F-1/2h-Ac, 1450°F-1h – cooled as noted; mill annealing cycle is 1450°F-1h-AC (after Ref. 7)

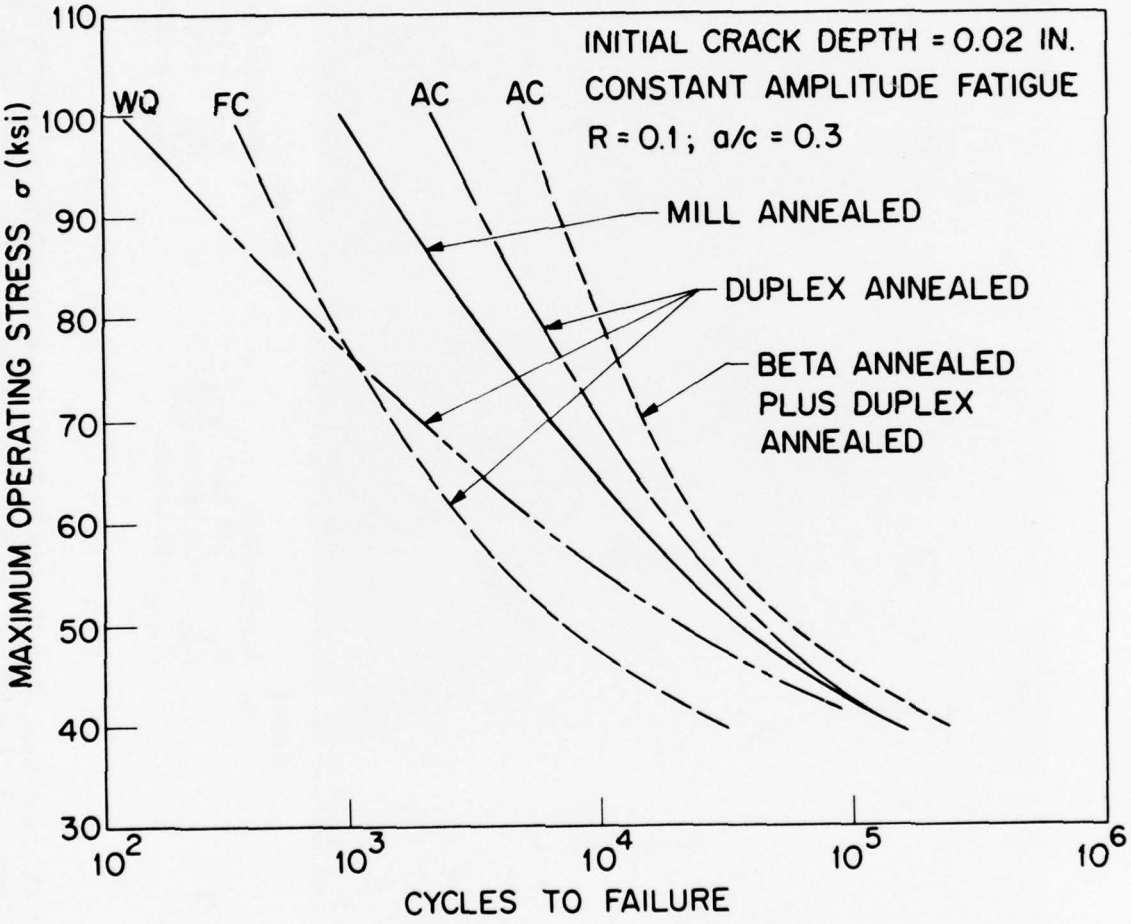

Fig. 65 Ti-6 Al-4V, 1-in. Plate, Effect of Heat Treatment on Structural Life Predicted by Computer Modelling. Beta plus duplex annealing cycle is 1825°F-1/2h-AC, 1775°F-1/2h-AC, 1450°F-1h-AC (this study). Duplex annealing cycle is 1775°F-1/2h-AC, 1450°F-1h-water quenched (WQ), air cooled (AC), or furnace cooled (FC); mill annealing cycle is 1450°F-1h-AC (after Ref. 7)

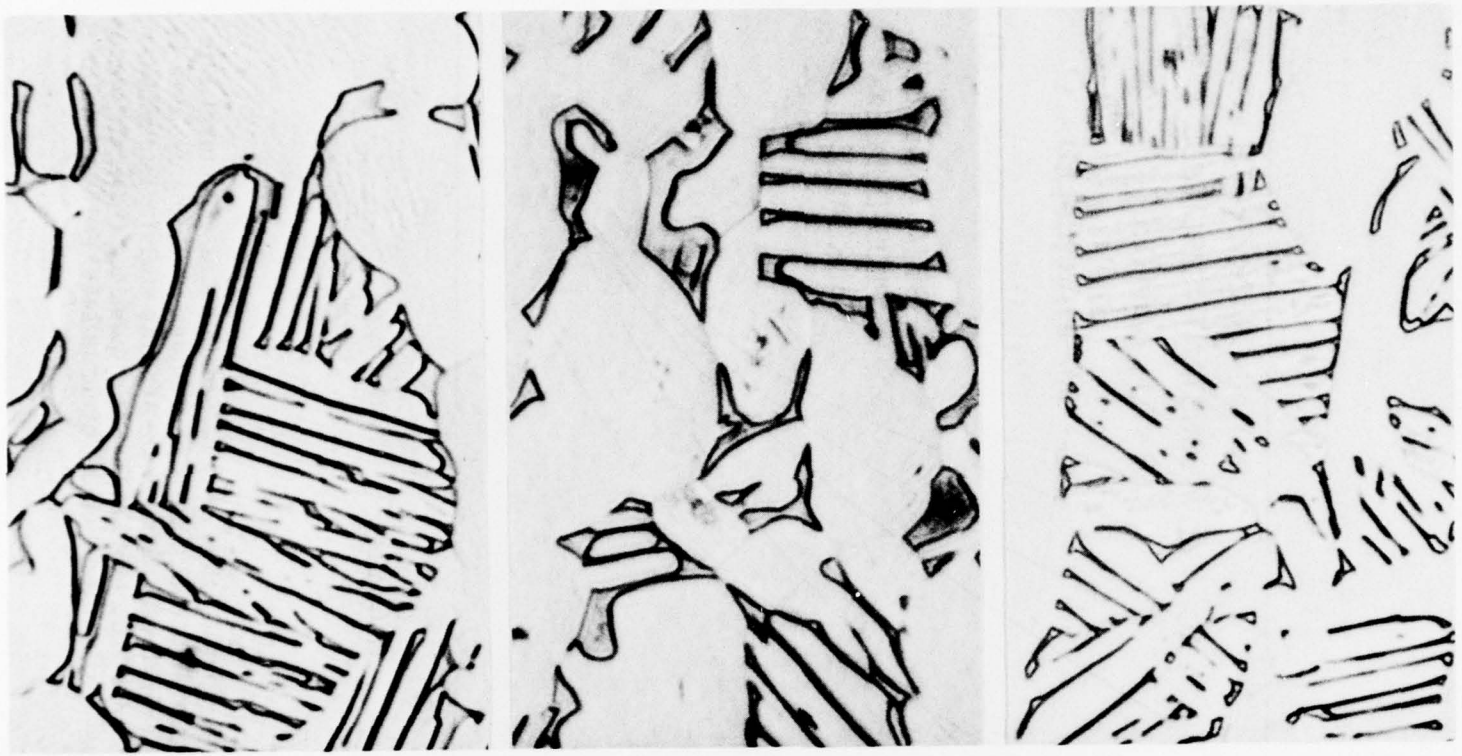

B9221

a. Water-Quenched:
F_{ty} = 141 ksi
K_{Ic} = 38 ksi-in.$^{1/2}$
K_{Iscc} = 34 ksi-in.$^{1/2}$

B9224

b. Air-Cooled:
F_{ty} = 138 ksi
K_{Ic} = 50 ksi-in.$^{1/2}$
K_{Iscc} = 30 ksi-in.$^{1/2}$

B9260

c. Furnace-Cooled:
F_{ty} = 141 ksi
K_{Ic} = 52 ksi-in.$^{1/2}$
K_{Iscc} = 22 ksi-in.$^{1/2}$

Fig. 66 Ti-6Al-4V Conditions 31, 2(R), and 32 From the First and Second Year's Studies. 1-in. Plate, 1775°F-1/2h-AC, 1450°F-1h – cooled as noted. 3000× (after Ref. 2)

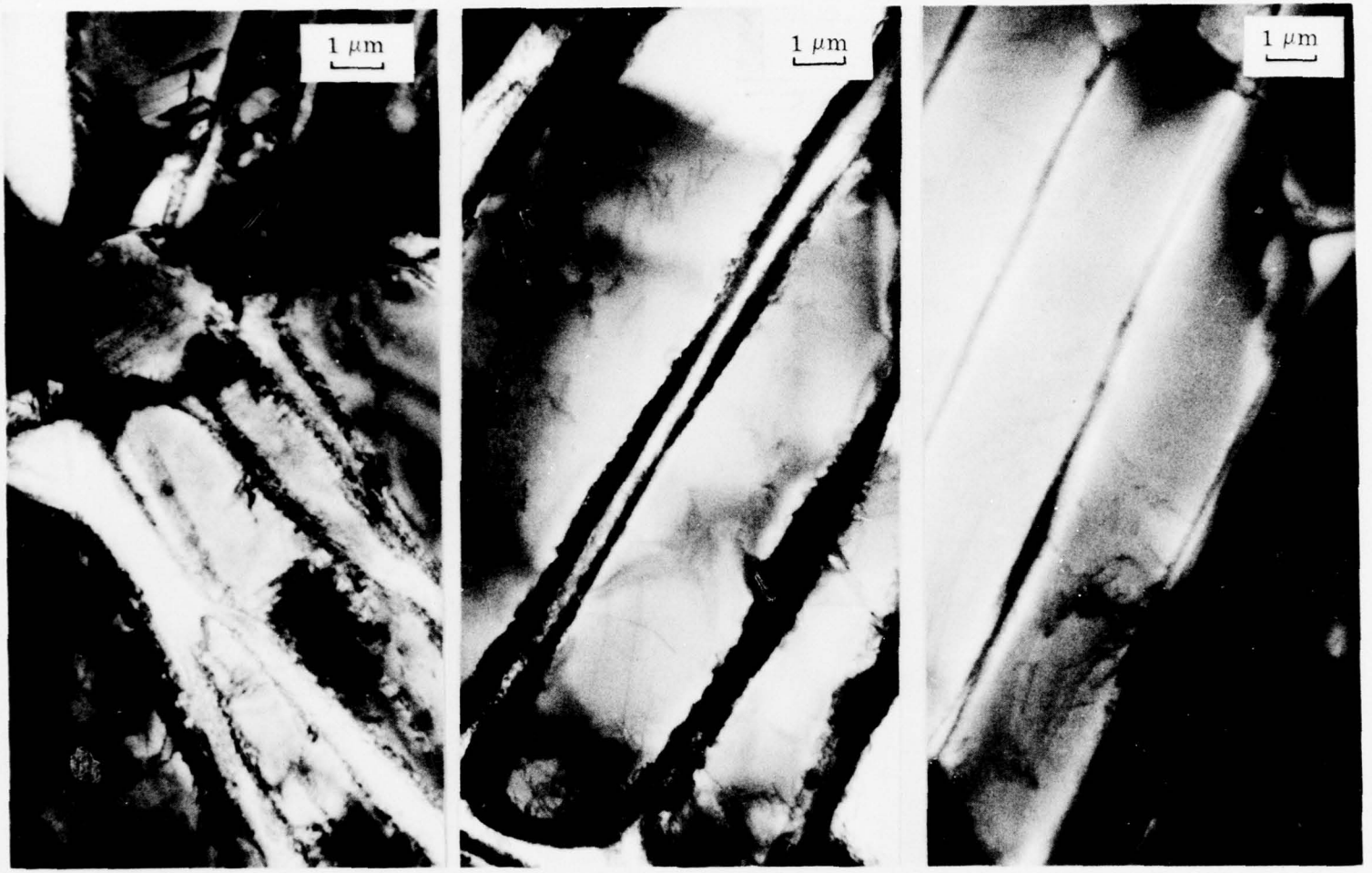

h873 7700× h866 7700× h882 7700×

a. Water-Quenched b. Water-Quenched c. Air-Cooled

Fig. 67 Ti-6Al-4V Conditions 31, 2(R), and 32; Duplex-Annealed and Water-Quenched, Air-Cooled, or Furnace-Cooled, Respectively

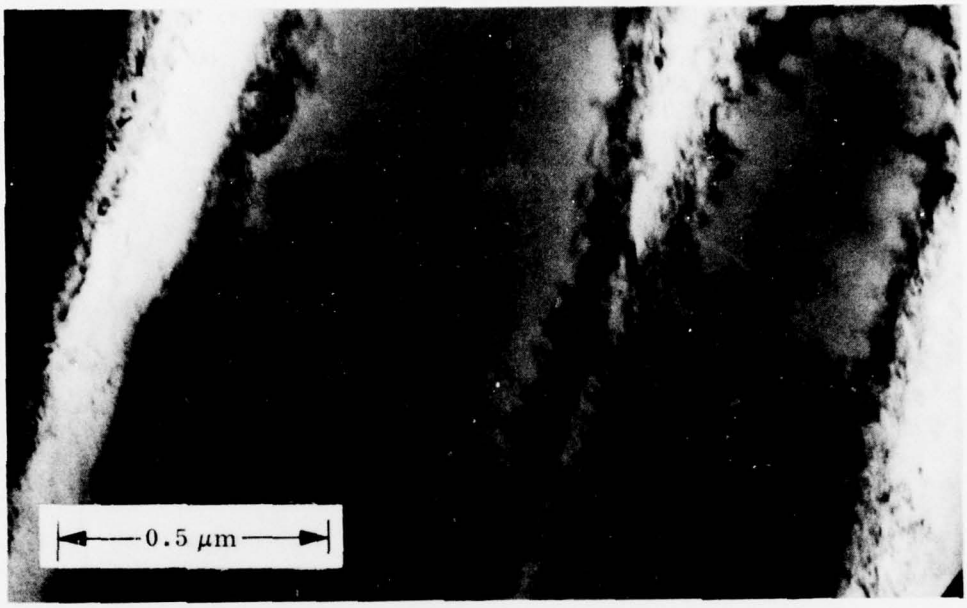

h874

a. Bright Field

h875

b. Dark Field

Fig. 68 *Ti-6Al-4V Condition 31:*
Duplex-Annealed and Water-Quenched

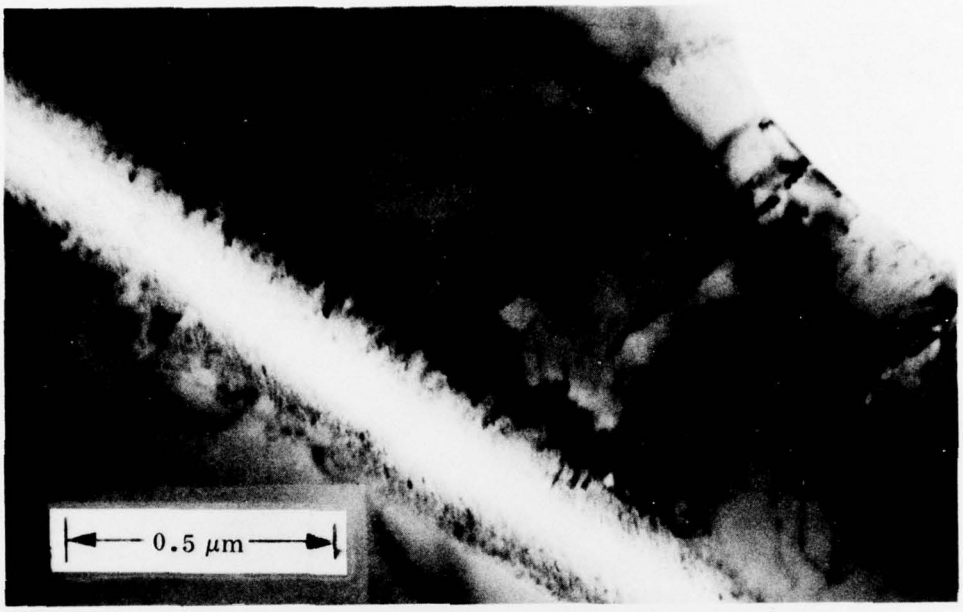

h870

a. Bright Field

h871

b. Dark Field

Fig. 69 Ti-6Al-4V Condition 2(R):
Duplex-Annealed and Air-Cooled

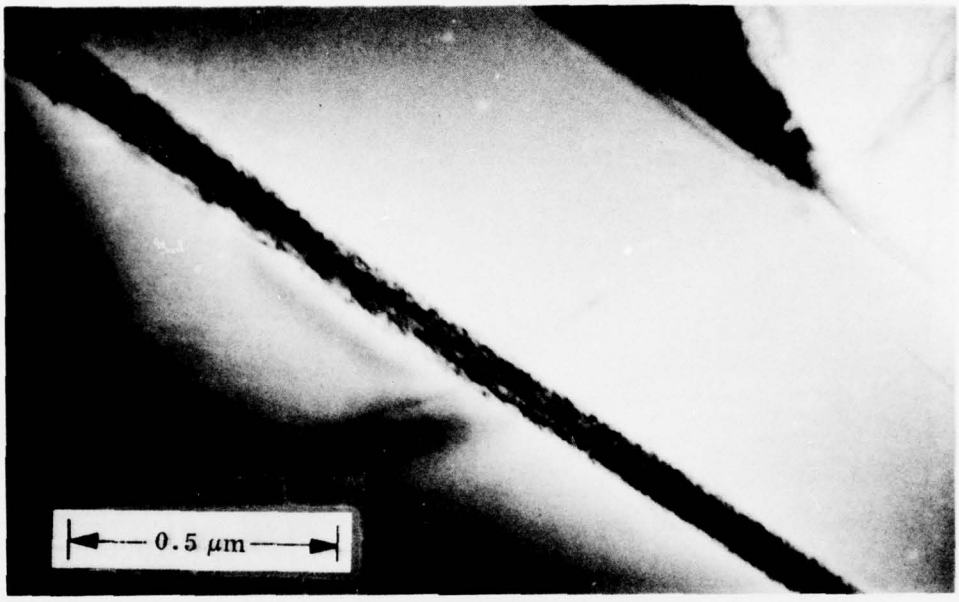

h776

a. Bright Field

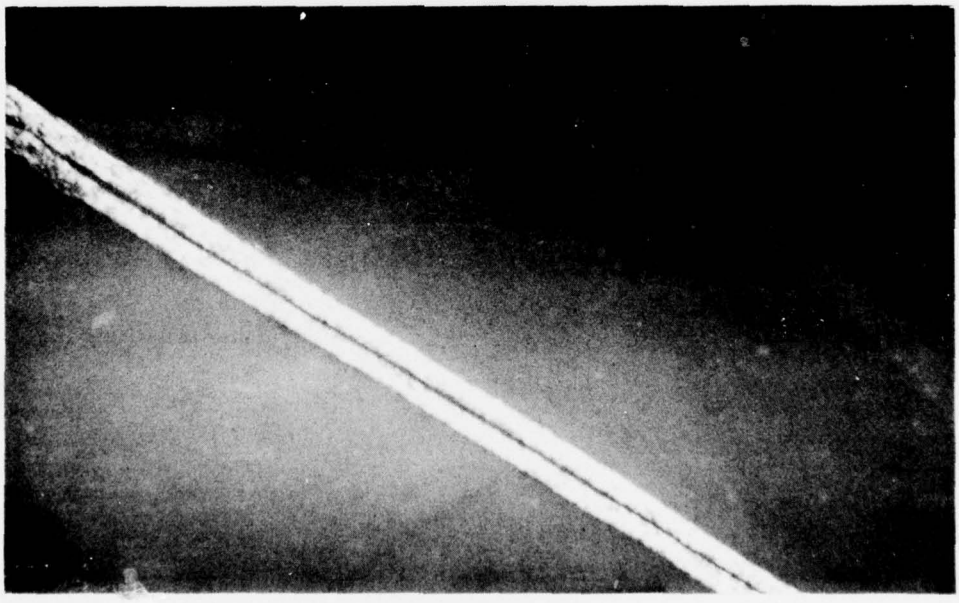

h775

b. Dark Field

Fig. 70 Ti-6Al-4V Condition 32:
Duplex-Annealed and Furnace-Cooled

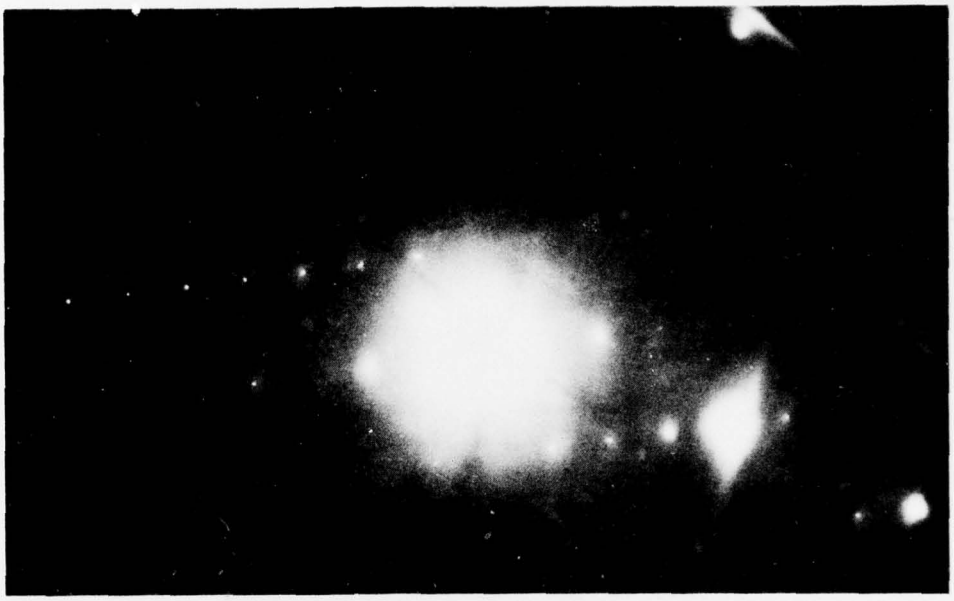

h712

a. Original Photograph

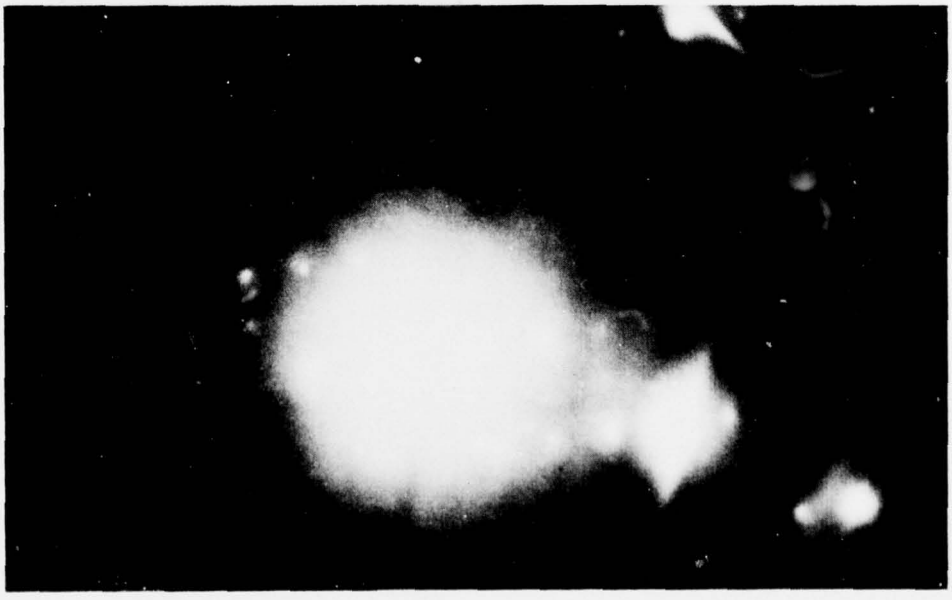

h712

b. Electronically Reprocessed Photograph

Fig. 71 Diffraction Pattern From Duplex-Annealed and Furnace-Cooled Specimen Showing Diffuse Spots at (h/2, k/2, ℓ)

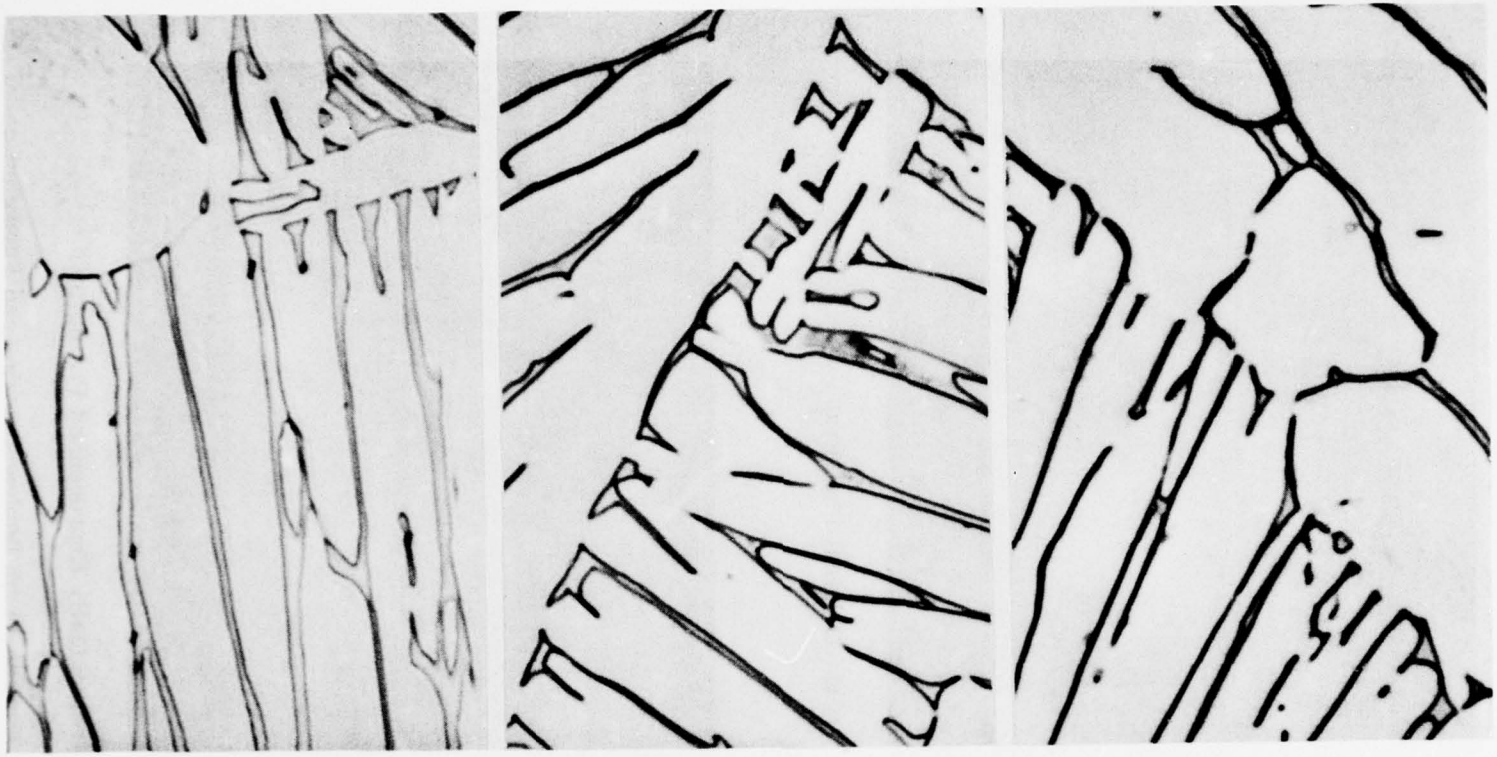

B9256

a. Water-Quenched:
F_{ty} = 118 ksi
K_{Ic} = 55 ksi-in.$^{1/2}$
K_{Iscc} = 43 ksi-in.$^{1/2}$

C1099

b. Air-Cooled:
F_{ty} = 124 ksi
K_Q = 85 ksi-in.$^{1/2}$
K_{Iscc} not measured

B9259

c. Furnace-Cooled:
F_{ty} = 137 ksi
K_{Ic} = 71 ksi-in.$^{1/2}$
K_{Iscc} = 33 ksi-in.$^{1/2}$

Fig. 72 Ti-6Al-4V Conditions 33, 7, and 34 From the First and Second Year's Studies. 1-in. Plate, 1850°F-1/2h-AC, 1775°F-1/2h-AC, 1450°F-1h – cooled as noted. 3000× (after Refs. 1 and 2)

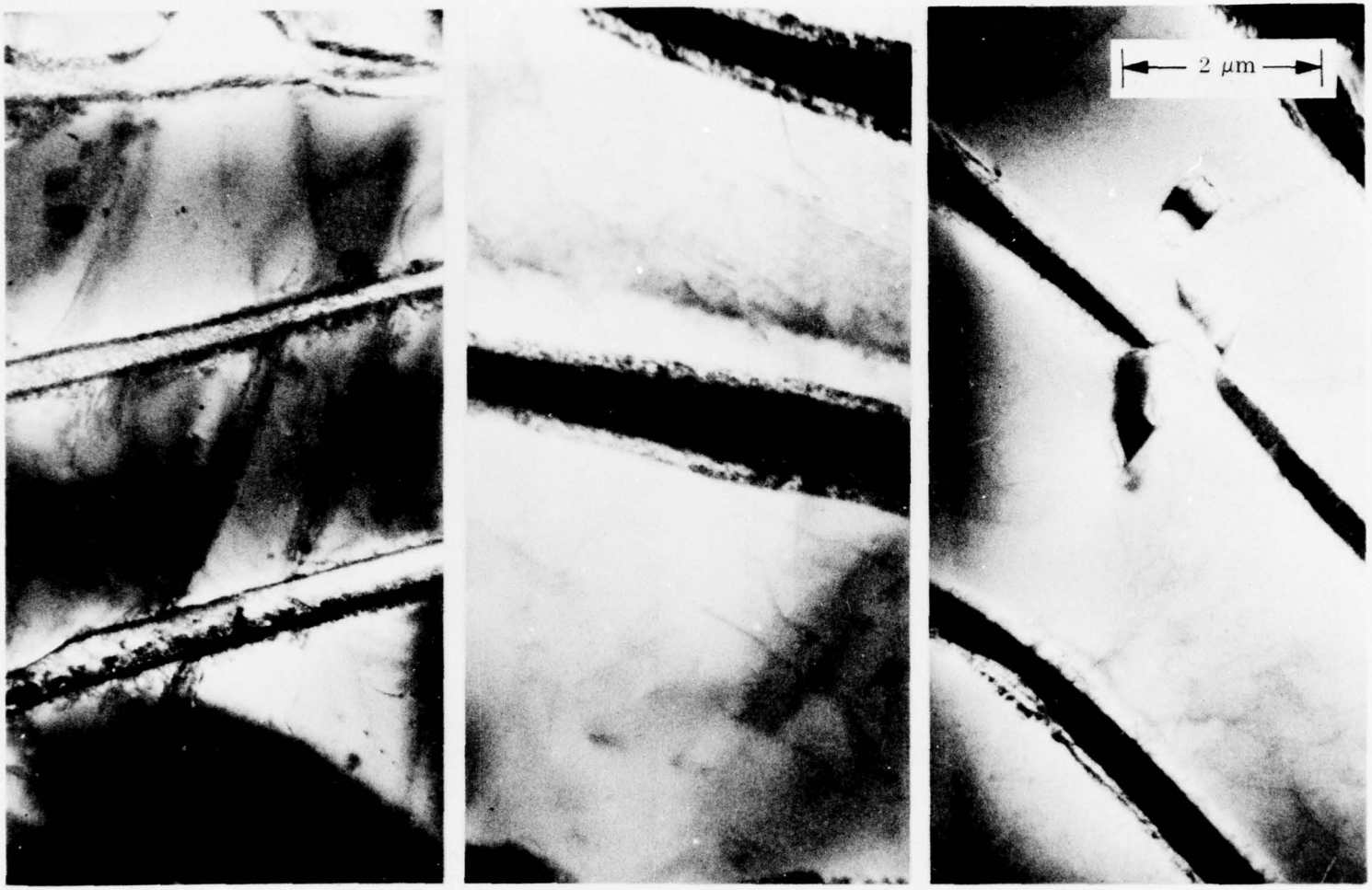

h827 h833 h830

a. Water-Quenched b. Air-Cooled c. Furnace-Cooled

Fig. 73 Ti-6Al-4V Conditions 33,7, and 34; Beta-Treated, Duplex-Annealed, and Water-Quenched, Air-Cooled, or Furnace-Cooled, Respectively

h829

a. Printed To Enhance Low Contrast Area

h829

b. Printed To Enhance High Contrast Area

Fig. 74 Diffraction Pattern From Beta-Treated and Duplex-Annealed Furnace-Cooled Specimen Showing Diffuse Spots at (h/2, k/2, ℓ)

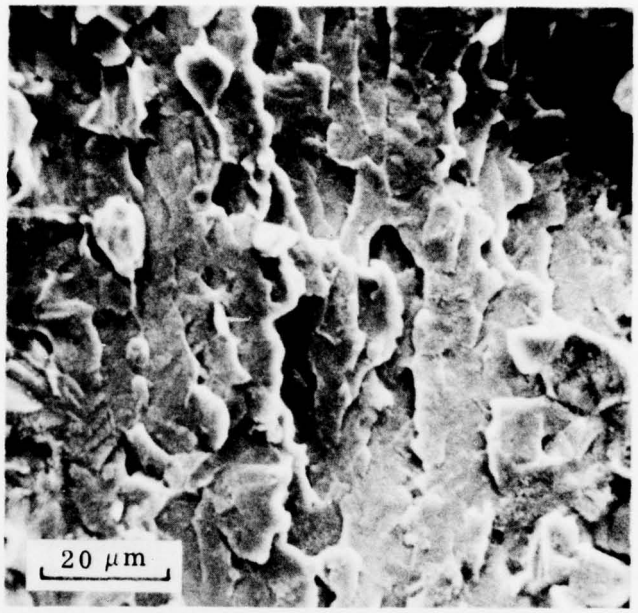

5JAF

a. Water-Quenched: $K_{Iscc} = 34$ ksi-in.$^{1/2}$

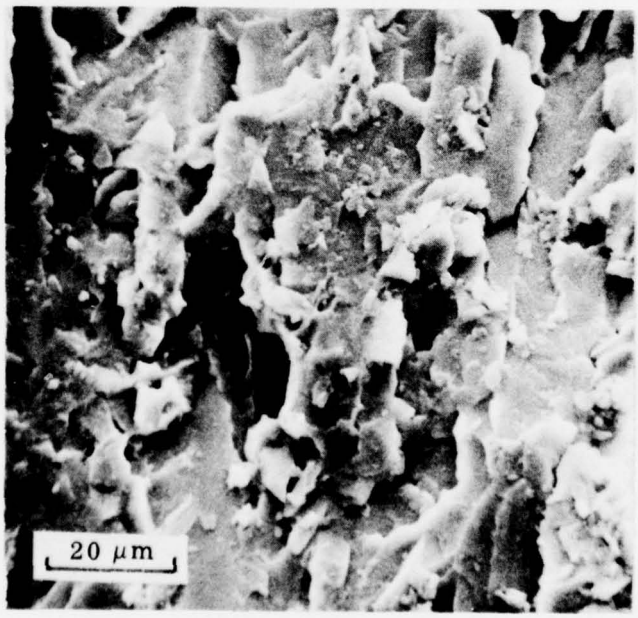

5JAW

b. Furnace-Cooled: $K_{Iscc} = 22$ ksi-in.$^{1/2}$

Fig. 75 Fracture Surfaces of Ti-6Al-4V Stress-Corrosion Cracked Specimens; Duplex-Annealed and Water-Quenched or Furnace-Cooled

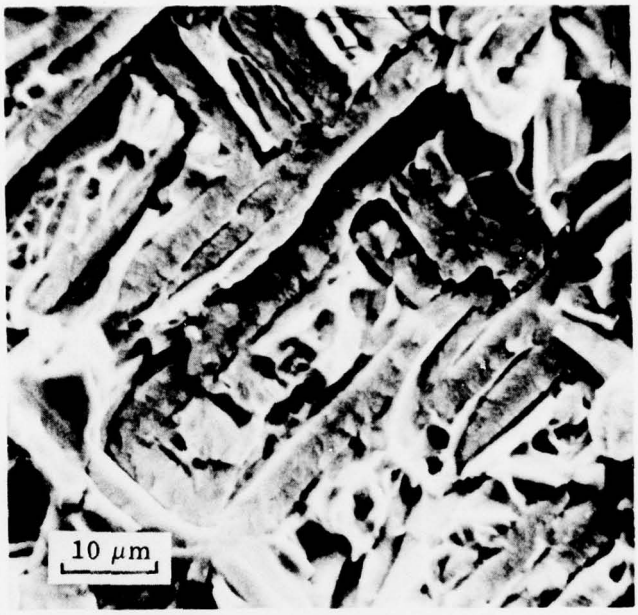

6IDS

a. Water-Quenched:
K_{Iscc} = 43 ksi-in.$^{1/2}$

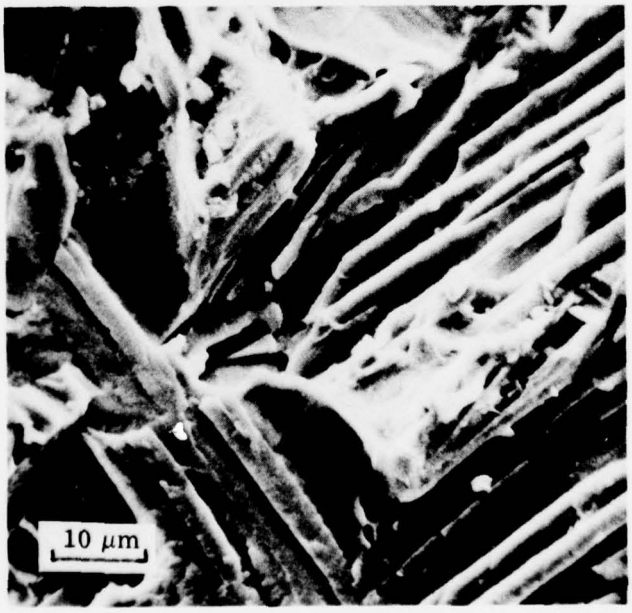

5IDX

b. Furnace-Cooled:
K_{Iscc} = 33 ksi-in.$^{1/2}$

Fig. 76 Fracture Surfaces of Ti-6Al-4V Stress-Corrosion Cracked Specimens; Beta-Treated, Duplex-Annealed and Water-Quenched or Furnace-Cooled

DISTRIBUTION LIST

Department of the Navy
Naval Air Systems Command
Washington, D.C. 20361
Attn: Mr. W. T. Highberger
AIR-52031D (10 copies)

Department of the Navy
Ships Systems Command
Washington, D.C. 20361
Attn: Code 03423

Chief of Naval Research
Department of the Navy
Washington, D.C. 20361
Attn: ONR 423, 471 (2 copies)

Director
U.S. Naval Research Laboratory
Metallurgy Division
Washington, D.C. 20390
Attn: Mr. D. Meyn (Code 6312)
Mr. C. D. Beachem (Code 6312)
Dr. G. Yoder (Code 6384)
Dr. B. B. Rath (Code 6490) (1 each)

Commanding Officer
Naval Air Development Center, Johnsville
Aero Materials Laboratory
Warminister, Pennsylvania 18974
Attn: Mr. F. S. Williams

Air Force Materials Laboratory
Wright-Patterson Air Force Base
Dayton, Ohio 45433
Attn: Codes LLM, LC, MXE, MBC, & LLS
(1 each)

USAEC Division of Reactor Development and Technology
Washington, D.C. 20545
Attn: Mr. J. M. Simmons, Chief Metallurgy Section

Department of the Interior
Bureau of Mines
Washington, D.C. 20240

U.S. Department of Commerce
National Bureau of Standards
Washington, D.C. 20234

National Academy of Sciences
National Materials Advisory Board
2101 Constitution Avenue
Washington, D.C. 20418
Attn: Dr. J. C. Lane

National Aeronautics and Space Administration
600 Independence Avenue
Washington, D.C. 20546

U.S. Army Materials & Mechanics Research Center
Watertown Arsenal
Watertown, Massachusetts 02172
Attn: Mr. S. Arnold

Commander
U.S. Army Munitions Command
Frankford Arsenal
Pitman Dunn Laboratory
Philadelphia, Pennsylvania 19137
Attn: Mr. K. Kleppinger

Battelle Memorial Institute
Defense Metals Information Center
505 King Avenue
Columbus, Ohio 43201

Avco Space Systems Division
Lowell Industrial Park
Lowell, Massachusetts 01851

Brush Wellman, Inc.
17876 St. Clair Avenue
Cleveland, Ohio 44110
Attn: Mr. Bryce King

The Boeing Company
Aerospace Division
P.O. Box 3707
Seattle, Washington 98124
Attn: Mr. E. C. Bovee

Dr. D. P. Ames
McDonnell Douglas Research Labs.
St. Louis, Missouri 63166

Defense Documentation Center
Cameron Station Bldg. 5
Alexandria, Virginia 22314
Attn: TISTA (14 copies)
Via: Naval Air Systems Command
Code AIR-50174
Washington, D.C. 20360

Clevite Corporation
Mechanical Research Division
540 East 105th Street
Cleveland, Ohio 44108
Attn: Mr. A. D. Schwope

The Franklin Institute Research Laboratories
Twentieth & Parkway
Philadelphia, Pennsylvania 19103
Attn: Technical Director

DISTRIBUTION LIST (Cont.)

Dr. John A. Schey
Department of Mechanical Engr.
University of Waterloo
Waterloo, Ontario
Canada N2L 3G1

Convair Division
General Dynamics
San Diego, California 92112
Attn: Mr. A. Hurlich

Dr. Charles Gilmore
School of Engineering and
Applied Science
George Washington University
Washington, D.C. 20006

IIT Research Institute
10 West 35th Street
Chicago, Illinois 60616
Attn: Dr. N. Parikh

Kawecki Berylco Industries
P.O. Box 1462
Reading, Pennsylvania 19603

Ladish Company
Packard Avenue
Cudahy, Wisconsin 53110
Attn: Mr. Joseph Picher
Librarian

Linde Company
Division of Union Carbide
P.O. Box 44
Tonawanda, New York 14152

Lockheed Missiles & Space Company, Inc.
P.O. Box 504
Sunnyvale, California 91088
Attn: Dr. F. A. Crossley
81-35/154
Dr. R. W. Fenn
47-01/154 (1 each)

Lycoming Division
Avco Corporation
550 South Main Street
Stratford, Connecticut 06497
Attn: Division Library

P. R. Mallory & Co., Inc.
3029 East Washington Street
Indianapolis, Indiana 46206
Attn: Technical Librarian

Martin Marietta Corporation
P.O. Box 5837
Orlando, Florida 32805
Attn: Dr. Richard C. Hall
Mail Point 275

Midwest Research Institute
425 Volker Boulevard
Kansas City, Missouri 64110

NASA Scientific & Technical
Information Facility
P.O. Box 33
College Park, Maryland 20740

Autonetics, Division of
Rockwell International Corporation
P.O. Box 4173
Anaheim, California 92803
Attn: Mr. A. G. Gross, Jr.
Dept. 522-92

Northrup Norair
3901 West Broadway
Hawthorne, California 90250
Attn: Technical Information
3343-32

Solar Division
International Harvester Company
2200 Pacific Highway
San Diego, California 92112
Attn: Dr. A. G. Metcalfe

TRW Inc., Jet & Ordnance Division
23555 Euclid Avenue
Cleveland, Ohio 44117
Attn: Elizabeth Barrett

United Aircraft Research Laboratory
East Hartford, Connecticut 06108
Attn: Mr. Roy Fanti

Vought Aeronautics Division
LTV Aerospace Corporation
P.O. Box 5907
Dallas, Texas 75222

Whittaker Corporation
Nuclear Metals Division
West Concord, Massachusetts 01718

Horizons Incorporated
2905 East 70th Street
Cleveland, Ohio 41404

Narmco Industries, Inc.
Research and Development Division
8125 Aero Drive
San Diego, California 92123
Attn: Technical Library

General Electric
Missile & Space Division
Materials Science Section
P.O. Box 8555
Philadelphia, Pennsylvania 91901
Attn: Technical Library

DISTRIBUTION LIST (Cont.)

Reynolds Metals Company
Reynolds Metals Building
Richmond, Virginia 23218
Attn: Technical Library

Artech Corporation
2816 Fallfax Drive
Falls Church, Virginia 22042
Attn: Mr. Henry Hahn

Massachusetts Institute of Technology
Department of Metallurgy and Material Science
Cambridge, Massachusetts 02139
Attn: Dr. R. Pelloux
Dr. N. J. Grant (1 each)

Massachusetts Institute of Technology
Department of Mechanical Engineering
Cambridge, Massachusetts 02139
Attn: Dr. R. O. Ritchie
Dr. A. Argon (1 each)

Dr. Donald E. Harrison
Westinghouse Electric Company
R&D Center
Beulah Road
Pittsburgh, Pennsylvania 15235

Dr. Kenneth A. Jackson
Bell Telephone Laboratories, Inc.
600 Mountain Avenue
Murray Hill, New Jersey 07974

General Electric Research Laboratory
Schenectady, New York 12301
Attn: Dr. Don Wood
Mr. David Lillie (1 each)

Stellite Division
Cabot Corporation
1020 West Park Avenue
Kokeno, Indiana 46901

Aluminum Company of America
1200 Ping Bldg.
Washington, D.C. 20036
Attn: Mr. G. B. Barthold

Pratt & Whitney Aircraft Corp.
400 Main Street
East Hartford, Connecticut 06108

Department of Metallurgical Engineering
Drexel University
32nd & Chestnut Streets
Philadelphia, Pennsylvania 19104

Dr. A. I. Mlavsky
Senior Vice President for Technology & Director of Corporate Technology Center
Tyco Laboratories, Inc.
16 Hickory Drive
Waltham, Massachusetts 02145

Commonwealth Scientific
500 Pendleton Street
Alexandria, Virginia 22314
Attn: Mr. A. P. Divecha

Martin Marietta Aluminum
Attn: Mr. Paul E. Anderson
(M/C 5401)
19200 South Western Avenue
Torrence, California 90509

Reactive Metals
Niles, Ohio 44446
Attn: Dr. H. Bomberger
Mr. H. Kessler
Dr. S. Seagle
Mr. W. Herman (1 each)

Mr. W. Spurr
The Boeing Company
12842 72nd Ave., N.E.
Kirkland, Washington 98033

Commander
Naval Air Systems Command Representative Atlantic
Naval Air Station
Norfolk, Virginia 23511

Commander
Naval Air Systems Command Representative Pacific
Naval Air Station, North Island
San Diego, California 92135

Commanding Officer
Naval Air Rework Facility (Code 34100)
Naval Air Station
Alameda, California 94501

Commanding Officer
Naval Air Rework Facility (Code 34100)
Marine Corps Air Station
Cherry Point, North Carolina 28533

Commanding Officer
Naval Air Rework Facility (Code 34100)
Naval Air Station
Jacksonville, Florida 32212

DISTRIBUTION LIST (Cont.)

Commanding Officer
Naval Air Rework Facility (Code 34100)
Bldg. 504
Naval Air Station
Pensacola, Florida 32508

Commanding Officer
Naval Air Rework Facility (Code 34100)
Naval Air Station, North Island
San Diego, California 92135

Commanding Officer
Naval Air Rework Facility (Code 34100)
Naval Air Station
Norfolk, Virginia 23511

Defense Advanced Research Project Agency
1400 Wilson Boulevard
Arlington, Virginia 22209
Attn: Dr. E. C. VanReuth

Rockwell International Science Center
P.O. Box 1082
1027 Camino Dos Rios
Thousand Oaks, California 91320
Attn: Dr. N. Paton
Dr. A. Thompson (1 each)

Pratt & Whitney Aircraft
Division of United Aircraft Corp.
Florida R&D Center
P.O. Box 2691
West Palm Beach, Florida 33402

Lockheed Missiles & Space Company, Inc.
Lockheed Palo Alto Research Laboratory
3251 Hanover Street
Palo Alto, California 94304
Attn: Dr. Thomas E. Tietz, 52-31/204

Titanium Metals Corporation of America
Henderson, Nevada 89015
Attn: Dr. Harry W. Rosenberg

Southwest Research Institute
8500 Culebra Road
P.O. Drawer 28510
San Antonio, Texas 78284
Attn: Dr. C. Gerald Gardner

Grumman Aerospace Corporation
Bethpage, L.I., New York 11714
Attn: Mr. R. Heitzmann (2 copies)
Dr. G. Geschwind (1 copy)

Mr. George Hsü
Manager of Industry Standards
Reynolds Metals Corp.
6601 W. Broad St.
Richmond, Virginia 23261

McDonnell Aircraft Co.
St. Louis, Missouri 63166
Attn: Mr. H. C. Turner

Dr. John K. Tien
Henry Krumb School of Mines
Columbia University
New York, New York 10027

Lockheed-Georgia Company
86 South Cobb Drive
Marietta, Georgia 30063
Attn: A. C. Fehrle, 72-26/Z28
W. C. Herron, 72-62/B4

Lockheed-California Company
P.O. Box 551
Burbank, California 91520
Attn: E. K. Walker, 74-50/B63
D. Pettit, 74-71/B204
J. Van Orden, 74-71/B229

Dr. J. L. Cavallaro, Code 2814
David Taylor Naval Ship R&D Center
Annapolis, Maryland 21402

Dr. J. C. Williams
Carnegie-Mellon University
Department of Metallurgy and Materials Science
Schenley Park
Pittsburg, Pennsylvania 15213